ASSIMILATION OF HYPERSPECTRAL INFRARED SOUNDER RADIANCES UNDER CLOUDY SKIES IN A REGIONAL NWP MODEL

By

Pei Wang

A dissertation submitted in partial fulfillment of

the requirements for the degree of

Doctor of Philosophy

(Atmospheric and Oceanic Sciences)

at the

UNIVERSITY OF WISCONSIN-MADISON

2016

Date of final oral examination: 25 April 2016

The dissertation is approved by the following members of the Final Oral Committee:

Steven A. Ackerman, Professor, Atmospheric and Oceanic Sciences

Jun Li, Distinguished Scientist, CIMSS/SSEC

Matthew Hitchman, Professor, Atmospheric and Oceanic Sciences

Tristan L'Ecuyer, Associate Professor, Atmospheric and Oceanic Sciences

Michael Morgan, Professor, Atmospheric and Oceanic Sciences

Abstract

Satellite measurements are an important source of global observations in support of numerical weather prediction (NWP). The assimilation of satellite radiances under clear skies has greatly improved NWP forecast scores. Since most of the data assimilation models are used for the clear radiances assimilation, an important step for satellite radiances assimilation is the clear location detection. Good clear detection could effectively remove the cloud contamination and keep the clear observations for assimilation. In this dissertation, a new detection method uses collocated high spatial resolution imager data onboard the same platform as the satellite sounders to help IR sounders subpixel cloud detection, such as the Atmospheric Infrared Sounder (AIRS) and Moderate Resolution Imaging Spectroradiometer (MODIS), the Crosstrack Infrared Sounder (CrIS) and Visible Infrared Imaging Radiometer Suite (VIIRS). The MODIS cloud mask provides a level of confidence for the observed skies to help AIRS Field-of-View (FOVs) cloud detection. By reducing the cloud contamination, a cold bias in the temperature field and a wet bias in the moisture field are corrected for the atmospheric analysis fields. These less cloud affected analysis fields further improve hurricane track and intensity forecast.

The availability of satellite observations that can be assimilated in the model is limited if only the clear radiances are assimilation, which is also used in most operational centers. An effective way to use the thermodynamic information under partially cloudy regions is to assimilate the “cloud-cleared” radiances (CCRs); CCRs are also called clear equivalent radiances. Because the CCRs are the equivalent clear radiances from the partially cloudy FOVs,

they can be directly assimilated into the current data assimilation models without modifications. The AIRS CCRs are assimilated and compared with the AIRS using stand-alone cloud detection and collocated cloud detection. The assimilation of AIRS cloud-cleared radiances directly affects the atmospheric fields in the surroundings away from the hurricane center at the analysis time. With the longer forecast time, the impacts from the environments are transferring to the center of the hurricane, and then further affect the speed of hurricane moving and the hurricane center locations. For the assimilation of AIRS cloud-cleared radiances, the cold air from both the surface level and on the 200 hPa is moving slower and weaker than the results using the stand-alone cloud detection method. The hurricane warm core and the radar reflectivity of the cloud-cleared AIRS assimilated are stronger than AIRS with stand-alone cloud detection. With the improvement of the atmospheric fields, the assimilation of cloud-cleared AIRS gives the smallest root mean square error (RMSE) of hurricane tract 72-hour forecast compared to the AIRS radiances using stand-alone cloud detection and collocated cloud mask cloud detection.

Acknowledgments

First and foremost, I would like to express my sincere gratitude to my research and academic advisors, Dr. Jun Li and Professor Steven A. Ackerman, for their guidance and support with my academics and this research. I thank Dr. Jun Li for giving me the opportunity to pursue my Ph.D, for supporting me in attending many conferences and colloquia, and for creating opportunities to communicate with researchers and scientists in the community.

I would like to thank the members of my Ph.D committee, Professors Matt Hitchman, Tristan L'Ecuyer, and Michael Morgan for their valuable, insightful comments, and encouragement throughout my graduate studies. The useful suggestions and challenging questions polished this work and made it better.

My warm thanks also go to Dr. Jinlong Li, Dr. Zhenglong Li, Dr. Yong-Keun Lee, for their constant help on my research questions, preparing data for my research study, and repeatedly revising and proofreading my manuscripts. I am truly grateful to have such a great research group in my Ph.D study period. Dr. Agnes Lim is the person whom I always turn to help when I meet any questions about the models and experiments. Her hard-work and conscientiousness always encourage me. I also would like to thank Maria Vasys, Debbie Weber, Sue Foldy and Kathy Kruger for their support during the past years.

I would like to gratefully acknowledge the following AOS and CIMSS people for their help in all kinds of ways: Allen Huang, Wenhua Wu, Yinghui Liu, Fuyao Wang, Shu Wu, Chianyi Liu, Jing Zheng, Yan Yu, Jiang Zhu, Feng Zhu, Alexa Ross, and Xiaowei Jiang.

Last but not least, my deepest gratitude goes to my husband, my daughter and my parents, who have encouraged me so much and always gave me confidence in my life. They are the people who I can turn to rain or shine, and always there supporting me. Thanks for the patience and endless love.

Table of Contents

Abstract ..... **i**

Acknowledgments ..... **iii**

Table of Contents ..... **v**

List of Tables ..... **vii**

List of Figures ..... **viii**

Chapter 1 Motivation and Introduction **1**

Chapter 2 Background **5**

2.1 Assimilating IR retrieved products 7

2.1.1 Retrieved products from IR sounders 8

2.1.2 About the assimilation of retrieved products 10

2.2 Assimilating IR sounder radiances 10

2.3 Challenges to assimilate IR sounder radiances in cloudy skies 12

Chapter 3 Models, Assimilation Systems, Hurricanes and Data used in this study **15**

3.1 Description of Models 15

3.1.1 Regional numerical weather prediction model 15

3.1.2 Data assimilation system 17

3.1.3 Radiative transfer model 18

3.2 Hurricanes 19

3.3 Data set used for assimilation 22

3.4 Experimental design 27

Chapter 4 Eliminating cloud contamination – clear location detection.....33
4.1 Methodology for clear location detection.....34
4.2 AIRS/MODIS for clear location detection.....36
4.2.1 Impact on analysis.....36
4.2.2 Impact on clear detection forecasts.....43
4.3 CrIS/VIIRS for clear location detection.....47
4.4 Summary.....50

Chapter 5 Use of thermodynamic information under partially cloudy skies.....53
5.1 Methodology for deriving cloud-cleared radiances.....55
5.2 Impact on analysis.....57
5.2.1 Coverage of AIRS radiances.....57
5.2.2 Analysis fields of temperature.....61
5.2.3 Comparing the analysis temperature profiles with radiosondes.....64
5.2.4 The hurricane locations at the analysis time.....67
5.3 Impact on cloud-cleared radiances forecasts.....70
5.3.1 Comparison with GOES-13 Imager brightness temperature observations.....70
5.3.2 Forecasts validation with radiosondes.....72
5.3.3 Hurricane track error and intensity error.....75
5.4 Summary.....79

Chapter 6 Analysis of thermodynamic fields of Hurricane Sandy..82
6.1 Case study of Hurricane Sandy.....83
6.2 The temperature fields on 500 hPa.....85
6.3 Sea level pressure, surface wind and the surface radar reflectivity.....89
6.4 The temperature fields, winds and geopotential height on 850 hPa.....92
6.5 The potential vorticity and the winds on 500 hPa.....96
6.6 Summary.....100

Chapter 7 Conclusions and future perspectives.....103

References.....110

List of Tables

Table 3.1 The used channels of AMSUA-A data onboard NOAA-15, NOAA-18, Metop-A, Aqua and NOAA-19 23

Table 3.2 The used channels of ATMS onboard S-NPP/JPSS 24

Table 3.3 Data used in the experiments for AIRS/MODIS clear detection 28

Table 3.4 Data used in the experiments for CrIS/VIIRS clear detection 29

Table 5.1 The number of radiosondes at different pressure levels from 1000 hPa to 150 hPa for Hurricane Sandy 64

List of Figures

Figure 2.1 AIRS temperature Jacobian (dBT/dT, unit: K/K) with a cloud-top pressure (CTP) of 700 hPa, and cloud optical thickness (COT) at 0.55 μm of 0.05 (upper) and 0.5 (lower), respectively 15

Figure 3.1 The model domain of the experiments for this study. 16

Figure 3.2 The best track (from CIMSS/SSEC) and the observed maximum wind speed (from NHC) of Hurricane Sandy (2012).....20

Figure 3.3 The best track (from CIMSS/SSEC) and the observed maximum wind speed (from NHC) of Hurricane Irene (2011).....21

Figure 3.4 The best track (from CIMSS/SSEC) and the observed maximum wind speed (from NHC) of Hurricane Ike (2008).....21

Figure 3.5 An example of AIRS spectrum (black) and the corresponding 281 channels (blue dots) selected for the NWP center. The red dots are selected 120 channels from 281 channels that were assimilated in this study.. 29

Figure 3.6 An example of CrIS spectrum (black) and the corresponding 399 channels (blue dots) selected for the NWP center. The red dots are selected 84 channels from 399 channels that were assimilated in this study.. 29

Figure 3.7 Assimilation cycle valid for the three experiments. The initial condition at 25 0600 UTC is interpolated from the global analysis. After the data assimilation (blue box), a 72-hour

forecast is carried out, and at the same time, the 6-hour short term forecast is used as the first guess for the next assimilation cycle.. 31

Figure 4.1 The brightness temperature (unit: K) for one AIRS granule indicated in Figure 4.2 at 0600 UTC on 25 October 2012..... 35

Figure 4.2 The collocated MODIS cloud mask for the small box area outlined by the rectangle in Figure 4.1.. 36

Figure 4.3 The weighting function of AIRS channel 210 (709.5659 cm^{-1}).. 38

Figure 4.4 AIRS stand-alone cloud detection (GSI) (left) and AIRS cloud detection with MODIS (right) for AIRS channel 210.. 38

Figure 4.5 The weighting function of AIRS channel 1447 (1345.31 cm^{-1}).. 39

Figure 4.6 AIRS alone cloud detection (GSI) (left) and AIRS cloud detection with MODIS (right) for AIRS channel 1447.. 39

Figure 4.7 The difference in temperature (upper, unit: K) and relative humidity (lower, unit: %) analysis between the two experiments (AIRS (MOD clr) – AIRS (GSI clr)) with the geopotential height (solid, unit: m) of AIRS (MOD clr) at 500 hPa at 0600 UTC on 25 October 2012.. 41

Figure 4.8 The difference in temperature (upper, unit: K) and relative humidity (lower, unit: %) analysis between the two experiments (AIRS (MOD clr)- AIRS (GSI clr)). The geopotential height (solid, unit: m) of AIRS (MOD clr) at 700 hPa at 0600 UTC on 25 October 2012.. 42

Figure 4.9 The 72-hour forecast hurricane track of best track (black), GTS+4AMSUA+AIRS (GSI blue) and GTS+4AMUSA+AIRS (MOD clr) at 1800 UTC 25 (a), 0000 UTC 26 (b), 0600 UTC 26 (c), 1200 UTC 26 (e) and 0000 UTC 27 (e) October 2012.....45

Figure 4.10 The track (top) and the maximum wind speed (bottom) forecast RMSE with AIRS (GSI clr) (blue) and AIRS (MOD clr) (red). Data are assimilated every 6-hour from 1800 UTC on 25 October to 0000 UTC on 27 October 2012, followed by 72-hour forecasts for Hurricane Sandy (2012) 46

Figure 4.11 The weighting function of CrIS channel 96 (709.37 cm^{-1}).. 47

Figure 4.12 The location at 0600 UTC 26 Oct 2012 where CrIS channel 96 (709.37 cm^{-1}) is flagged clear with stand-alone cloud detection (upper) and with VIIRS cloud detection (lower) on visible imagery (10.7 μm) from GOES-13 for Hurricane Sandy (2012)..…..49

Figure 4.13 The track (top) and the maximum wind speed (bottom) forecast RMSE with CrIS stand-alone cloud detection (blue) and CrIS/VIIRS cloud detection (red). Data are assimilated every 6-hour from 0600 UTC on 25 October to 0000 UTC on 27 October 2012, followed by a 72-hour forecast for Hurricane Sandy (2012).. 51

Figure 5.1 AIRS brightness temperature (BT) spectral (red, unit: K) with MODIS spectral response function (SRS) of channels (dashed). MODIS channel numbers are marked in the figure. Black with blue circle is MODIS channels used in cloud-clearing and QC, grey is not used. 57

Figure 5.2 The locations at 1800 UTC 25 October 2012 where AIRS channel 210 (709.5659 cm^{-1}) is assimilated in GSI for AIRS (GSI clr) (lower left red), AIRS (MOD clr) (upper blue) and AIRS (MOD cld-clr) (lower right green).....58

Figure 5.3 The weighting function of AIRS channel 787 (917.3062 cm^{-1}).....59

Figure 5.4 The locations at 1800 UTC 25 October 2012 where AIRS channel 787 (917.3062 cm^{-1}) is assimilated in GSI for AIRS (GSI clr) (lower left red), AIRS (MOD clr) (upper blue) and AIRS (MOD cld-clr) (lower right green).....60

Figure 5.5 The difference in temperature (shaded, unit: K) analysis between AIRS (MOD cld-clr) and AIRS (MOD clr) with temperature (contour, unit: K) of AIRS (MOD cld-clr) at 500 hPa at 1800 UTC 25 October 2012.....62

Figure 5.6 The difference in temperature (shaded, unit: K) analysis between AIRS (MOD cld-clr) and AIRS (MOD clr) with temperature (contour, unit: K) of AIRS (MOD cld-clr) at 850 hPa at 1800 UTC 25 October 2012.....63

Figure 5.7 Temperature BIAS (left) and STD (right) using radiosonde for AIRS (GSI clr) (dash-dot black, unit: K), AIRS (MOD clr) (solid blue, unit: K) and AIRS (MOD cld-clr) (dashed red, unit: K) at analysis time for Hurricane Sandy 65

Figure 5.8 Temperature BIAS (left) and STD (right) using radiosonde for AIRS (GSI clr) (dash-dot black, unit: K), AIRS (MOD clr) (solid blue, unit: K) and AIRS (MOD cld-clr) (dashed red, unit: K) at analysis time for Hurricane Irene 66

Figure 5.9 The location of radiosondes are used to compare with analysis fields at 0000 UTC 26 October 2012.....67

Figure 5.10 The track error of Hurricane Sandy (2012) at analysis time from 1800 UTC 25 October to 0000 UTC 27 October, 2012.....68

Figure 5.11 The number of assimilated AIRS radiances at channel 210 of Hurricane Sandy (2012) at analysis time from 1800 UTC 25 October to 0000 UTC 27 October, 2012 69

Figure 5.12 The brightness temperature of GOES-13 channel 4 (11 μm) observations (upper, unit: K), simulated 72-hour forecast brightness temperature of AIRS (MOD clr) (mid left) and AIRS (MOD cld-clr) (mid right), the difference of brightness temperature between observations and AIRS (MOD clr) (lower left) and between observations and AIRS (OD cld-clr) (lower right) at 1800 UTC 28 October 2012.....71

Figure 5.13 BIAS (left column) and STD (right column) for 24-hour (upper panel), 48-hour (middle panel), and 72-hour (lower panel), forecasts of temperature profiles between the AIRS (GSI clr) (dash-dot black, unit: K) and radiosondes, AIRS (MOD clr) (solid blue line, unit: K) and radiosondes, and AIRS (MOD cld-clr) (dashed red line, unit: K) and radiosondes from 1000 hPa to 150 hPa for Hurricane Sandy.....74

Figure 5.14 The track (top) and maximum wind speed (bottom) forecast RMSE with AIRS (GSI clr) (blue), AIRS (MOD clr) (red) and AIRS (MOD cld-clr) (green). Data are assimilated every 6-hour from 1800 UTC on 25 October to 0000 UTC on 27 October 2012, followed by 72-hour forecasts for Hurricane Sandy (2012).....77

Figure 5.15 The track (top) and maximum wind speed (bottom) forecast RMSE with AIRS (GSI clr) (blue), AIRS (MOD clr) (red) and AIRS (MOD cld-clr) (green). Data are assimilated every 6-hour from 1200 UTC on 22 August to 0000 UTC on 24 August 2011, followed by 72-hour forecasts for Hurricane Irene (2011).....78

Figure 5.16 The track (top) and maximum wind speed (bottom) forecast RMSE with AIRS (GSI clr) (blue), AIRS (MOD clr) (red) and AIRS (MOD cld-clr) (green). Data are assimilated every 6-hour from 1800 UTC on 5 September to 0000 UTC on 7 September 2008, followed by 72-hour forecasts for Hurricane Ike (2008).....79

Figure 6.1 The tracks of Hurricane Sandy (2012) for a 72-hour forecast from 1800 UTC 26 October to 1800 UTC 29 October 2012.....83

Figure 6.2 The track error of GTS+AMSUA+AIRS (GSI) (blue line), GTS+AMSUA+AIRS clr (red line) and GTS+AMSUA+AIRS clrcld (green line) comparing to the best track for 72-hopur forecast of Hurricane Sandy (2012) from 1800 UTC 26 October to 1800 UTC 29 October 2012 84

Figure 6.3 The locations at 1800 UTC 26 October 2012 where AIRS channel 210 (709.5659 cm^{-1}) is assimilated in GSI for AIRS (GSI clr) (lower left red), AIRS (MOD clr) (upper blue) and AIRS (MOD cld-clr) (lower right green).....86

Figure 6.4 The difference in temperature (shaded, unit: K) between AIRS (MOD cld-clr) and AIRS (MOD clr) with geopotential height (contour, unit: m) of AIRS (MOD cld-clr) at 500 hPa for 0-hour forecast (a), 24-hour forecast (b), 48-hour forecast (c) and 72-hour forecast (d) from 1800 UTC 26 October 2012.....88

Figure 6.5 The surface radar reflectivity (shaded, unit: dBz), sea level pressure (contour, unit: hPa) and surface wind (vector, unit: m/s) of AIRS (GSI clr) ((a) (c) (e) (g)) and AIRS (MOD cld-clr) ((b) (d) (f) (h)) for 0-hour forecast ((a) (b)), 24-hour ((c) (d)), 48-hour forecast ((e) (f)), and 72-hour forecast ((g) (h)) from 1800 UTC 26 October 2012.....90

Figure 6.6 The temperature fields (shaded, unit: K), geopotential height (contour, unit: m) and winds (vector, unit: m/s) on 850 hPa of AIRS (GSI clr) ((a) (c) (e) (g)) and AIRS (MOD cld-clr)

((b) (d) (f) (h)) for 0-hour forecast ((a) (b)), 24-hour forecast ((c) (d)), 48-hour forecast ((e) (f)), and 72-hour forecast ((g) (h)) from 1800 UTC 26 October 2012.....94

Figure 6.7 The potential vorticity (shaded, unit: PVU) and winds (vector, unit: m/s) on 200 hPa of AIRS (GSI clr) ((a) (c) (e) (g)) and AIRS (MOD cld-clr) ((b) (d) (f) (h)) for 0-hour forecast ((a) (b)), 24-hour ((c) (d)), 48-hour forecast ((e) (f)), and 72-hour forecast ((g) (h)) from 1800 UTC 26 October 2012.....98

Chapter 1

Motivation and Introduction

Society has long desired to accurately forecast the weather. What will the weather be like this afternoon? Tomorrow? Next week? An accurate weather forecast is very important for both our daily life and the whole society. For a successful accurate weather forecast, Bjerknes (1911) outlined two conditions: (1) The present state of the atmosphere (or the analysis fields) must be characterized as accurately as possible; (2) the intrinsic laws, according to which the subsequent states develop out of the preceding ones, must be known. The basic atmospheric motion equations and basic conservation laws are the components of the theoretical support for the atmospheric intrinsic laws. For practical implementation, Bjerknes subdivided the two conditions into three partial problems: (1) the observation component; (2) the diagnostic or analysis component; and (3) the prognostic component. These three problems are the key components for improving weather forecasts.

Based on Bjerknes' three partial problems, with the dense global observation system of today, there are two ways to further improve the weather forecast: improve the diagnostic or analysis component, that is improves the initial conditions through the advanced data assimilation systems; or improves the prognostic component, which is to improve the numerical modeling with advanced numerical methods by better representing the dynamic processes of the

atmosphere. This study focuses on the former because the current observations are not efficiently used by the analysis system.

Data assimilation uses both observations and short-term forecasts to estimate the initial conditions (Kalnay, 2003). In the modern NWP, both traditional observations and satellite observations can be assimilated in the system, and provide useful atmospheric initial condition information for improving the weather forecasts. Traditional measurements from the surface and radiosonde are the traditional measurements used in forecasting, including the SYNOP (for land surface observations), SHIP (for sea surface observations) and TEMP (for upper air observations) (Daley, 1991). The weather observations have high temporal and spatial resolution are also available for operational centers, such as the satellite observations, the lidar and radar data, and the GPS Radio Occultation (RO) data. The satellite measurement is an important type of global observation in support of NWP. Because most traditional observations are over populated land regions, satellite observations compensate for those areas where traditional observations are limited or rare, such as over oceans and the Southern Hemisphere. High temporal resolution is another advantage of satellite observations. Even over land, satellite observations are able to fill the gaps between the radiosonde locations and their launch times. In addition, the number of the radiosondes is becoming declined in the near future (McPherson, 1999), which indicates that the satellite measurements are becoming more important observations. The methodologies and applications for improving the satellite infrared radiances assimilation on hurricane forecast are discussed in the dissertation.

To date, the assimilation of satellite data is mostly under clear skies only, especially for infrared (IR) sounder data. Due to many satellite IR sounders measure both atmospheric profiles and clouds, the data impact of the IR observations mainly comes from the clear observations (not

affected by clouds) at most operational centers. In data assimilation system, the radiative transfer model, the background error covariance, the observation error covariance and etc. are suitable for the clear radiances assimilation. Studies (e.g. Pangaud et al., 2009; Wang et al., 2014) found that if the cloudy radiances are assimilated as clear observations, the analysis fields would be degrade and make the NWP forecasts results worse. Reliable cloud detection is essential and one of the challenges in assimilating advanced IR sounder radiances. The current cloud detection scheme for satellite radiances is the clear channel detection (McNally and Watts, 2003) based on the first-guess departures (e.g., by comparing the observed brightness temperature and the simulated brightness temperature calculated through the forward model from the background), which potentially generates considerable risk for confusing the cloud detection by falsely assimilating observed cloudy radiances as clear radiances. Improved cloud detection could improve detection of clear field-of-views (FOVs) and improve the assimilation of IR radiances. The collocated high spatial resolution imager data can help IR sounder sub-pixel cloud detection and characterization (Li et al., 2004).

By applying spatially and temporally collocated high spatial resolution imager cloud mask, the thermodynamic information and cloud properties at the IR sounder sub-pixel level can be well separated. The collocated imager information improves the sounder cloud detection, and then further improved the weather forecasts (Wang et al., 2014). In this dissertation, the impact of the cloud detection on AIRS radiance assimilation has been investigated, and the collocated high spatial resolution (1 km) MODIS (Moderate resolution Imaging Spectroradiometer) cloud mask product is used for AIRS sub-pixel cloud detection. The methodology can also be applied on CrIS (Crosstrack Infrared Sounder) sounder cloud detection. Collocated high spatial

resolution VIIRS (Visible Infrared Imaging Radiometer Suite) cloud mask product is used for CrIS sub-pixel cloud detection.

Good cloud detection can effectively remove the cloud contamination and keep the clear observations for assimilation. However, the clear IR observations constitute only a small portion of the total IR observations. The percentage of completely clear-sky observations from the High-Resolution Infrared Radiation Sounder (HIRS) is around 25% (Wylie et al., 1994), and the percentage of AIRS is less than 10% (Huang and Smith, 2004). Therefore, the percentage of IR observations which can be assimilated in the operational system is as few as 5% of the total observations (McNally and Watts, 2003). Expanding radiance assimilation into partially cloudy regions is needed to maximize the utility of advanced IR sounder data. Research using cloudy radiances directly has been ongoing, but significant challenges remain. An effective way to use the thermodynamic information under partially cloudy regions is to assimilate the "cloud-cleared" radiances (CCRs) or cloud-removed radiances (Smith, 1968; Smith et al., 2004); CCRs are also called clear equivalent radiances. The cloud-cleared radiance is the equivalent clear radiances, which can be assimilated in the current models without modifications. The AIRS cloud-cleared radiances can be calculated combining the information from MODIS and AIRS radiances (Li et al., 2005). The assimilation of AIRS cloud-cleared radiances are compared with the stand-alone cloud detection and the collocated MODIS cloud detection. The atmospheric environment fields of the three experiments are discussed to help us understand how the AIRS cloud-cleared radiances assimilation improves the hurricane track forecast.

The dissertation is structured as follows. Chapter 2 presents an overview of the satellite IR data assimilation, focusing on the IR sounder radiances and retrieved products assimilation and the challenges of IR radiances under cloudy skies. Chapter 3 describes the conventional data,

satellite data, the data assimilation system and regional NWP model used for this study. The detailed of the experimental design and the hurricane cases are also explained in the Chapter 3. Chapter 4 introduces the IR radiances cloud detection method using the collocated high spatial resolution cloud mask, and the application of this method on the IR assimilation and forecast. Chapter 5 discussed the cloud-clearing method and the application of AIRS cloud-cleared radiances assimilation on hurricane case studies. The analysis fields and the forecast results of AIRS cloud-cleared radiances assimilation are compares with AIRS using GSI stand-alone cloud detection and MODIS cloud mask cloud detection experiments. Chapter 6 further studies the improvement on the hurricane structures and atmospheric environment variables with assimilating the AIRS cloud-cleared radiances. Besides hurricane track, the dynamic fields of hurricane structures, such as temperature, wind, PV and etc. are shown in details. Chapter 7 summarizes the dissertation results and the future work.

Chapter 2

Background

Satellite observations are an important component of global observations in support of weather forecast. Both the retrievals and the direct radiances from the satellite measurements are assimilated in the NWP models. The assimilation of the retrievals was carried out in the early studies. Dey et al. (1989) compared the assimilation of statistical derived soundings and the physical derived soundings. It was found that the physical satellite soundings performed consistently better in both hemispheres. Le Marshall (1988) found that the physical soundings significantly improved the moisture field in both nowcasting and the NWP. However, the soundings are highly related to the background fields, and the observation error of the retrieval profiles is hard to calculate. Kelly et al. (1991) compared the satellite soundings and the first guess fields and found large departures between them. To reduce the error characterization in the satellite soundings, the direct assimilation of the satellite radiance was considered in the NWP centers.

Radiance assimilation was first applied to the global data by modifying the one-dimensional non-linear optimal estimation scheme at the European Center for Medium-Range Weather Forecasts (ECMWF) in June 1992 (Eyre et al., 1993). And then the operational three-dimensional variation assimilation (3D-Var) systems were developed for radiance assimilation in

the early 1990s' (Parrish and Derber, 1992; Derber et al., 1991; Courtier et al., 1993). The assimilation of the retrievals was replaced by assimilation of the direct radiances since 1995 at the National Center for Environmental Prediction (NCEP) (Derber and Wu, 1998). After that, the satellite radiances are becoming directly assimilated in the other operational centers and research studies (Guthier et al., 1999; Laroche et al., 1999; Lorenc et al., 2000). Based on the recent studies, contributions from satellite data, especially from infrared (IR) and microwave (MW) sounders such as AIRS, Infrared Atmospheric Sounding Interferometer (IASI), CrIS, Advanced Microwave Sounding Unit-A (AMSU-A), Advanced Microwave Sounding Unit-B (AMSU-B), Microwave Humidity Sounder (MHS) etc., are becoming the most important observations in operational centers (Le Mashall et al., 2005, 2006; Kelly and Thepaut, 2007; Cardinali, 2009). MW and IR sounders have the largest impact on forecast skills in all satellite observations (Cucurrull et al., 2014; Joo et al., 2013; Garand et al., 2013).

2.1 Assimilating IR retrieved products

Severe weather systems are usually accompanied with heavy clouds and precipitation. The regions with clouds and precipitation are expected to have large impacts on forecast accuracy, because they are meteorologically sensitive areas (McNally, 2002). To avoid the limitations and uncertainties associated with direct assimilation of the cloud-affected radiances (Errico et al., 2007; Geer and Bauer et al., 2011), in recent studies, the cloud properties and the related moisture information are retrieved from the cloudy regions and then further assimilated into the models. The advantages of assimilating the retrieval products are that (i) it is easier to handle the non-linearity of the moist physical process (Moreau et al., 2004); (ii) it is

straightforward to apply the quality controls before the retrievals are passed on to the assimilation models (Bauer et al., 2006a, 2006b; Geer et al., 2008); (iii) it avoids using the forward radiative transfer model to calculate the brightness temperature from the model background in the cloudy regions. Therefore, assimilating the clouds and rainfall products retrieved from satellite data is used in operational and research studies.

2.1.1 Retrieved products from IR sounders

IR observations are very sensitive to clouds, which has two sides for satellite data assimilation. On the one hand, reliable cloud detection is required for IR sounder assimilation, which helps the cloud contamination or cloud pixels that are removed from the clear sky assimilation; on the other hand, high spatial resolution IR imager data provides the high quality of observed cloud characteristics, such as the cloud fraction and cloud height, which could be assimilated in the system to improve the atmospheric analysis and forecasts fields.

The cloud fraction and height from satellite imagers are used to help initialize mesoscale systems in the Met Office (Macpherson et al., 1996; Renshaw and Francis, 2011). Information on the cloud fraction and height from the Spinning Enhanced Visible and Infrared Imager (SEVIRI) is converted to humidity pseudo-observations, and then the humidity profiles are assimilated in the system in a similar way as radiosondes. Some modifications for assimilating the humidity are noted by Renshaw and Francis (2011).

The cloud-top pressure and temperature data from the GOES imager have been used operationally in the Rapid Update Cycle (RUC) since April 2002 (Kim and Benjamin, 2001;

Benjamin et al., 2004a; Benjamin et al., 2004b). The GOES single FOV cloud-top pressure provides information on the cloud locations, though not the multiple layers or the cloud optical depths (Li et al., 2001). The clouds or hydrometeors are removed in the model where there are no observed clouds, and the cloud water and/or ice are added in the model where there are observed clouds. Assimilating GOES cloud-top improves the 3-hour forecast of cloud-top pressure and frontal cloud band. Otkin (2010) used an ensemble Kalman filter method (Evensen, 1994) to assimilate the simulated clear and cloudy observations of the Advanced baseline Imager (ABI), which is to be launched onboard GOES-R. It is shown that the assimilation of the IR brightness temperature both under clear-sky and cloudy-sky largely provided the cloud fields.

The retrieved temperature and moisture profiles (Li and Huang 1999; Li et al., 2000) as well as surface emissivity (Li et al., 2007; Li and Li, 2008) from IR sounders provide useful information for improving NWP. The temperature and moisture soundings from the hyperspectral infrared sounders have high vertical resolution and accuracy. Using the high quality temperature and moisture sounding data, the track errors for Hurricane Ike (2008) and Typhoon Sinlaku (2008) are reduced and the hurricane intensity forecasts are improved (Li and Liu, 2009; Liu and Li, 2010). Zheng et al. (2015) assimilated the AIRS clear-sky temperature profiles in the hurricane environment, which improves the hurricane track forecast and the hurricane moisture environment. Assimilating AIRS soundings derived in cloud-contaminated areas significantly increases the weather forecast skill during the midlatitude boreal winter conditions (Reale et al., 2008). Zavodsky et al. (2007) indicated that the AIRS retrievals provided a positive impact on improving the weather forecast skill.

2.1.2 About the assimilation of retrieved products

Assimilating retrieved products is an alternative way to extend the assimilation of satellite observations from clear skies to cloudy skies. The retrieved products bring information about the cloud-affected observations in the system to improve the hydrometeor process and cloud properties in the analysis and forecast atmospheric fields. However, several problems of assimilating the retrieved products are addressed: (i) the retrieved products are highly dependent on the first guess. If the first guess differs significantly from the model background, the analysis fields are degraded by the mismatch of the large departures (Geer et al., 2008); (ii) the variables assimilated in the model usually are cloud-top pressure, TCWV, and rain rate. However, there are more variables that can be retrieved, such as the surface wind, the vertical profiles of temperature, moisture, cloud and precipitation. The information is missed by only assimilating one or two variables in the system (Okamoto and Derber, 2006); (iii) the retrieved cloud properties or the precipitation are usually converted to humidity profiles to affect the analysis fields. This process needs to be done carefully as adding or removing the moisture information at the wrong vertical level would degrade the forecast skills (Renshaw and Francis, 2011). Therefore, it is still worth the efforts to study the direct assimilation of satellite observations under cloudy sky.

2.2 Assimilating IR sounder radiances

Currently there are mainly four methodologies for IR sounder radiance assimilation: (1) the first method is clear location, which is to find clear FOVs so that radiances in clear FOVs can

be assimilated. The advantage of this method is that radiance assimilation in clear skies is quite mature and the radiative transfer model (RTM) in clear skies is also reliable; the disadvantage is that only a small percentage of the data are used. (2) The second method is clear channel detection. This method is used to find radiances of those channels not affected by clouds, for example, choosing radiances in those channels with weighting function, or Jacobian (dBT/dT) peaks above the clouds. The advantage of this method is that more data are used in radiance assimilation, especially some data are used in cloudy skies (e.g., in low cloud situations), the disadvantage is that the channels with weighting peaks above the cloud top can still be partially contaminated by clouds. (3) The third methodology is direct assimilation of radiances in cloudy skies, which is still quite challenging. (4) The fourth methodology is to use cloud-cleared radiances instead; this method removes the cloud effect in IR FOV(s) by using additional information in cloudy skies and obtaining the clear equivalent radiances or so-called cloud-cleared radiances (CCRs), so that the CCRs can be treated as clear radiances in assimilation. The advantage of this method is that the CCRs can be assimilated as clear radiances under partially cloudy skies; the disadvantage is that additional information is needed and the CCR observation errors are amplified compared to the clear sky radiances.

Based on difference sources of additional information, three cloud-clearing methods have been developed. The first method, called the background based cloud-clearing method, is based on the background or first-guess fields. The cloud-cleared CrIS radiances based on the background cloud-clearing method are assimilated at the National Centers for Environmental Prediction (NCEP) for research study (Liu et al., 2015). The advantage of this method is that it is easy to implement into the operational systems. But the cloud-cleared information is only based on the background or the first-guess fields, which generate considerable risk if the forecasts used

as the background in cloudy regions have large uncertainties. The second method is using the MW (i.e., AMSU-A) data to help the IR (i.e., AIRS) obtain cloud-cleared IR radiances (Susskind et al. 2003). Usually MW sounders have relatively coarse spatial resolution (i.e., 45 km for AMSU-A at nadir) compared to IR sounders (i.e., 13.5 km for AIRS at nadir); as a result, the cloud-cleared IR sounders are degraded from the higher spatial resolution to the coarse spatial resolution of the MW sounders. The third cloud-clearing method uses high spatial resolution imager data (i.e., MODIS) to help the IR (i.e., AIRS) obtain cloud-cleared IR radiances under partially cloudy regions (Li et al., 2005). It removes the cloud effect from an IR sounder FOV with partial cloud cover by using collocated clear sky imager IR radiances. For example, by spatially averaging MODIS IR radiances into an AIRS FOV, and spectrally averaging AIRS into MODIS spectral bands, an important cloud-clearing parameter called N* can be calculated, by applying N* to the whole AIRS radiance spectrum, AIRS cloud-cleared radiances on a single FOV basis can be obtained for radiance assimilation in NWP. The advantage of this method is that it keeps the original high spatial resolution of the IR data (i.e., 13.5 km at nadir for AIRS cloud-cleared radiances). The details of the third cloud-clearing method and the applications of this method is discussed in this dissertation Chapter 5.

2.3 Challenges to assimilate IR sounder radiances in cloudy skies

For IR sounders, direct assimilation of radiances is particular challenging because (1) both NWP and radiative transfer models (RTM) have larger uncertainties in cloudy regions, (2)

there is a significant change in the temperature Jacobians at cloud level, and (3) satellite observations and NWP may be inconsistent on clouds (e.g., satellite sees clouds but NWP does not, vice versa). Figure 2.1 shows the AIRS temperature Jacobian (dBT/dT, unit: K/K) using the Community Radiative Transfer Model (CRTM) with a cloud-top pressure (CTP) of 700 hPa, and cloud optical thickness (COT) at 0.55 μm of 0.05 (upper) and 0.5 (lower), respectively. It can be seen that when the cloud is thin, the temperature Jacobians are quite smooth vertically while when the cloud is thicker, there is a large temperature Jacobian change at cloud level, making the assimilation of temperature information from radiances very difficult in cloudy skies. Another challenge is the higher nonlinearity in assimilation when clouds present (Bauer et al. 2011).

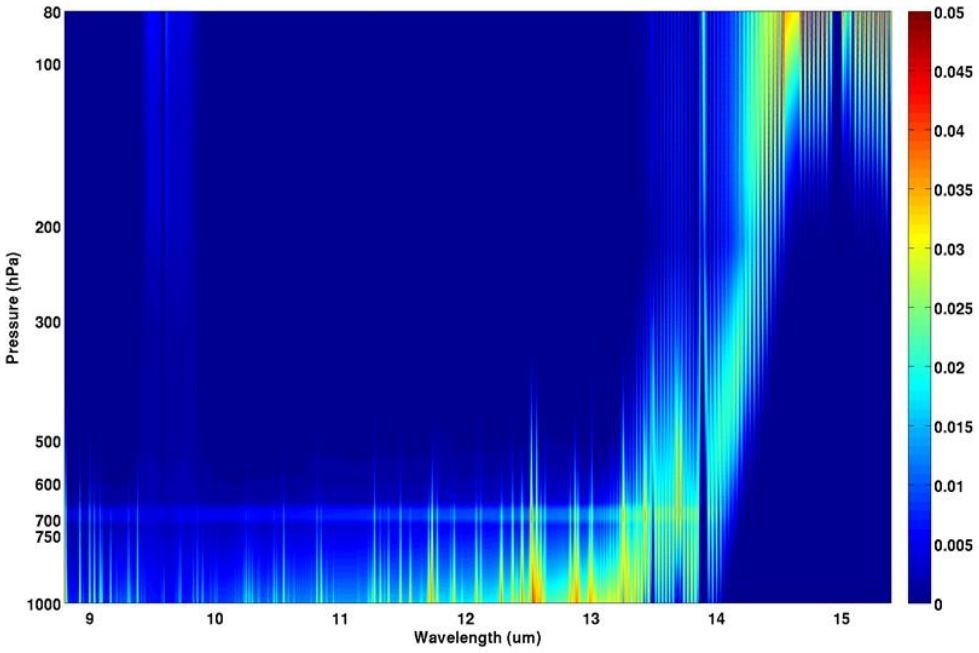

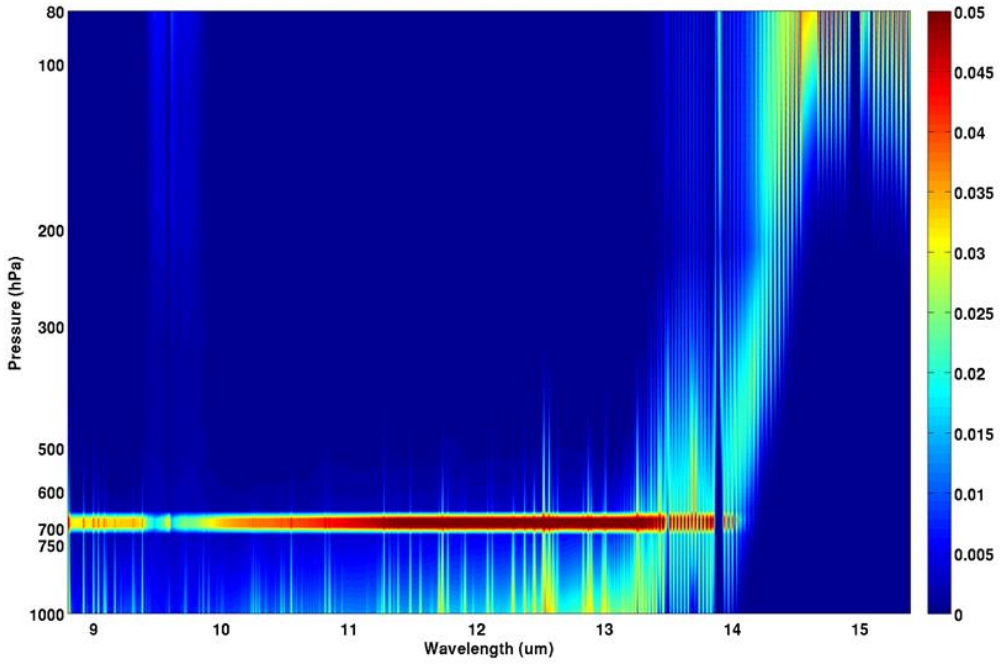

Figure 2.1 AIRS temperature Jacobian (dBT/dT, unit: K/K) with a cloud-top pressure (CTP) of 700 hPa, and cloud optical thickness (COT) at 0.55 μm of 0.05 (upper) and 0.5 (lower), respectively.

Chapter 3

Models, Assimilation Systems, Hurricanes and Data used in this study

3.1 Description of Models

3.1.3 Regional numerical weather prediction model

The advanced research version of the Weather Research and Forecasting (WRF-ARW) model version 3.2.1 is used as the NWP system. WRF is a mesoscale NWP model, which is designed for both research and operational forecasting. The NCAR Mesoscale and Microscale Meteorology Division support WRF-ARW for the community. The equation set for WRF-ARW is fully compressible, Eulerian and non-hydrostatic in flux form on a mass based terrain following vertical coordinate system [Skamarock et al. 2008]. In WRF-ARW, several physical schemes are available for various research purposes, such as data assimilation development and studies, parameterized-physics research, air quality modeling atmosphere-ocean coupling and idealized simulations. WRF-ARW is used in daily runs for regional NWP short-term forecasts, such as NCEP Rapid Refresh (RAP), and SDAT.

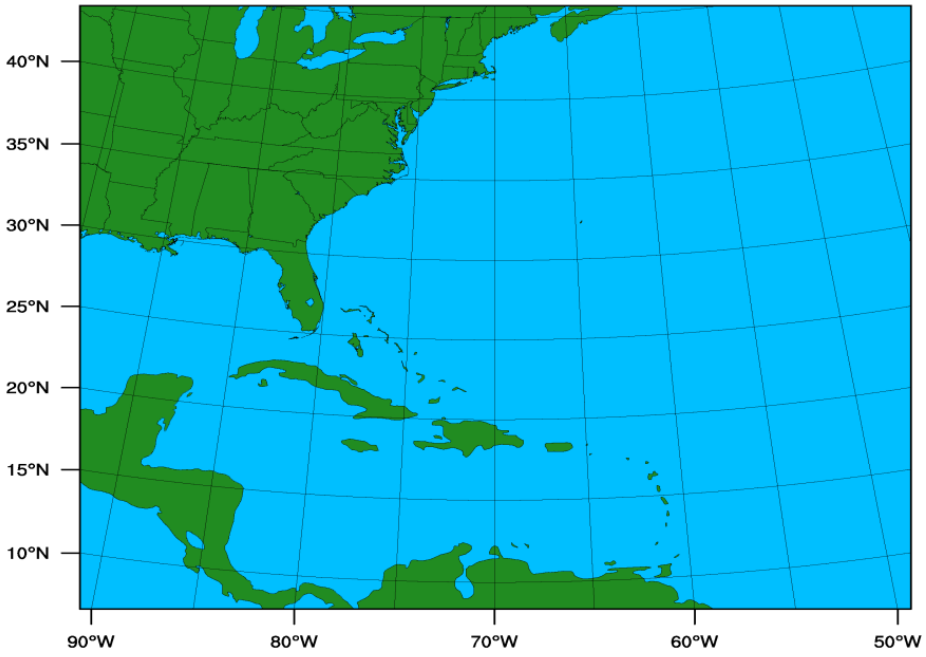

Figure 3.1 The model domain of the experiments for this study.

In this study, the horizontal domain covers an area from $6°N$ to $51°N$ and $40°W$ to $100°W$ on the Lambert Conformal Conic projection as shown in Figure 3.1. Since hurricanes are the weather systems that we want to focus on, the model domain covers a large area of the North Atlantic Ocean, the East and the Mid-West of the American, Cuba, the Gulf of Mexico and the very north of the South America. The horizontal resolution in the domain is 12 km with 400×350 grid points, and the vertical is from the surface to 10 hPa instead of the default 50 hPa in WRF model. The microphysics scheme used is the WRF Single-Moment six-class scheme (WSM6) by Hong and Lim [2006]. Longwave and shortwave radiation schemes used are the RRTMG scheme [Iacono et al., 2008]. The planetary boundary layer is the Yonsei University scheme (YSU) [Hong et al., 2006], and the cumulus parameterization option is the Kai-Fritsch scheme [Kain, 2004].

3.1.2 Data assimilation system

The Gridpoint Statistical Interpolation (GSI) system version 3.1 from the Developmental Testbed Center (DTC) is used as the data assimilation model. GSI is primarily a three-dimensional incremental variational (3D-Var) system with modules developed for advanced features for both global and regional applications (Wu et al., 2002; Kleist et al., 2009). GSI is an operational assimilation system developed jointly by, NASA and NCAR. DTC transitioned the operational GSI system into a community system to be used in the public domain for study, research or any purpose. It is capable of assimilating various kinds of observations from conventional data to aerosol observations and satellite radiance data. GSI system is now widely used in research community (Schwartz et al., 2012; Zhang et al., 2013; Lim et al., 2014).

The major application of GSI version 3.1 is a 3D-Var data assimilation system. For variational data assimilation method, it minimizes a penalty function with respect to the atmospheric state using background information, the observations and the physical and dynamical constraints (DTC, 2012). It is assumed that the background error distributions and the observation error distributions are Gaussian, with no bias and the background and observation errors are uncorrelated. The maximum likelihood atmospheric state can be obtained by the minimization of the cost function (Lorenc, 1986), which is:

$$J(x) = \frac{1}{2}(x - x_b)^T B^{-1}(x - x_b) + \frac{1}{2}(y - H(x))^T R^{-1}(y - H(x)) + J_c$$

Where

x: Analysis fields

x_b: Background fields (first guess), or the initial estimate given by the model state vector

B: Background error covariance matrix

H: Observation operator (or forward model), which transforms the grid point analysis to observation space

y: Observations

R: Observational error covariance matrices, which comprises of the covariance of instrumental observation errors and the covariance of representativeness error in the observations.

J_c: Constraint terms (i.e., dynamical and moisture constraint)

The background profile x_b is from the NWP model. The background error covariance matrix B is derived from the differences between the background field and observations (Derber and Bouttier, 1999). The cost function is the sum of the squared residuals of the analysis to the background and observations. Correlation between observational errors is neglected. The minimized cost function is found by an iterative process, and it gives the best analysis results.

3.1.3 Radiative transfer model

For satellite radiance assimilation, a forward radiative transfer model (RTM) is required to calculate the radiance from the background. The radiance calculated from the background is compared with the observations, and then the adjustment for the atmosphere is made by the difference between the calculated and observed radiances. In GSI, the Community Radiative Transfer Model (CRTM) has been implemented and used as the RTM. It is developed by the

Joint Center for Satellite Data Assimilation (JCSDA), and it includes the forward operator, tangent-linear, adjoint and K-matrix to transform the grid point analysis to observational space [Han et al., 2006; Weng 2007; Chen et al. 2010; Chen et al. 2012]. It has the capability to simulate the microwave and infrared radiances observed by instruments onboard variety satellites, such as AMSU-A onboard NOAA-15, NOAA-18, Metop-A; AMSU-A and AIRS onboard Aqua; ATMS and CrIS onboard Suomi NPP.

3.2 Hurricanes

Hurricanes Sandy (2012), Irene (2011) and Ike (2008) over the Atlantic Ocean are the selected case studies for the assimilation and forecast experiments. Hurricane Sandy was a very destructive hurricane during the 2012 Atlantic hurricane season (Figure 3.2). It was a late-season hurricane that developed on 1200 UTC 22 October in the southwestern Caribbean Sea, and then moved northward. By 25 October when Sandy made landfall in Cuba it was a Category 3 storm. After passing the Bahamas, Sandy turned toward the northeast around 1200 UTC 27 October and its speed increased again by 1200 UTC 27 October. On 28 October, Sandy passed southeast of North Carolina and turned to the northwest. By 2100 UTC 29 October, Sandy became an extratropical storm and the center of post-tropical Cyclone Sandy made landfall at about 2300UTC near Brigantine, New Jersey (Blake et al., 2013). Throughout its path across seven countries, Sandy caused widespread destruction with estimated damage over $68 billion (U.S. dollars), and the total fatalities were at least 286. The total losses of Hurricane Sandy put it second only to Hurricane Katrina (2005).

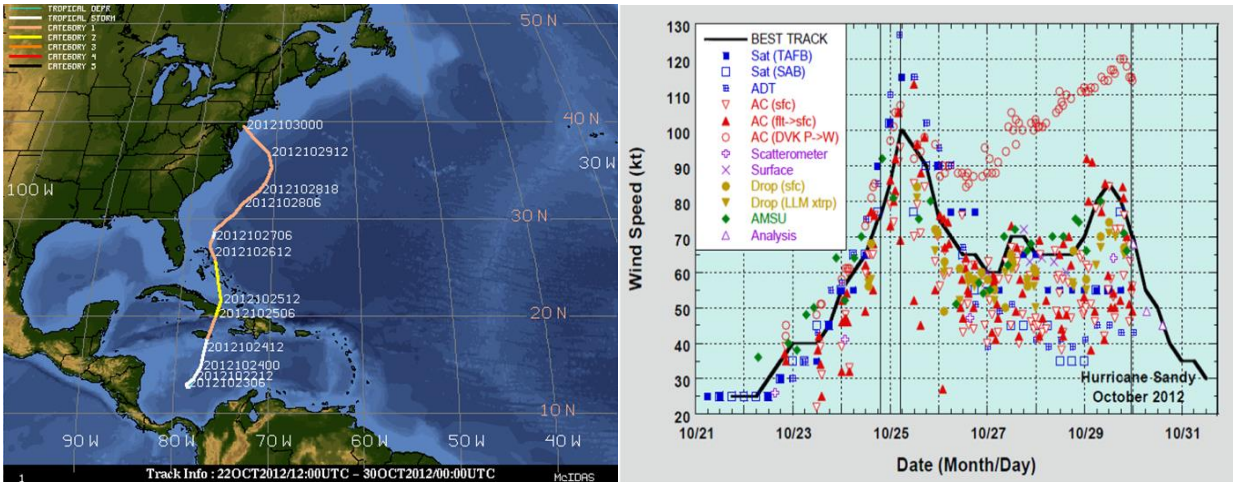

Figure 3.2 The best track (from CIMSS/SSEC) and the observed maximum wind speed (from NHC) of Hurricane Sandy (2012).

Hurricane Irene (2011) formed east of the Lesser Antilles on 0000 UTC 21 August 2011. By 1200 UTC 24 August, it had increased in strength to become a major hurricane (Category 3) and turned northward (Figure 3.3). It passed offshore the east coast of Florida and Georgia around1200 UTC 25 August. Irene made landfall near Cape Lookout, North Carolina at 1200 UTC 27 August. Irene continued to move north and northeastward and made landfall again near Atlantic City, New Jersey at 0935 UTC on 28 August 2011 (Avila and Cangialosi, 2011). Irene killed at least 56 people and caused an estimated $15.6 billion in total damage in the United States.

Hurricane Ike (2008) was a destructive tropical cyclone that became a hurricane by 1800 UTC 3 September 2008, and a Category 4 storm at 0600 UTC 4 September (Figure 3.4). It moved from North Atlantic Ocean westward and made landfall in Cuba around 0200 UTC 8 September. Ike continued moving westward across Cuba and then turned northwest to make final landfall in Texas on 0700 UTC 13 September (Berg, 2009). Ike was directly responsible for at

least 103 deaths throughout its path. The damages from Ike in U. S. are estimated at $29.5 billion with additional $7.3 billion in Cuba.

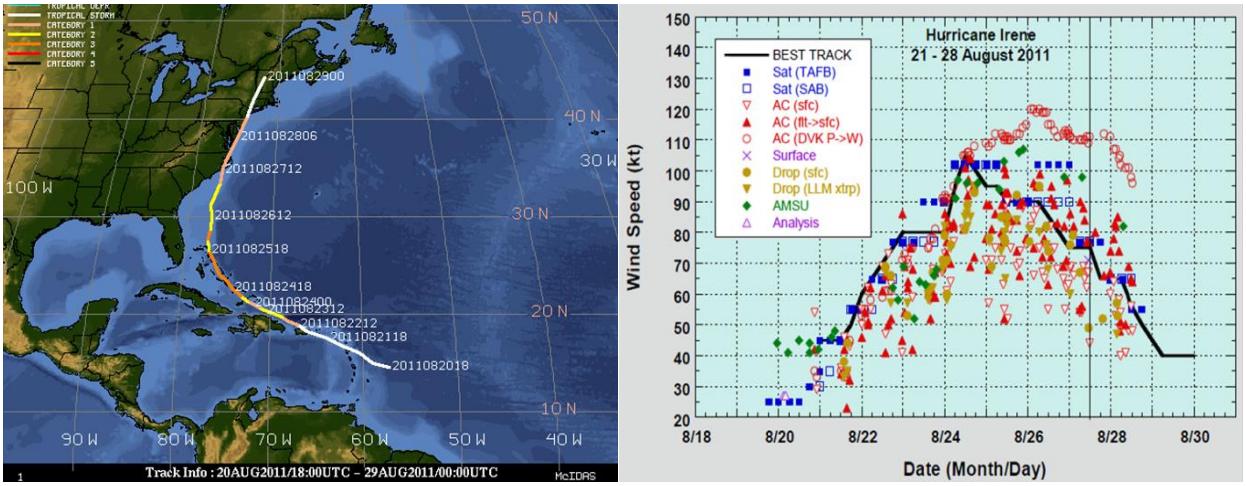

Figure 3.3 The best track (from CIMSS/SSEC) and the observed maximum wind speed (from NHC) of Hurricane Irene (2011).

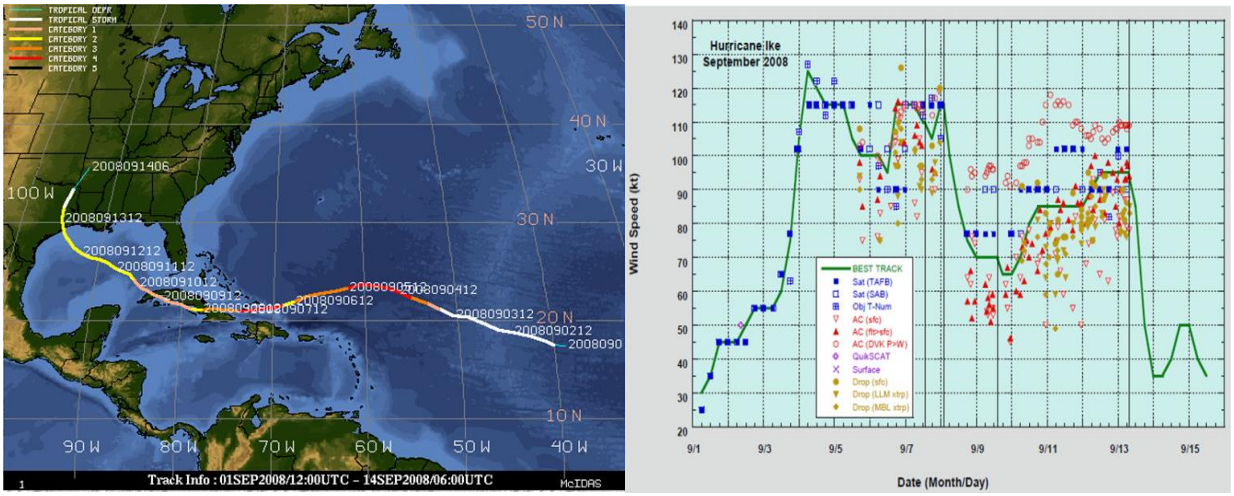

Figure 3.4 The best track (from CIMSS/SSEC) and the observed maximum wind speed (from NHC) of Hurricane Ike (2008).

3.3 Data set used for assimilation

3.3.1 NCEP FNL data

The NCEP FNL (Final) operational global analysis data are used as the background and the boundary conditions for the regional model. The FNL data are on 1-degree by 1-degree grids globally for every six hours. This product is from the Global Data Assimilation System (GDAS), and it made with the same model which NCEP uses in the Global Forecast System (GFS). But the FNLs are delated than the operational results, which allows more observational data can be assimilated in GDAS and get more accurate forecasts than GFS.

3.3.2 GTS data

Data from the World Meteorological Organization's (WMO) Global Telecommunication System (GTS) are used in this study. GTS includes all the conventional data both from the global upper air and surface weather observations. The data include the land surface, marine surface, radiosonde, pibal and aircraft reports. These reports include the pressure, the geopotential height, temperature, moisture and wind. The report time intervals are from hourly to 12 hourly. The data available time is every 6 hourly. In the data set, the observational error and the quality control for each data type and each observation are encoded together with the observations. The GTS data are used as one of the data set of the control experiment in this study.

3.3.3 AMSU-A data

The Advanced Microwave Sounding Unit-A (AMSU-A) sensor is a multi-channel temperature and moisture sounder with 15 channels at microwave frequencies ranging from 23.8

GHz to 89.0 GHz. It scans across the satellite track at 30 viewing angles covering ±48.95 degrees, with a nominal FOV of 1.1° and 3.3 ° (16 km and 49 km at nadir) (Diak et al., 1992; Weng et al., 2003). The priority of the AMSU-A is to provide the atmospheric information in the presence of the clouds. The AMSU-A observations are also used as one of the data set of the control experiment. The AMSU-A onboard NOAA-15, NOAA-18, Metop-A, Aqua and NOAA-19 are used with a thinning box of 60 km in this study. The used channels are followed the same channel set of GDAS, which are listed in table 3.1.

Table 3.1 The used channels of AMSU-A data onboard NOAA-15, NOAA-18, Metop-A, Aqua and NOAA-19.

Channel	**NOAA-15**	**NOAA-18**	**Metop-A**	**Aqua**	**NOAA-19**
1	Use	Use	Use		Use
2	Use	Use	Use		Use
3	Use	Use	Use		Use
4	Use	Use	Use		Use
5	Use	Use	Use		Use
6	Use	Use	Use		Use
7	Use	Use			Use
8	Use	Use	Use	Use	
9	Use		Use	Use	Use
10	Use	Use	Use	Use	Use
11		Use	Use	Use	Use
12	Use	Use	Use	Use	Use
13	Use	Use	Use	Use	Use
14		Use			
15	Use	Use	Use		Use

3.3.4 ATMS data

The Advanced Technology Microwave Sounder (ATMS) onboard Suomi National Polar-Orbiting Operational Environmental Satellite System Preparatory Project satellite (S-NPP) and the Joint Polar Satellite System (JPSS) is a cross-track scanner with 22 channels in bands from 23.8 GHz through 183.3 GHz, combing all the channels of the preceding AMSU-A and AMSU-B sensors. It was designed to have three antenna beam-widths, 1.1°, 2.2°, and 5.2°, providing spatial resolution of 16 km, 32 km, and 75 km at nadir, respectively (Muth et al., 2005). The assimilated ATMS channels in this study are listed in table 3.2, which is also following the channel set by GDAS.

Table 3.2 The used channels of ATMS onboard S-NPP/JPSS

Channel	**ATMS**	**Channel**	**ATMS**	**Channel**	**ATMS**
1	Use	9	Use	17	Use
2	Use	10	Use	18	Use
3	Use	11	Use	19	Use
4	Use	12	Use	20	Use
5	Use	13	Use	21	Use
6	Use	14	Use	22	Use
7	Use	15			
8	Use	16	Use		

3.3.5 MODIS data

MODIS on the Earth Observing System (EOS) Terra and Aqua satellites has 36 broadband spectral bands covering from 0.4 μm to 14.4 μm. MODIS is the instrument aimed for the biological and physical measurements of the earth and atmosphere systems. Some of the selected MODIS channels have been used to study the atmosphere properties, such as atmospheric temperature and moisture profiles, aerosol properties, and the cloud properties (Barnes et al., 1998). The daily global cloud products from MODIS with a high spatial resolution of 1 km are retrieved by combining the observed infrared and visible radiances (King et al., 2003; Platnick et al. 2003; Ackerman et al., 1998). The MODIS 1-km cloud products include, but are not limited to, the cloud mask (confident clear, probably clear, confident cloudy and probably cloudy) (Ackerman et al., 1998), the cloud-phase mask (water clouds, ice clouds and mixed phase) (Strabala et al., 1994; Baum et al., 2000), the cloud classification mask (CCM) (Li et al., 2003; Li et al., 2007), the cloud particle size (CPS), and the cloud optical thickness (COT) (King et al., 2003; Platnick et al., 2003). The high resolution cloud mask from MODIS is applied in this study, to provide reliable cloud detection for AIRS FOVs. Besides, the MODIS radiance is also used to get the cloud-cleared for AIRS FOVs. The detailed will be discussed in the following parts.

3.3.6 AIRS data

AIRS is a high spectral resolution sounder with 2378 channels covering the visible, near-infrared and infrared spectrum from 0.40 μm to 15.4 μm (Aumann et al., 2003). The infrared spectrum is from 3.74 μm to 15.4 μm, and the aim for AIRS infrared is the get an accurate atmospheric temperature and moisture profiles from the surface to the higher atmosphere. The

spatial footprint of the instrument is 13.5 km at nadir (with a nominal FOV of 1.1°) and a ±49.5° scan width. Two strong CO_2 absorption bands (centered at 15.5 μm and 4.3 μm) and a strong water vapor absorption band (centered at 6.3 μm) are occurred in AIRS spectral. Some other absorption bands, such as CH_4, O_3 and CO are also occurred within the AIRS spectral.

3.3.7 VIIRS data

The Visible Infrared Imaging Radiometer Suite (VIIRS) is one of the major instruments onboard S-NPP and JPSS. VIIRS has 22 spectrum from 0.412 μm to 12.01 μm with 16 moderate resolution channels (750 m at nadir) and 6 imaging resolution channels (375 m at nadir) (Lee et al., 2006). The VIIRS observations are designed mainly to measure the clouds and Earth surface variables. It provides high spatial resolution cloud products containing CM (Hutchison et al., 2005), CP (Pavolonis and Heidinger, 2004; Godin, 2014), cloud top parameters (Baker, 2012), COT, and effective radius (Godin, 2014). The high resolution cloud product is collocated with the CrIS FOVs and help the Cross-track Infrared Sounder (CrIS) better identify cloud.

3.3.8 CrIS data

CrIS onboard the Suomi-NPP and JPSS with 1305 channels from 3.92 μm to 15.38 μm. It was launched on 28 October 2011. The spatial footprint of the instrument is 14 km at nadir and 1km vertical layer, and the scanned swath is 2200 km. CrIS provides unprecedented information about atmospheric temperature and moisture profiles with high vertical resolution and good accuracy. CrIS could also measure the atmospheric chemistry and detect the concentration of the greenhouse gases in the atmosphere (Han et al., 2013). The CrIS is one of the operational

satellite measurements to verify the operational application of the cloud detection with collocated high spatial resolution cloud mask in this study.

3.4 Experimental design

In this study, three experiments have been carried out to demonstrate the impact of the AIRS radiances assimilation (Table 3.3). The GTS and AMSUA are assimilated in all the experiments, and the AIRS radiances data are different in the experiments.

- GTS+AMSUA+AIRS (GSI clr) or AIRS (GSI clr) for simplicity;
- GTS+AMSUA+AIRS (MOD clr) or AIRS (MOD clr);
- GTS+AMSUA+AIRS (MOD cld-clr) or AIRS (MOD cld-clr).

All three experiments assimilate the GTS, AMSU-A radiances and AIRS radiances. The differences are the AIRS radiances: GSI clr uses the GSI stand-alone cloud detection for AIRS clear radiances; MOD clr uses collocated MODIS cloud mask for AIRS clear radiances; and MOD cld-clr uses MDOSI cloud mask for AIRS clear radiances and AIRS/MODIS cloud-clearing for additional AIRS radiances. To avoid the complexity of land surface (i.e. emissivity), only AIRS cloud-lceared radiances over ocean are used in the assimilation experiments. The comparison between AIRS (GSI clr) assimilation and AIRS (MOD clr) assimilation is discussed in Chapter 4. And the impacts from additional cloud-cleared AIRS radiances on hurricane forecasts are discussed in the Chapter 5.

Because AIRS/MODIS are the satellites for research study, to apply the methodologies and the schemes on the operational satellite instruments, CrIS and VIIRS satellite observations are

discussed in this study. The high spatial resolution cloud products from VIIRS are collocated with CrIS FOVs to help CrIS better identify clouds. The comparison between CrIS stand-alone cloud detection and the CrIS/VIIRS cloud detection are carried out (Table 3.4). The experiments, the assimilation cycling, the forecast time periods, and the hurricane cases are following the AIRS/MODIS cloud detection.

Table 3.3 Data used in the experiments for AIRS/MODIS clear detection (Italics indicate the AIRS radiance data with different methods, AIRS (GSI clr) uses the AIRS-alone cloud detection, AIRS (MOD clr) is AIRS/MODIS cloud detection, and AIRS (MOD cld-clr) is the AIRS/MODIS cloud-clearing method.)

Experiment	**GTS**	**AMSUA**	**AIRS (GSI clr)**	**AIRS (MOD clr)**	**AIRS (MOD cld-clr)**
GTS+AMSUA+AIRS (GSI clr)	**Yes**	**Yes**	***Yes***		
GTS+AMSUA+AIRS (MOD clr)	**Yes**	**Yes**		***Yes***	
GTS+AMSUA+AIRS (MOD cld-clr)	**Yes**	**Yes**			***Yes***

It is assumed that the observations are independent and the observational errors are uncorrelated. Thinning is applied to the satellite radiances assimilation. The thinning mesh is 60 km for AMSU-A, and 120 km for AIRS. The background error covariance matrix and observation error table used in GSI follows the NCEP operational system, i.e. North American Mesoscale Forecast System (NAM) (McCarty et al., 2009). The bias correction has two parts in GSI system: air mass bias and satellite scan dependent bias. In this study, the initial bias coefficients are from the NCEP GFS. The air mass bias correction coefficient is updated based

on the previous results for each cycling run. Therefore, the bias correction coefficients of the three experiments are different.

Table 3.4 Data used in the experiments for CrIS/VIIRS clear detection.

Experiment	GTS	AMSUA	CrIS (GSI clr)	CrIS (VIIRS clr)
GTS+AMSUA+CrIS (GSI clr)	**Yes**	**Yes**	***Yes***	
GTS+AMSUA+CrIS (VIIRS clr)	**Yes**	**Yes**		***Yes***

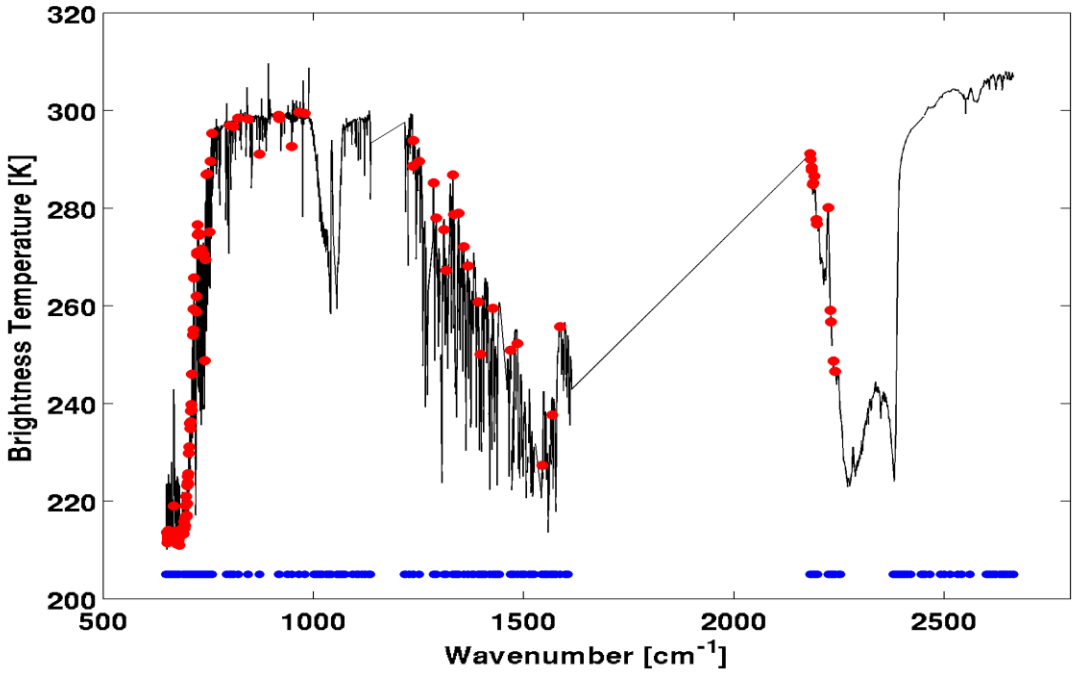

Figure 3.5. An example of AIRS spectrum (black) and the corresponding 281 channels (blue dots) selected for the NWP center. The red dots are the selected 120 channels from 281 channels that were assimilated in this study.

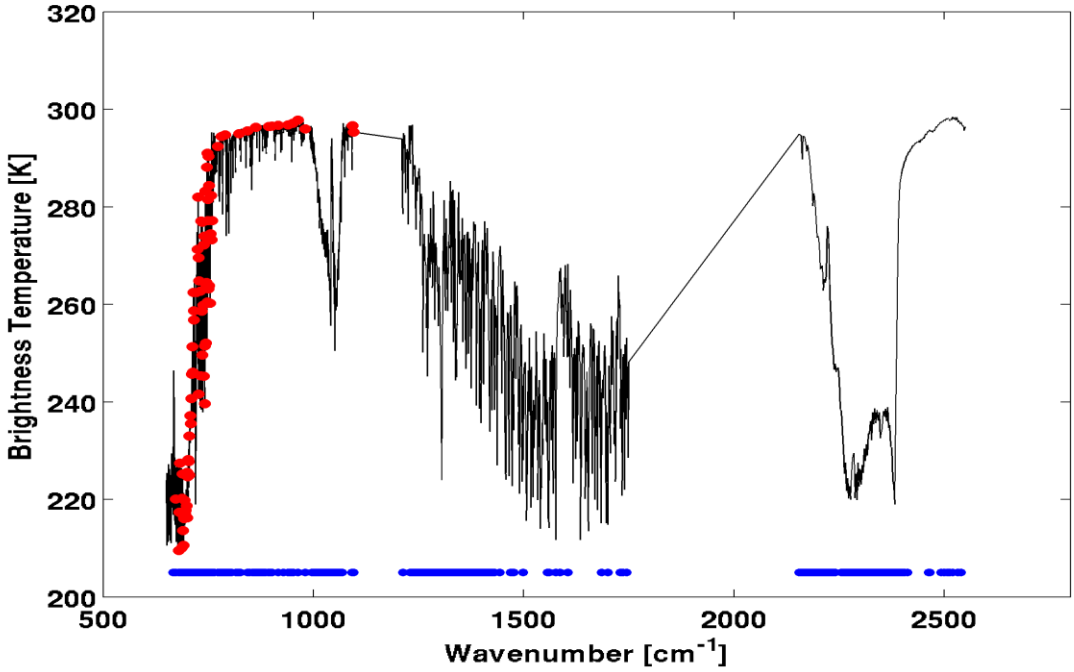

Figure 3.6. An example of CrIS spectrum (black) and the corresponding 399 channels (blue dots) selected for the NWP center. The red dots are the selected 84 channels from 399 channels that were assimilated in this study.

Based on Goldberg et al. (2003), 281 channels of 2378 AIRS channels are selected for NWP centers by NOAA NESDIS. But not all of the 281 channels of AIRS are used in the GSI system. Due to the local thermal equilibrium effects, large innovation differences and dominated penalty function, 152 channels are selected from the 281 channels based on the NCEP operational center (Jung, 2008). Spectral channels located in the shortwave spectrum and those with significant ozone absorption are rejected in the regional assimilation. Combining the NCEP operational and the regional model channel selections, there are 120 channels assimilated in the GSI in this study (Figure 3.5). The surface channel assimilation follows the same schemes as

demonstrated by Lim et al. (2014). All the experiments used the same set of AIRS channels in this study.

The total number of CrIS infrared sounding channels is 1305 spread over 3 bands covering the longwave (655-1095 cm^{-1}), midwave (1210-1750 cm^{-1}) and shortwave (2155-2550 cm^{-1}) (Gambacorta and barnet, 2011). 399 CrIS channels are selected based on the NOAA/NESDIS physically-based methodology for the near real time studies. These channels include 24 surface temperature and emissivity sounding channels, 87 temperature sounding channels, 62 water vapor, 53 O_3, 27 CO, 54 CH_4, 53 CO_2, 24 N_2O, 28 HNO_3 and 24 SO_2 sounding channels. 84 channels are assimilated in GDAS operational system and GSI (Figure 3.6). The channels assimilated from CrIS are temperature sounding channels.

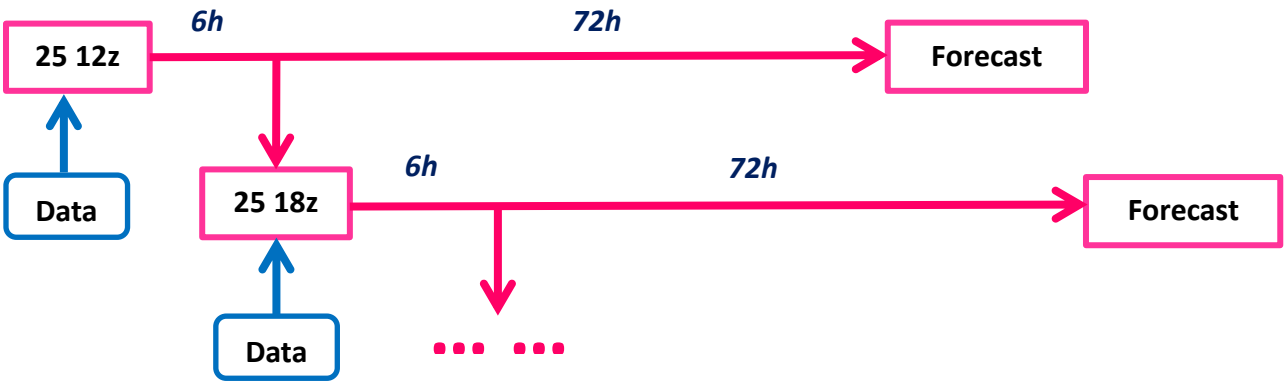

Figure 3.7. Assimilation cycle valid for the three experiments. The initial condition at 25 0600 UTC is interpolated from the global analysis. After the data assimilation (blue box), a 72-hour forecast is carried out, and at the same time, the 6-hour short term forecast is used as the first guess for the next assimilation cycle.

To verify the data impact, three hurricanes are selected to simulate as the case studies. For the Hurricane Sandy experiments, the assimilation time is from 1800 UTC 25 October to 0000

UTC 27 October at every 6-hour cycle with a +/- 1.5 hour assimilation window. A 72-hour forecast, from 1800 UTC 28 October to 0000 UTC 30 October 2012 followed (Figure 3.7). The experiments for Hurricane Irene and Ike are similar to those for Hurricane Sandy. The assimilation time for Irene is from 1200 UTC 22 August to 0000 UTC 24 August. The forecast time was run from 1200 UTC 25 August to 0000 UTC 27 August 2011. The assimilation time for Hurricane Ike is from 1800 UTC 5 September to 0000 UTC 7 September, and the forecast time is from 1800 UTC 5 September to 0000 UTC 10 September 2008.

Because the regional models are limited area models (LAM), the lateral boundary conditions (LBC) are required to be updated at various time steps with the model integrating forward in time. The LBC is updated from the global model, which helps to slow down the propagation of the lateral boundary errors into the domain under study over time (Warner et al., 1997). In this study, the LBC is updated every 6 hour from the NCEP FNL data, and the new LBC with the analysis fields together to do the forecast through WRF-ARW model.

Chapter 4

Eliminating cloudy contamination – clear location detection

To date, in many operational centers, the clouds contribution from the satellite sounders are neglected, so the core parts in the model, or more broadly the data assimilation system (DAS) (i.e. the control vectors, the radiative transfer model, the background error covariance, the observation error covariance and the linearized physical parameters) are designed for the clear radiances assimilation. If the cloudy radiances are assimilated as clear radiances, there will be a negative impact on the quality of NWP analysis (Pangaud et al., 2009). Therefore, reliable cloud detection is one important step before the satellite data assimilation. Improved cloud detection could reduce the incorrect detection of clear fields of view (FOVs) and improve the assimilation of IR radiances.

The major method for cloud detection in most systems is to calculate the first-guess departures (i.e. by comparing the observed brightness temperature and the simulated brightness temperature calculated through forward model from the background). If the first-guess departures are larger than the threshold, then the observations are rejected as cloudy. So, this approach requires very accurate atmospheric temperature analysis, as well as the accurate

simulated clouds from the first-guess. The model can capture the large scale clouds, and due to the large first-guess departures, the deep convective clouds are detected and removed. However, for the thin clouds or under partially cloudy regions, the difference of radiances between the clouds and the clear skies is small. For the low clouds where the temperature contrast from the surface is small, the first-guess departures are potential within the threshold value. In these regions, if the first-guess departure is smaller than the threshold, the observed cloudy radiances are assimilated as clear sky in the NWP model, which introduces cloud contamination and degrades the analysis fields. In addition, in the case of clear observations from satellite while NWP has clouds, the clear observations will be discarded in the assimilation based on the first-guess departure.

4.1 Methodology for clear location detection

MODIS on the Earth Observing System Terra and Aqua satellites provides multispectral broadband radiance measurements and cloud products at a spatial resolution of 1 km. With a collocation methodology developed by Nagle (1998), AIRS sub-pixel cloud detection and characterization can be derived by taking advantage of high spatial resolution MODIS cloud products. For example, the MODIS cloud mask can be used for AIRS sub-pixel cloud detection, and the 1 km MODIS cloud phase and cloud type mask can be used for AIRS sub-pixel cloud characterization, both of which are useful for quality control in assimilating cloudy radiances. In recent experiments with WRF/GSI, it is found that some clear pixels are identified as cloudy while cloudy pixels are identified as clear in the GSI system. While the data assimilation suffers from these misclassifications (Hu and Xue, 2006), a better cloud detection could reduce the

cloudy data mismatch and improve the assimilation. The impact of cloud detection on AIRS radiance assimilation has been investigated, and the collocated high spatial resolution (1 km) MODIS cloud mask product is used for AIRS sub-pixel cloud detection.

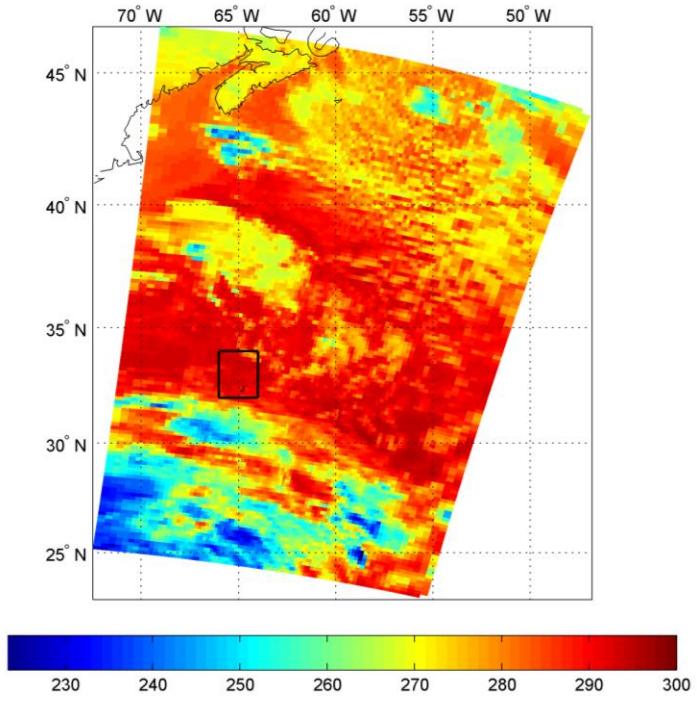

Figure 4.1 The brightness temperature (unit: K) for one AIRS granule indicated in Figure 4.4 at 0600 UTC on 25 October 2012.

To better understand the advantage of AIRS sub-pixel cloud detection with the MODIS cloud mask, one granule of AIRS brightness temperature (BT) is shown in Figure 4.1 and the collocated MODIS high resolution cloud mask is shown in Figure 4.2. Figure 4.2 reveals the collocated MODIS cloud mask for a small area outlined in Figure 4.1. The AIRS sub-pixel clear mask can be easily derived based on the MODIS cloud mask; there are four possible categories for each MODIS pixel: confident clear, probably clear, uncertain and cloudy. Only the AIRS

sub-pixels filled with the MODIS confident clear mask are considered clear footprints for assimilation and forecast experiments. Otherwise, the AIRS sub-pixels are removed due to the cloud contamination.

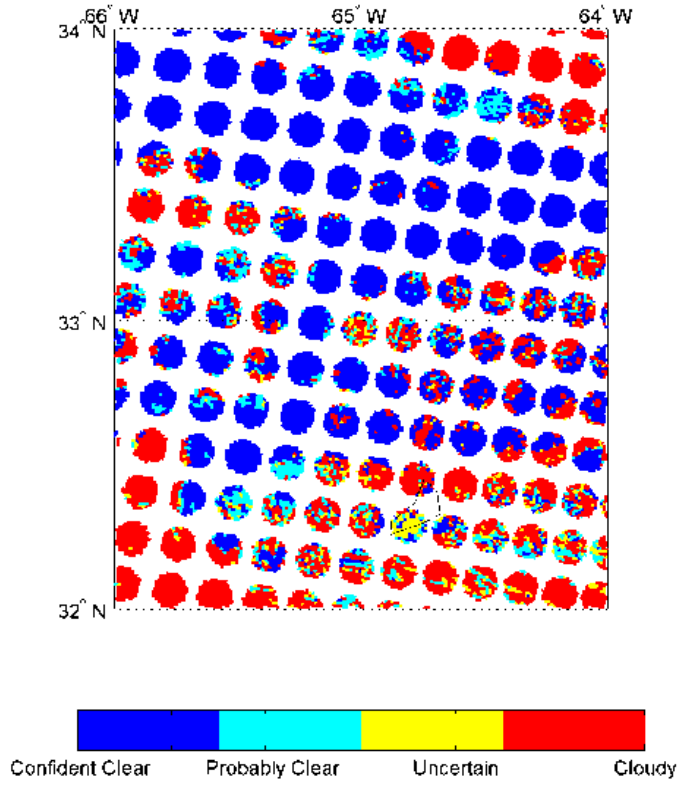

Figure 4.2 The collocated MODIS cloud mask for the small box area outlined by the rectangle in Figure 4.1.

4.2 AIRS/MODIS for clear location detection

4.2.1 Impact on analysis

To compare the data coverage of AIRS radiance data assimilated using two different cloud detection methods, AIRS channel 210 (709.5659 cm^{-1}) and channel 1477 (1345.31 cm^{-1}) are selected as temperature sensitive channel and moisture sensitive channel respectively. The weighting function peaking of AIRS channel 210 is at around 450 hPa (Figure 4.3). The left panel of Figure 4.4 shows the AIRS data coverage using the GSI stand-alone cloud detection method (AIRS (GSI clr) as short), while the right panel shows the AIRS data coverage using collocated MODIS cloud detection method (AIRS (MOD clr)). Similarly, the data coverage of AIRS channel 1477 (1345.31 cm^{-1}) with the weighting function peaking around 700 hPa (Figure 4.5) is shown in Figure 4.6. For both channel 210 and channel 1477, there are some mismatched observations in the West Atlantic and north of South America between AIRS (MOD clr) and AIRS (GSI clr); the AIRS (MOD clr) sees much less clear footprints than the AIRS (GSI clr). As mentioned, only channels detected as cloud-free are assimilated by GSI, therefore, the reduced amount of data is due to more accurate cloud detection with the MODIS high spatial resolution cloud mask product. The mismatched areas are the cloudy regions according to the MODIS cloud mask. The GSI cloud detection failed to reject them and assimilated them as clear sky radiances, which could potentially degrade the analysis field due to the cloud contamination. After MODIS cloud detection, although we have less AIRS pixels left to assimilate, we have high quality of the data and more confidence of the data. The cloud contamination from AIRS pixels is removed by the collocated MODIS cloud mask, which improves the analysis fields.

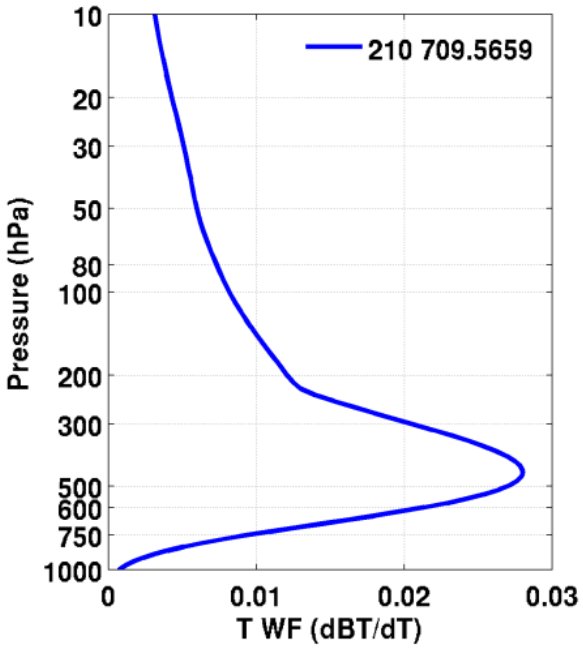

Figure 4.3 The weighting function of AIRS channel 210 (709.5659 cm^{-1}).

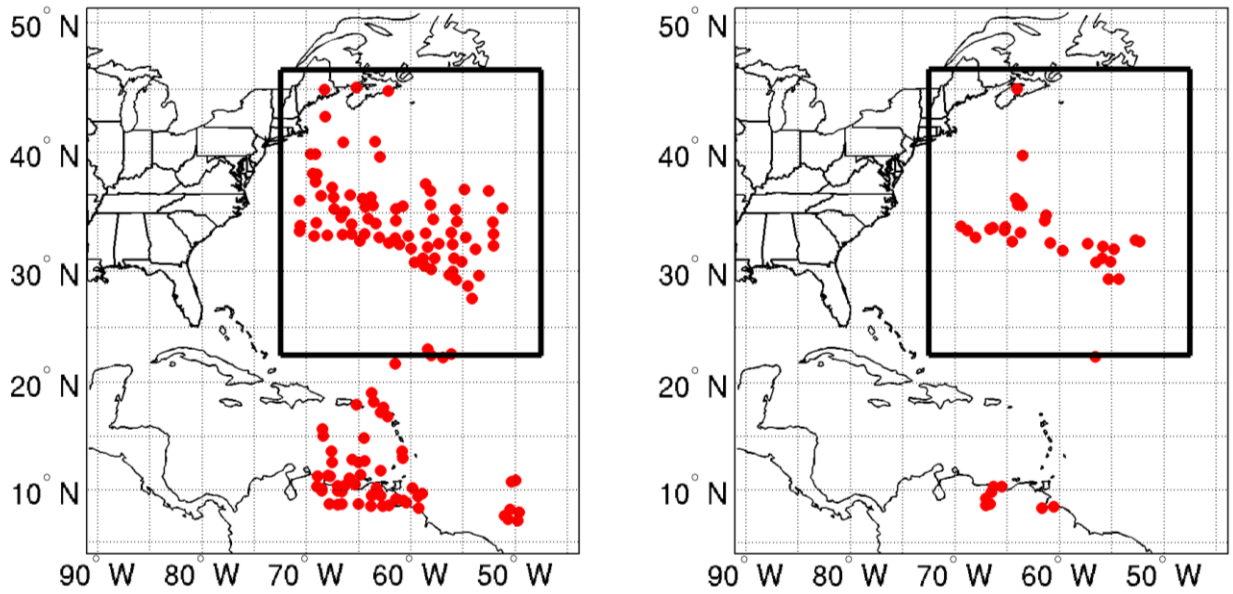

Figure 4.4 AIRS stand-alone cloud detection (GSI) (left) and AIRS cloud detection with MODIS (right) for AIRS channel 210.

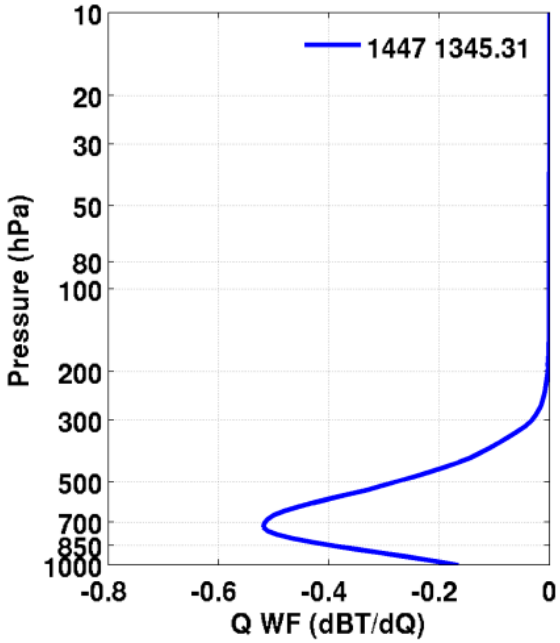

Figure 4.5 The weighting function of AIRS channel 1447 (1345.31 cm^{-1}).

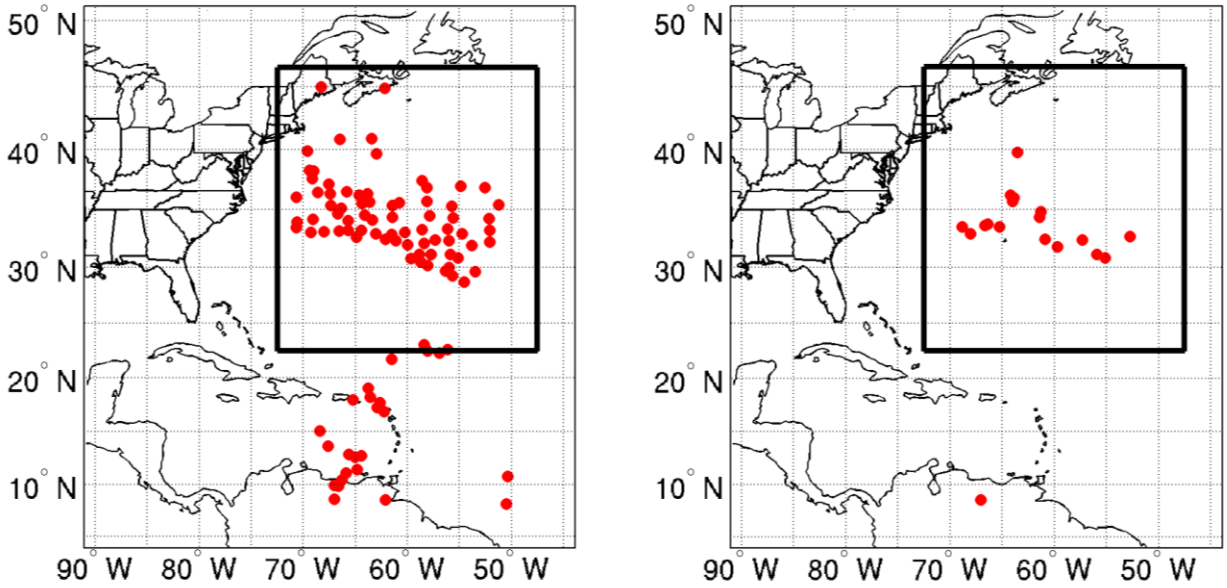

Figure 4.6 AIRS alone cloud detection (GSI) (left) and AIRS cloud detection with MODIS (right) for AIRS channel 1447.

To see the impact of different cloud detection methods on the assimilation, the difference between the temperature and relative humidity of the analysis field between AIRS (MOD clr) and AIRS (GSI clr) at 06 UTC on 25 October 2012 is shown in Figure 4.7 and 4.8. In general, unsuccessful cloud detection results in more cloud contamination in the radiance assimilation. Consequently, the analysis could either be colder or wetter than it should be, or some combination. In this case, for the 500 hPa in Figure 4.7, the analysis change is dominated by temperature; the AIRS (MOD clr) analysis is warmer than AIRS (GSI clr) due to less cloud contamination. The impact of moisture field is subtle at 500 hPa. For 700 hPa in Figure 4.8 the analysis change is visible in both temperature and moisture fields. The temperature of AIRS (MOD clr) is about 1 K warmer than AIRS (GSI clr) in the northwest of Atlantic Ocean and 0.6 K warmer in the east of Hurricane Sandy. The relative humidity (RH) of AIRS (MOD clr) is nearly 30% drier in the northwest of Atlantic Ocean, and around 10% drier in the east of Hurricane Sandy. The different behaviors in 500 (Figure 4.7) and 700 hPa (Figure 4.8) are determined by the assimilation method, which is closely related to the background covariance matrix (Derber and Bouttier, 1999). No attempt is made to validate as to whether the analysis change in Figure 4.7 and 4.8 are reasonable or not. Instead, WRF-ARW is used to conduct forecasts for Hurricane Sandy. We speculate that better analyses will yield better hurricane forecasts.

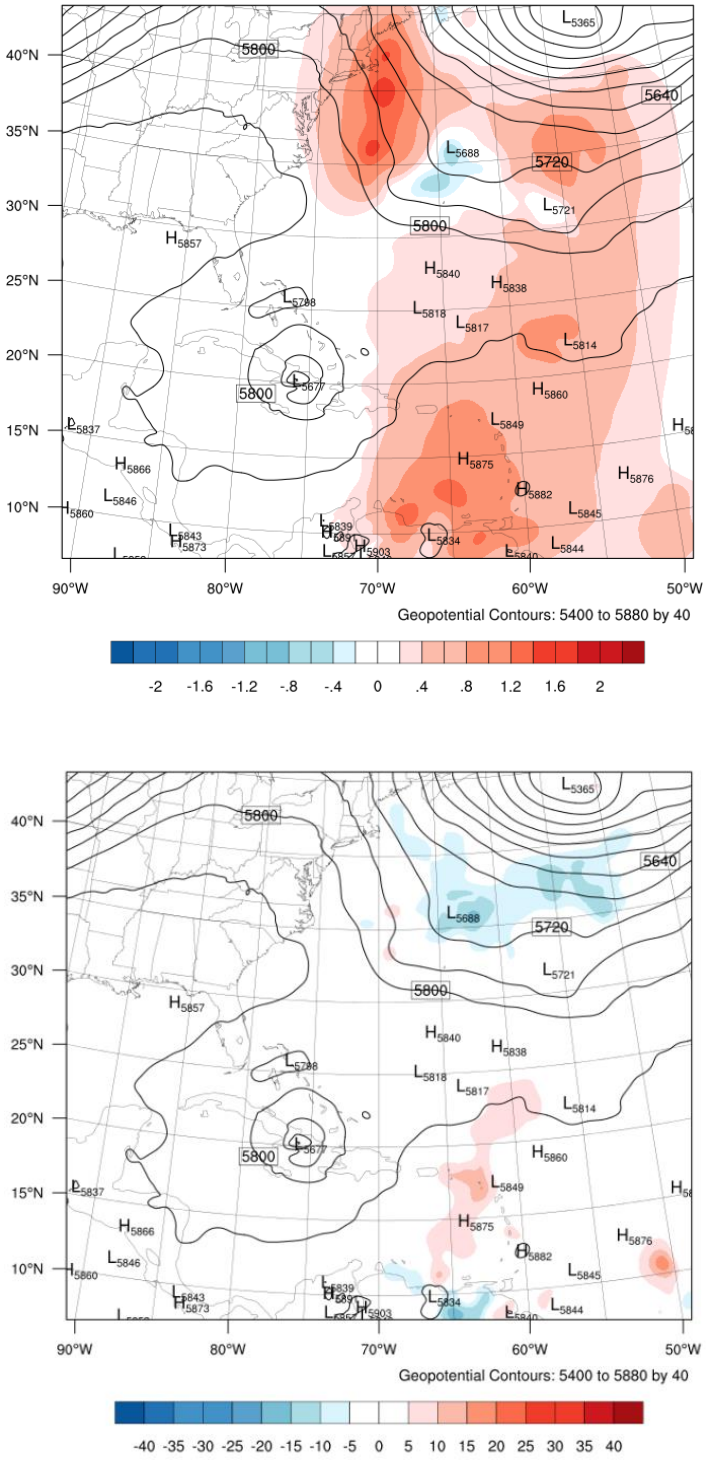

Figure 4.7 The difference in temperature (upper, unit: K) and relative humidity (lower, unit: %) analysis between the two experiments (AIRS (MOD clr) – AIRS (GSI clr)) with the geopotential height (solid, unit: m) of AIRS (MOD clr) at 500hPa at 0600 UTC on 25 October 2012.

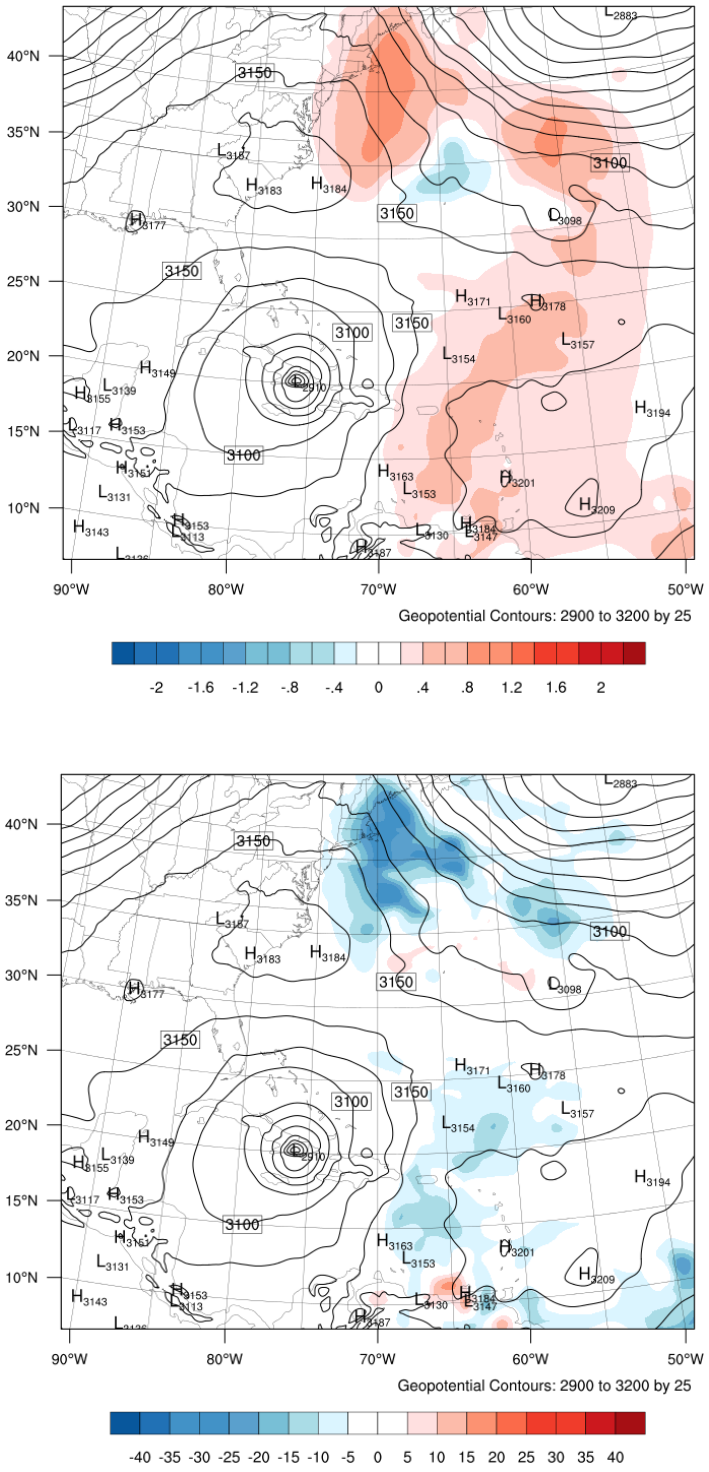

Figure 4.8 The difference in temperature (upper, unit: K) and relative humidity (lower, unit: %) analysis between the two experiments (AIRS (MOD clr) – AIRS (GSI clr)). The geopotential height (solid, unit: m) of AIRS (MOD clr) at 700hPa at 0600 UTC on 25 October 2012.

4.2.2 Impact on clear detection forecasts

Hurricane forecast are validated against the actual storm track and its intensity with time (the best track and observations data were obtained from NOAA's NHC). The 72-hour hurricane track of AIRS (GSI clr), AIRS (MOD clr) are compared with the best track. The hurricane track is located using the minimum sea level pressure. The movement of the hurricane reflects the both the atmospheric environmental fields and the hurricane structures (discussing in details in Chapter 6).

At 1800 UTC 25 October (Figure 4.9 (a)), the forecast hurricane track of AIRS (GSI clr) and AIRS (MOD clr) is very similar. The impacts of the different AIRS data sets are not very obvious on the hurricane track. At 0000 UTC 26 (Figure 4.9 (b)), from 68-hour to 72-hour, the AIRS (GSI clr) is moving faster than the best track, but AIRS (MOD clr) collocated with cloud mask could slow the hurricane movement and make it close to the best track. At 0600 UTC 26 (Figure 4.9 (c)), 1200 UTC 26 (Figure 4.9 (d)) and 1800 UTC 26 (Figure 4.9 (e)), the 72-hour forecasts of AIRS (MOD clr) is always better than AIRS (GSI clr). The location and pattern of the hurricane track forecasts of AIRS (MOD clr) are closer to the best track. Only at 000 UTC 27 (Figure 4.9 (f)), the AIRS (MOD clr) is closer to the best track at the first 48-hour, but AIRS (GSI clr) is closer to the best track from 48-hour to 72-hour. Since at the last time step, the effects from the land or terrain is becoming important, which would affect the hurricane forecasts.

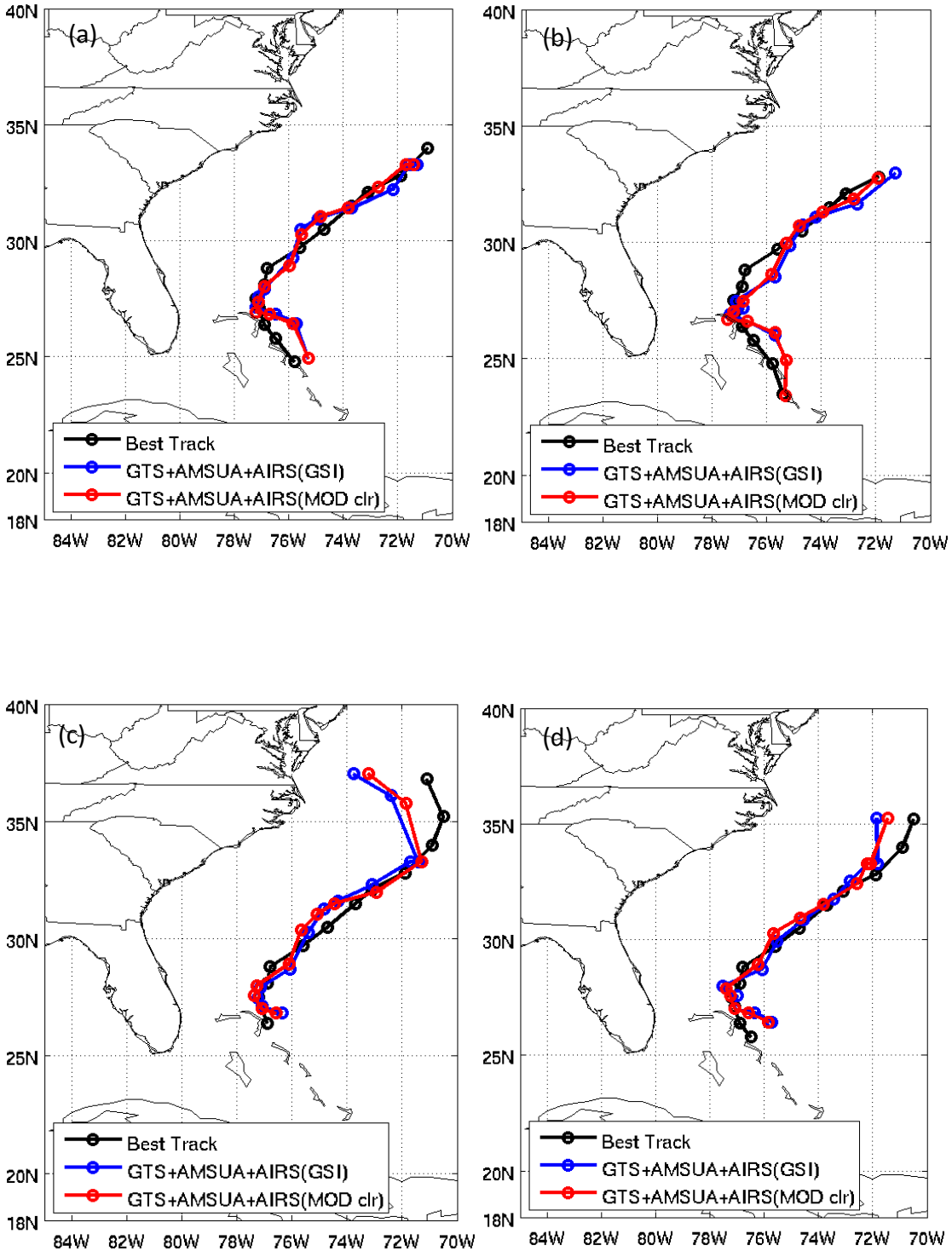
(a)
(b)
(c)
(d)
40N
35N
30N
25N
20N
18N
84W
82W
80W
78W
76W
74W
72W
70W
Best Track
GTS+AMSUA+AIRS(GSI)
GTS+AMSUA+AIRS(MOD clr)

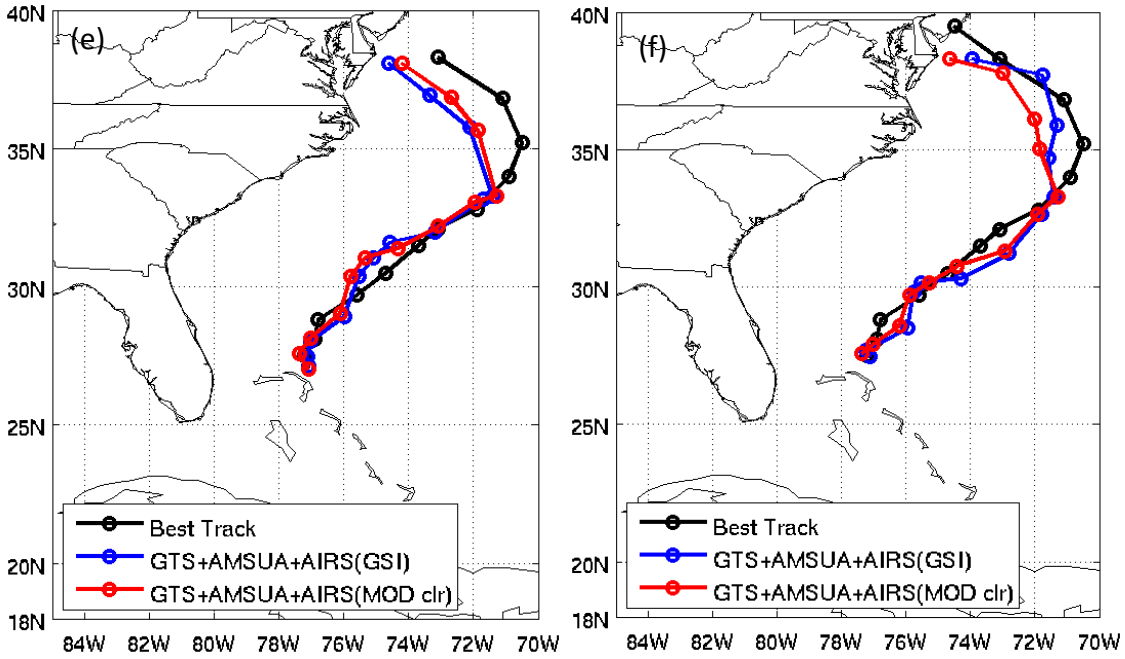

Figure 4.9 The 72-hour forecast hurricane track of best track (black), GTS+4AMSUA+AIRS (GSI) (blue) and GTS+4AMSUA+AIRS (MOD clr) (red) at 1800 UTC 25 (a), 0000 UTC 26 (b), 0600 UTC 26 (c), 1200 UTC 26 (d), 1800 UTC 26 (e) and 0000 UTC 27 (e) October 2012.

Hurricane track and intensity (characterized by either the minimum sea level pressure (MSLP), or maximum wind speed (MSW)) are two important parameters for hurricane forecasts (Merrill, 1988). Figure 4.10 shows the root mean square error (RMSE) of the hurricane track (upper) and the maximum wind speed (lower) of the 72-hour forecasts for Hurricane Sandy. The RMSE of GTS+AMSUA+AIRS (GSI clr) (blue) uses the AIRS stand-alone cloud detection, and the GTS+AMSUA+AIRS (MOD clr) (red) uses the AIRS/MODIS cloud detection method. For the hurricane track, the RMSE is smaller with the AIRS (MOD clr) cloud detection, especially after 18 hours. The average improvement of the hurricane track RMSE from the AIRS (GSI clr) cloud detection to the AIRS (MOD clr) cloud detection is obvious. For the maximum wind speed, the forecasts with AIRS (MOD clr) cloud detection are comparable to the forecast with

AIRS (GSI clr) cloud detection, with only a slight advantage. So for the intensity forecast, the impact of the AIRS (MOD clr) cloud detection is neutral.

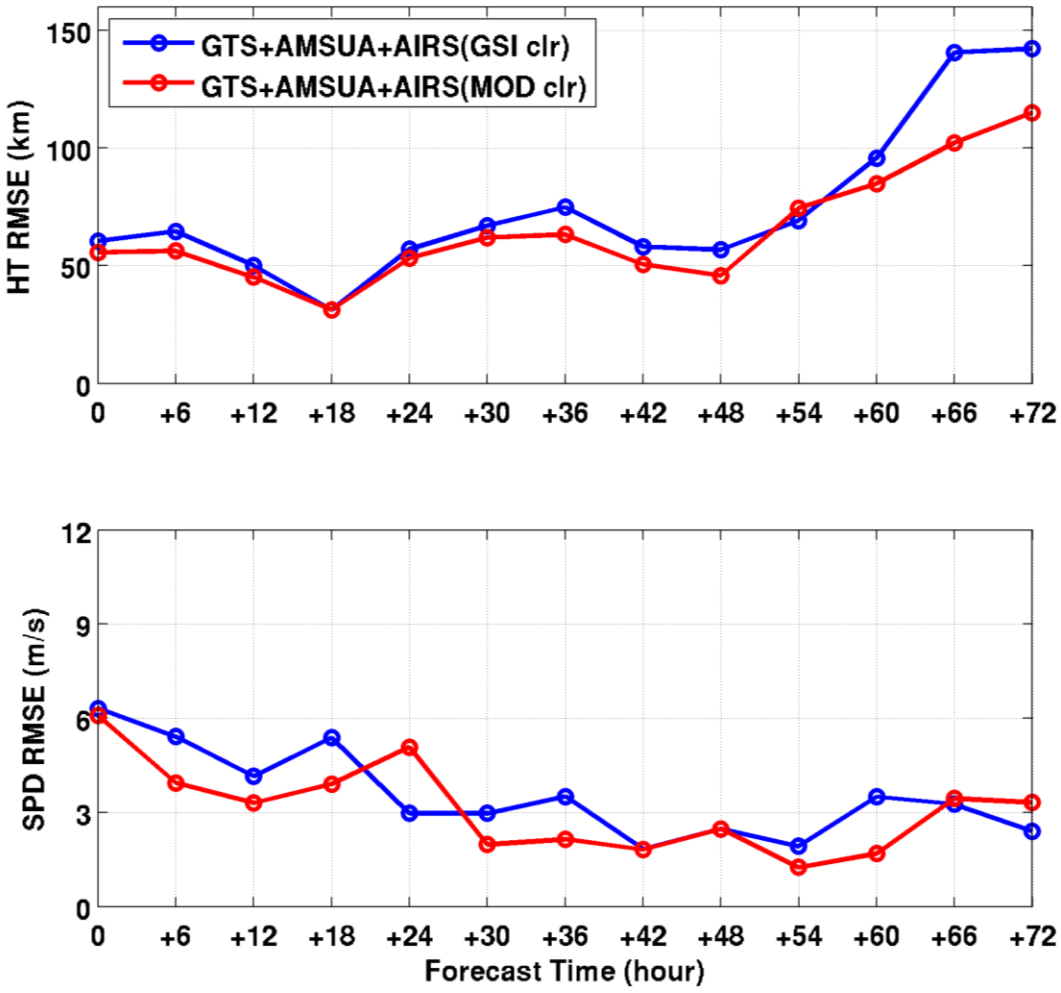

Figure 4.10 The track (top) and the maximum wind speed (bottom) forecast RMSE with AIRS (GSI clr) (blue) and AIRS (MOD clr) (red). Data are assimilated every 6-hour from 1800 UTC on 25 October to 0000 UTC on 27 October 2012, followed by 72-hour forecasts for Hurricane Sandy (2012).

4.3 CrIS/VIIRS for clear location detection

CrIS and VIIRS are onboard the Suomi-NPP/JPSS, and VIIRS could provide high spatial resolution cloud mask and other cloud properties. Similar to AIRS and MODIS, the methodology of collocated high resolution of cloud mask to help IR FOV cloud detection can also be applied on the cloud detection of CrIS radiances. The cloud properties and the cloud mask from VIIRS can be collocated to the corresponding CrIS FOVs; the clear FOVs of CrIS are selected and assimilated in the data assimilation system, and the cloud contaminated CrIS FOVs are removed before data assimilation.

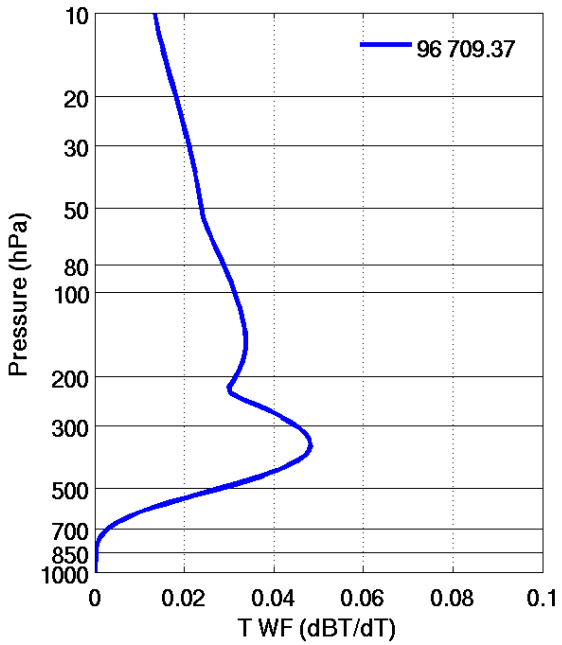

Figure 4.11 The weighting function of CrIS channel 96 (709.37 cm^{-1}).

To compare the two cloud detection methods on CrIS radiances assimilation, the GSI cloud detection and the collocated VIIRS cloud detection are used for Hurricane Sandy (2012) case study. CrIS channel 96 is selected to compare the data coverage using the two methods. Figure 4.11 gives the weighting function (or Jacobian) for CrIS channel 96 (709.37 cm-1). The weighting function peak for this channel is around 350-400 hPa. The weighting function for this channel is very broad, which has high risk to be affected by clouds. The green dots in the upper panel of Figure 4.12 are the CrIS data coverage with GSI stand-alone cloud detection method. The green dots in the lower panel of Figure 4.12 are the CrIS data coverage with VIIRS cloud detection, respectively, for CrIS channel 96. To identify the cloud contamination, the Geostationary Operational Environmental Satellites (GOES-13) Imager brightness temperature (BT) at 10.7 μm is overlapped in this region. The cloudy regions have low brightness temperature in GOES-13 imager data. It can be seen that the GSI stand-alone cloud detection method assimilated some CrIS data affected by clouds as clear radiances (see the boxes in Figure 4.12), especially at the northeast of the hurricane vortex and the front area close to the Great Lakes. With the collocated VIIRS high spatial resolution cloud mask for CrIS clear detection, the cloud affected radiances are removed before radiance assimilation, which avoids degrading the analysis fields. Since CrIS and VIIRS are onboard the operational satellite, this method could be used in operations.

The forecast results of CrIS radiances assimilation using VIIRS cloud detection method and using GSI stand-alone cloud detection method are shown in Figure 4.13. The experiments are assimilated the GTS, AMSU-A radiances, ATMS radiances and CrIS radiances data using GSI data assimilation system. The clear radiances from CrIS observations are mostly in the regions surrounding the hurricanes, which has more impacts for the surrounding thermodynamic

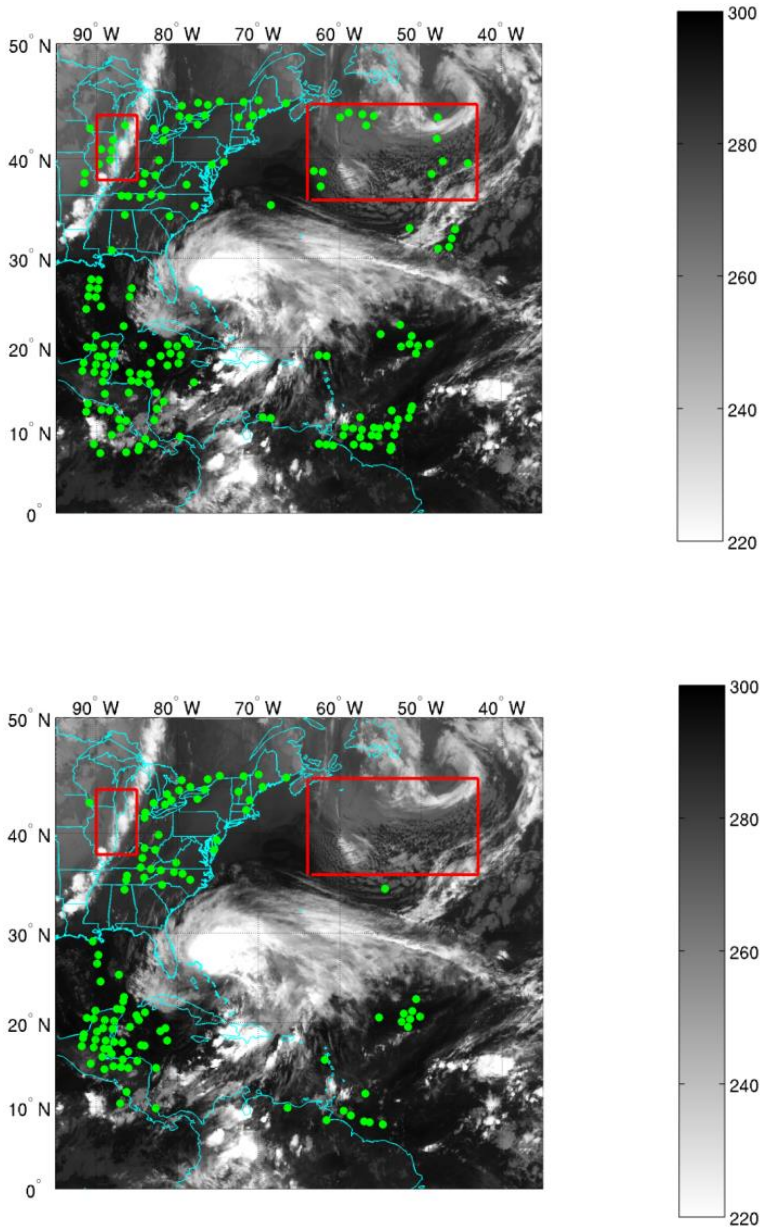

Figure 4.12 The locations at 0600 UTC 26 Oct 2012 where CrIS channel 96 (709.37 cm^{-1}) is flagged clear with stand-alone cloud detection (upper) and with VIIRS cloud detection (lower) on visible imagery (10.7 μm) from GOES-13 for Hurricane Sandy (2012).

fields. With the accumulated forecast time, the impacts from the sounding thermodynamic fields would affect the hurricane structures, the speed of the hurricane movement, the hurricane intensity and etc. Compared to the GSI stand-alone cloud detection (blue lines in Figure 4.13), the assimilation of CrIS radiances using VIIRS cloud detection (red lines in Figure 4.13) reduces the hurricane track RMSE in the 72-hour forecasts. The track RMSE of CrIS/VIIRS cloud detection is around 5-20 km less than GSI stand-alone cloud detection. The RMSE of maximum wind speed (SPD) is comparable with these two cloud detection methods. So for the hurricane intensity forecast, the impact of CrIS/VIIRS cloud detection is neutral.

4.4 Summary

Cloud detection is one of the challenges in assimilating advanced IR sounder radiances. Improved cloud detection could reduce the incorrect detection of clear FOVs and improve the assimilation of IR radiances. Most operational centers are using clear channel detection and figure-guess check method to detect clouds, which has the potential risk of assimilating the cloudy radiances as clear skies. The collocated high spatial resolution imager data could help IR sounder FOV cloud detection, and the cloud contaminated IR FOVs are removed before data assimilation.

Due to AIRS and MODIS onboard the same platform, MODIS can provide high spatial resolution cloud properties and cloud mask for AIRS cloud detection. If the AIRS FOVs collocated with MODIS cloud mask give confident clear, then the AIRS FOVs will be assimilated in the data assimilation system; if the AIRS FOVs collocated with MODIS cloud mask indicate the cloud combination, the AIRS FOVs will be removed before data assimilation.

Therefore, the data used for assimilation have high quality and without cloud contamination. Similarly, the cloud mask from VIIRS could collocate with CrIS FOVs and help CrIS do cloud detection before data assimilation.

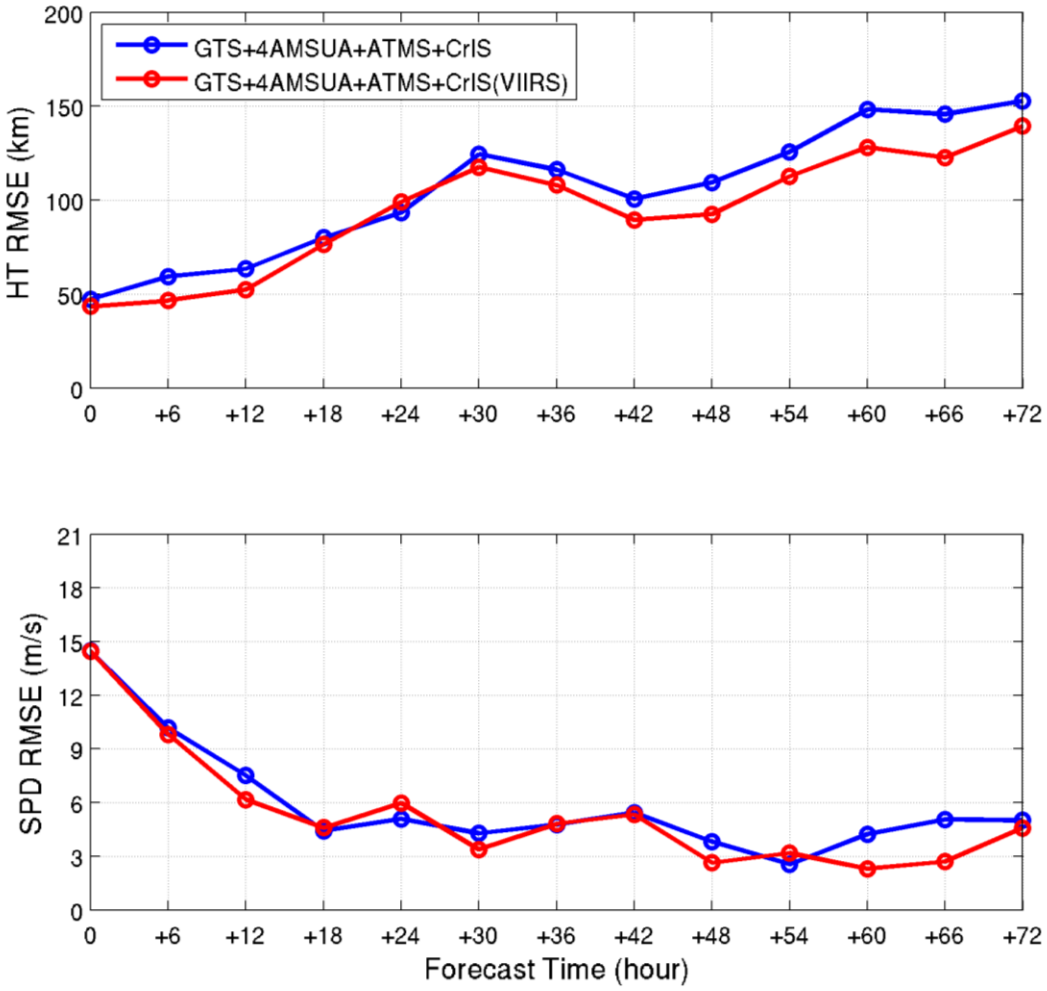

Figure 4.13 The track (top) and the maximum wind speed (bottom) forecast RMSE with CrIS stand-alone cloud detection (blue) and CrIS/VIIRS cloud detection (red). Data are assimilated every 6-hour from 0600 UTC on 25 October to 0000 UTC on 27 October 2012, followed by a 72- hour forecast for Hurricane Sandy (2012).

The stand-alone cloud detection method is plugged into the GSI system, and the sub-pixel cloud detection method is collocated the cloud mask from MODIS or VIIRS. The data locations of assimilated IR radiances with stand-alone cloud detection generally agree with the MODIS or VIIRS cloud detection; however, there are some mismatched areas that the stand-alone cloud detection allows more cloud-contaminated radiances into the GSI system, causing a cold bias in the temperature field and a wet bias in the moisture field. This bias affects the forecasts of hurricane track and intensity. The 72-hour forecasts of Hurricane Sandy (2012) indicate that the hurricane track forecasts are improved with AIRS/MODIS cloud detection and CrIS/VIIRS cloud detection compared to the stand-alone cloud detection method. The hurricane track RMSE reduced around 30 km using AIRS/MODIS cloud detection from stand-alone method. The RMSE of the hurricane track is improved on average over the 72-hour forecast period. This improvement is more evident after 30-hour in the forecasts. After collocated the high spatial resolution imager data, the clear radiances are mostly in the regions surrounding the hurricanes, which has more impacts for the surrounding thermodynamic fields. The maximum wind speed is neutral during the whole forecast period. These results indicate that the AIRS/MODIS and CrIS/VIIRS cloud detection algorithm could benefit the hurricane track forecast by reducing the cloud-contaminated radiances into the assimilation system.

Chapter 5

Use the thermodynamic information under partially cloudy skies

Good cloud detection could effectively remove the cloud contamination and keep the clear observations for assimilation. However, the availability of satellite observations that can be assimilated in the model is limited if only the clear radiances are assimilated. Clouds affect a large percentage of observations from IR sounders. The chance of a FOV being affected by clouds is approximately 75% for HIRS (Wylie et al., 1994) and around 87% for AIRS (Rienecker et al., 2008). This means that a majority of IR sounder radiance observations are abandoned if only clear-sky IR radiances are used. To expand advanced IR sounder radiance assimilation in cloudy regions, research has been conducted on assimilating the cloudy radiances directly (Heilliette and Garand, 2007; Pavelin et al., 2008). Stengel et al. (2013) assimilated the Spinning Enhanced Visible and Infrared Imager cloud-affected IR radiances with a four-dimensional incremental variational assimilation (4D-Var) system and reduced forecast fields normalized error between 500 hPa and 200 hPa by 4%, the forecast error of geopotential height and humidity by 1%, and forecast error of wind direction by 1-3% in the upper troposphere. However, some negative impacts were noted in the lower troposphere. To date, cloudy radiances

have not been effectively used operationally due to various factors: modeling clouds in NWP, calculating equivalent radiances from radiative transfer models, and observing the vertical structures of cloud parameters (fraction, liquid water content, and phase) (Errico et al., 2007; Geer and Bauer, 2011).

The availability of observations that can be effectively assimilated is limited if only clear IR radiances are used. The direct assimilation of the cloudy radiances is full of challenges. To enable assimilating the thermodynamic information in partially cloudy regions, cloud-cleared radiances are assimilated into a regional NWP model in this chapter. Cloud-cleared radiance is the clear equivalent radiance under partially cloudy region. In this chapter, we use AIRS cloud-cleared radiances since the AIRS clear radiances have been successfully used in operational NWP forecasts. The cloud-cleared radiances can be assimilated as clear radiances without changes for the data assimilation systems. We have compared stand-alone AIRS cloud-cleared radiances with those benefiting from collocation with MODSI – so called AIRS/MODIS cloud clearing (Li et al., 2005). This method retrieves clear column radiances through combining collocated multiband MDOSI IR clear radiances and the AIRS cloudy radiances (Li et al., 2004). One advantage of this method is that no NWP background information is needed in the AIRS/MODIS cloud-clearing technique. MODIS is used to cloud clear the AIRS radiances as well as to quality control the cloud-cleared radiances (Goldberg et al., 2005). Based on the statistical results (Rienecker et al., 2008), approximately 13% of the AIRS FOVs are under clear skies, and an additional 21% of the AIRS FOVs can be cloud cleared successfully.

5.1 Methodology for deriving cloud-cleared radiances

Smith et al. (2004) had discussed several possible methods of extracting atmospheric thermodynamic information from cloud-contaminated hyperspectral infrared measurements: (1) cloud-clearing method based upon the spatially adjacent cloud contaminated radiances, (2) retrieval method using the assumption of opaque and overcast cloudy conditions, where only sounding down to the cloud level is possible, and (3) retrieval or assimilation method using an accurate cloud radiative transfer model, which physically accounts for absorption and scattering of cloud particles within the field of view (FOV) of the measurements. Unlike the other two methods, the first approach handles clouds indirectly by using multiple spatial FOVs to extract the clear portion of the observations. In other words, cloud-clearing extracts the radiance arising from the clear air portion of partly cloudy FOVs by extrapolating spatially coherent cloudy radiances, thus permitting profile soundings to the surface or the assimilation of radiances as in the clear field of view case.

Using the collocated clear portion of MODIS IR radiances within the two adjacent AIRS FOVs' cloudy radiances, a cloud-clearing parameter call N* can be derived by spatially averaging MODIS clear radiances to AIRS footprints, and spectrally convolving AIRS radiances to MODIS bands by applying MODIS Spectral Response Functions (SRFs) to AIRS radiance spectrum (see Figure 5.1 for the MODIS SRFs overlaying on an AIRS brightness temperature spectrum). Once N* is derived, it can be applied to the cloudy radiances from these two FOV's measurements and derive the clear equivalent radiance spectrum representing the common clear portion of radiances within the two adjacent AIRS FOVs. This N* concept for AIRS/MODIS cloud-clearing was described by Smith et al. (2004) with a single MODIS band (11 μm) and was

further expanded to using MODIS multi-spectral bands (Li et al., 2005) through optimal cloud-clearing.

Once the cloud-cleared AIRS radiance spectrum is produced, quality control (QC) is carried out through checking the differences between the simulated AIRS cloud-cleared MODIS band radiances (through spectral convolution with related MODIS band SRFs), using most of the MODIS bands from the IR shortwave to longwave spectral regions, and the collocated MODIS clear radiance observations (Goldberg et al., 2005). These differences must all be smaller than the predetermined expected error. Otherwise, the whole cloud-cleared AIRS spectra are rejected for assimilation. Nine MODIS infrared bands (22 (3.959 μm), 24 (4.465 μm), 25 (4.515 μm), 28 (7.325 μm), 30 (9.73 μm), 31 (11.03 μm), 32 (12.02 μm), 33 (13.335 μm), and 34 (13.635 μm)) are used in both the cloud-clearing and QC process. The MODIS bands 20 (3.750 μm), 23 (4.050 μm) and 27 (6.715 μm) are not used in both cloud-clearing and QC because of the convolution error introduced by the spectral gaps in the AIRS spectrum; and band 21 is not used due to the large detector noise; and bands 35 (13.935 μm) and 36 (14.235 μm) are not used due to the calibration error of the spectral response function .

A threshold of 0.3 K is set for quality control on the differences between the simulated AIRS cloud-cleared (convolved to MODIS IR bands) radiances and the MODIS IR band clear radiance observations in this study. Therefore, the AIRS cloud-cleared radiances have high quality and can be treated as equivalent clear radiances for assimilation, and the technique for assimilating clear sky radiances can be applied directly to the cloud-cleared radiances without modification of GSI system.

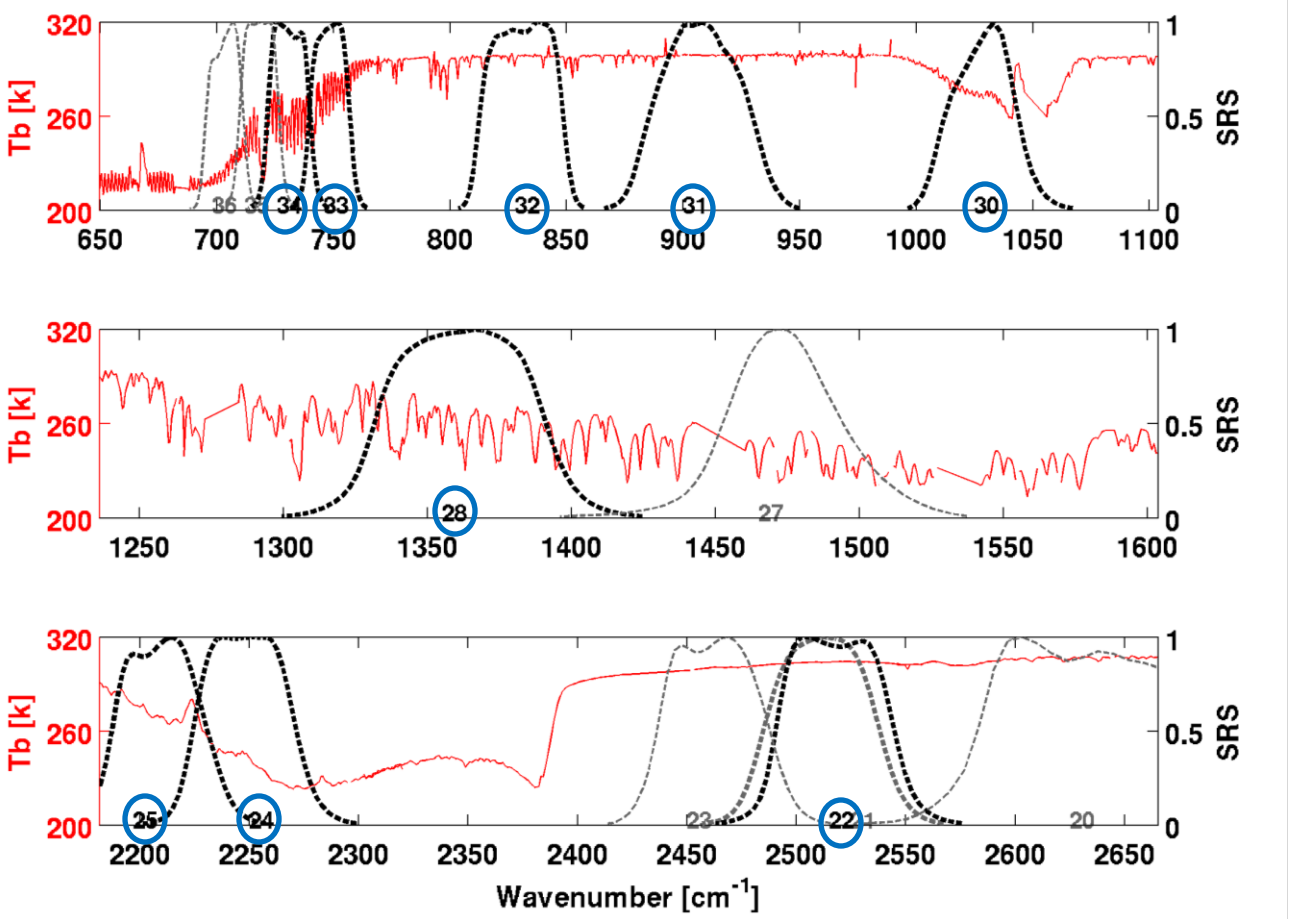

Figure 5.1 AIRS brightness temperature (BT) spectral (red, unit: K) with MODIS spectral response function (SRS) of channels (dashed). MODIS channel numbers are marked in the figure. Black with blue circle is MODIS channels used in cloud-clearing and QC, grey is not used.

5.2 Impact on analysis

5.2.1 Coverage of AIRS radiances

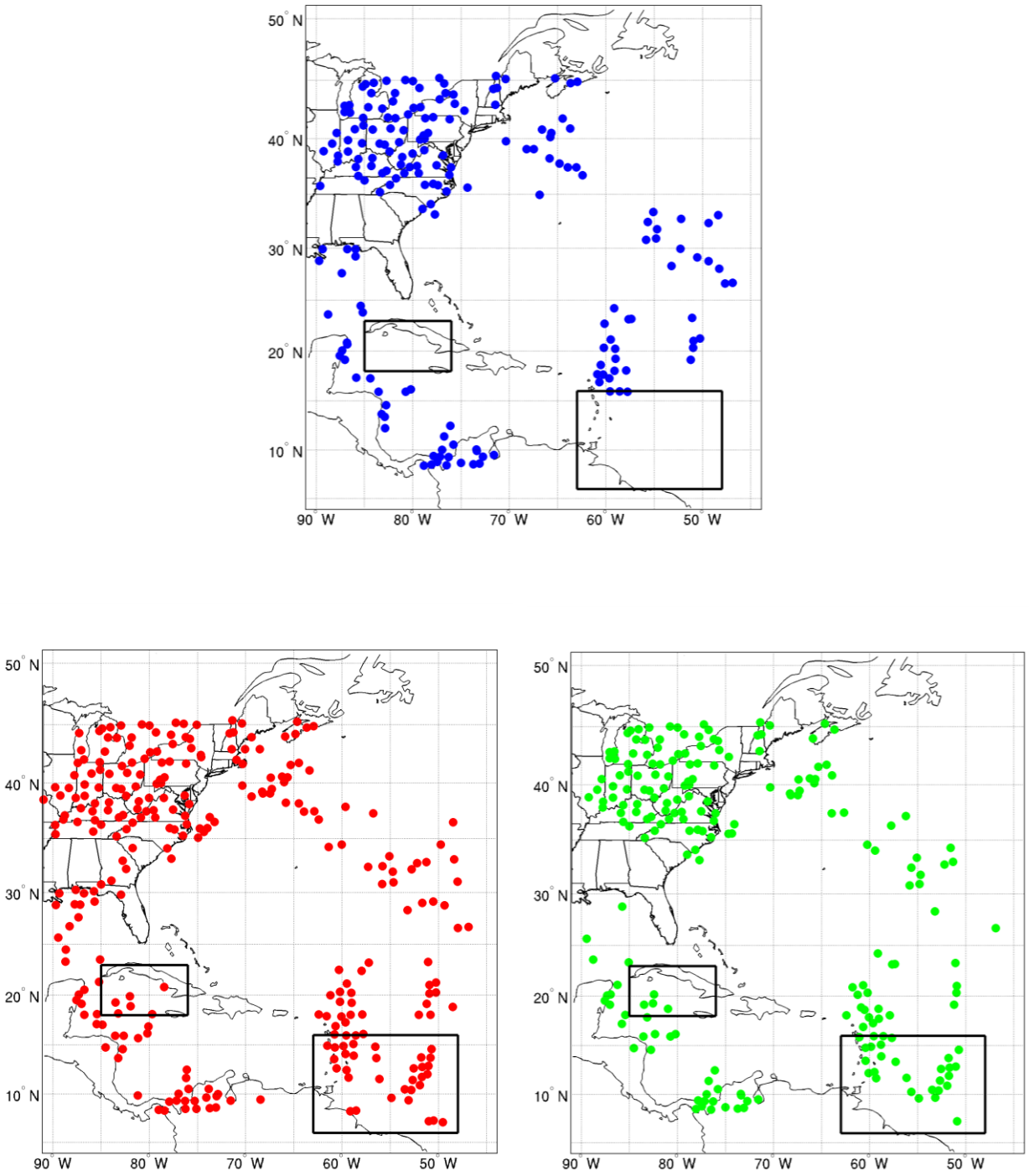

Figure 5.2. The locations at 1800 UTC 25 October 2012 where AIRS channel 210 (709.5659 cm^{-1}) is assimilated in GSI for AIRS (GSI clr) (lower left red), AIRS (MOD clr) (upper blue) and AIRS (MOD cld-clr) (lower right green).

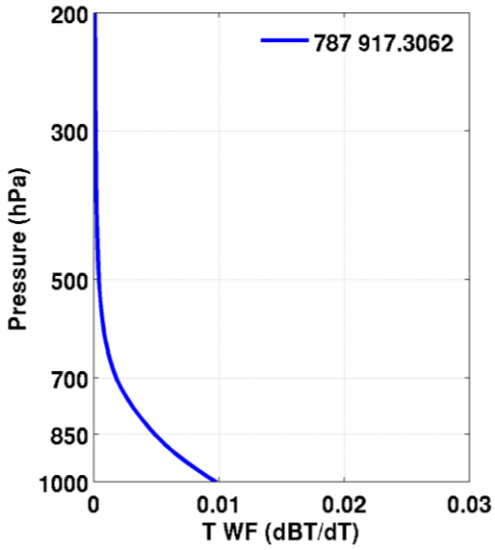

Figure 5.3 The weighting function of AIRS channel 787 (917.3062 cm^{-1}).

The number and quality of observations highly affected the data assimilation results. Better quality observations assimilated usually leads to better analysis/forecast. On the other hand, poor quality observations, even a small percentage, may pose significant negative impacts on the analysis and forecast. The data coverage of AIRS radiances assimilated of channel 210 (709.5659 cm-1) in GSI at 1800 UTC 25 October 2012 is shown in Figure 5.2, and the channel of 787 (917.3062 cm-1) is shown in Figure 5.4. The peak of the weighting function for channel 210 is at around 450 hPa (Figure 5.3). The channel 787 is surface channel with the weighting function peak is at surface level (Figure 5.4). For channel 210, the number of assimilated AIRS FOVs is 283 for AIRS (GSI clr), 186 for AIRS (MOD clr), and 211 for AIRS (MOD cld-clr). For channel 787, the number of assimilated AIRS FOVs is 92 for AIRS (GSI clr), 43 for AIRS (MOD clr), and 47 for AIRS (MOD cld-clr). For both of these two channels, with more accurate cloud detection with the MODIS high spatial resolution cloud mask product (Ackerman et. al., 1998; Ackerman et. al., 2008), the number of AIRS (MOD clr) assimilated radiances is smaller

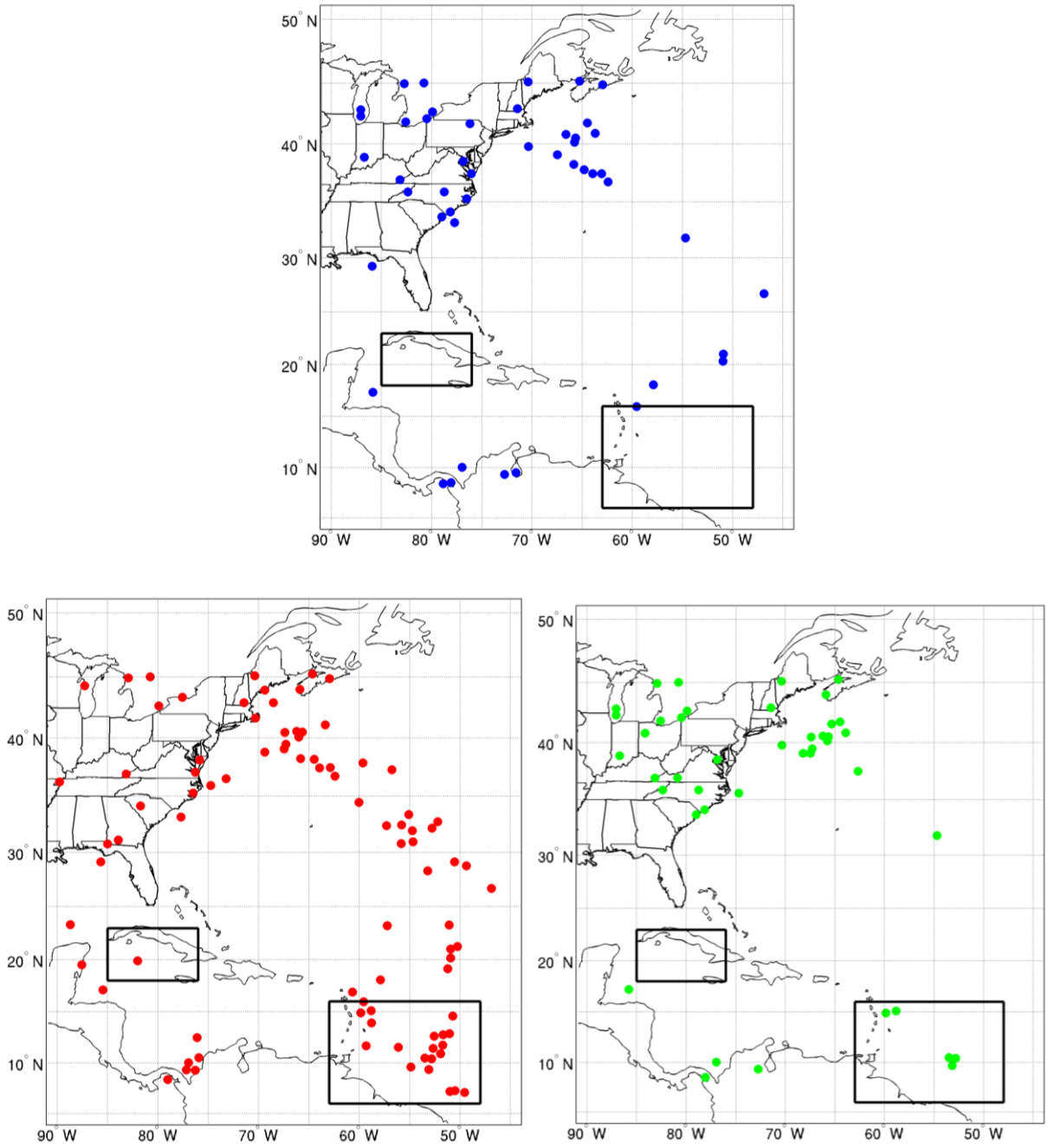

Figure 5.4 The locations at 1800 UTC 25 October 2012 where AIRS channel 787 (917.3062 cm^{-1}) is assimilated in GSI for AIRS (GSI clr) (lower left red), AIRS (MOD clr) (upper blue) and AIRS (MOD cld-clr) (lower right green).

than with the GSI stand-alone cloud detection, which greatly reduces the possibility of cloud contamination. The number of AIRS (MOD cld-clr) is more than the number of AIRS (MOD clr) indicates that cloud-clearing method could provide extra clear equivalent radiances effectively assimilated in the data assimilation model.

Comparing AIRS (GSI clr) and AIRS (MOD clr), some mismatches are found in the Caribbean Sea and south of the North Atlantic Ocean. The mismatched regions are cloudy regions according to the MODIS cloud mask, but assimilated as clear-sky in GSI, which potentially bias the analysis fields. The two black rectangles show where cloud-cleared radiances increase the number of observations in partially cloudy regions which are rejected by AIRS (MOD clr) but incorrectly accepted by AIRS (GSI clr). More data are assimilated in AIRS (MOD cld-clr) than AIRS (clr), because the cloud-clearing method generates AIRS clear equivalent radiances for assimilation in some partially cloudy regions addition to the AIRS (MOD clr). These additional cloud-cleared radiances increase the number of quality observations that cloud be assimilated by GSI and therefore improve the analysis and forecast.

5.2.2 Analysis fields of temperature

The assimilation of advanced IR radiances provides the atmospheric thermodynamic information for improving NWP initialization. Impact on initialization (or the analysis fields), due to different schemes of assimilating AIRS radiances, is analyzed in the following part.

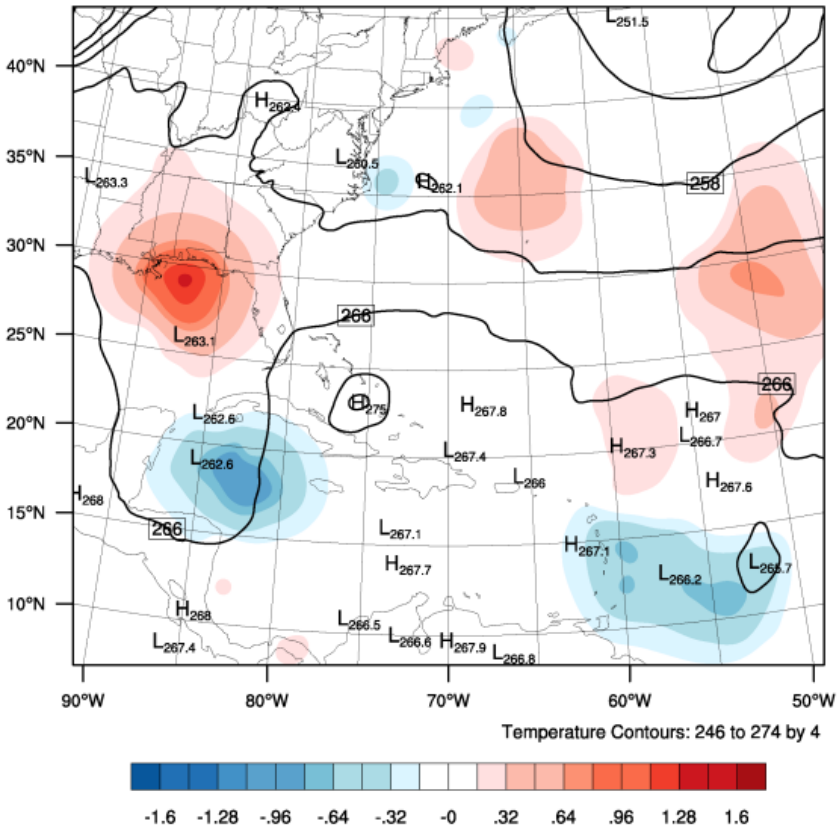

Figure 5.5 The difference in temperature (shaded, unit: K) analysis between AIRS (MOD cld-clr) and AIRS (MOD clr) with temperature (contour, unit: K) of AIRS (MOD cld-clr) at 500 hPa at 1800 UTC 25 October 2012.

The temperature and its difference between AIRS (MOD cld-clr) and AIRS (MOD clr) on the analysis fields at 1800 UTC on 25 October 2012 are shown in Figure 5.5. The cloud-clearing method extracts the radiance arising from the clear air portion of partly cloudy FOVs to represent the thermodynamic information in partially cloudy regions. It is therefore expected that the analysis from the cloud-cleared radiances is warmer than that from the cloud contaminated clear radiances, such as the Florida area. However, there are regions over the Caribbean Sea and south of the North Atlantic Ocean in Figure 5.5 showing the opposite. Careful examination from high quality MODIS cloud mask reveals that those regions have no clear radiances. As a result, the

analysis with thermodynamic information of AIRS (MOD clr) is not much different from the background. The pattern of temperature difference fields on 850 hPa (Figure 5.6) is quite similar to the pattern on 500 hPa. But the value of the difference is much smaller, with the difference range between -0.8 K to 0.8 K.

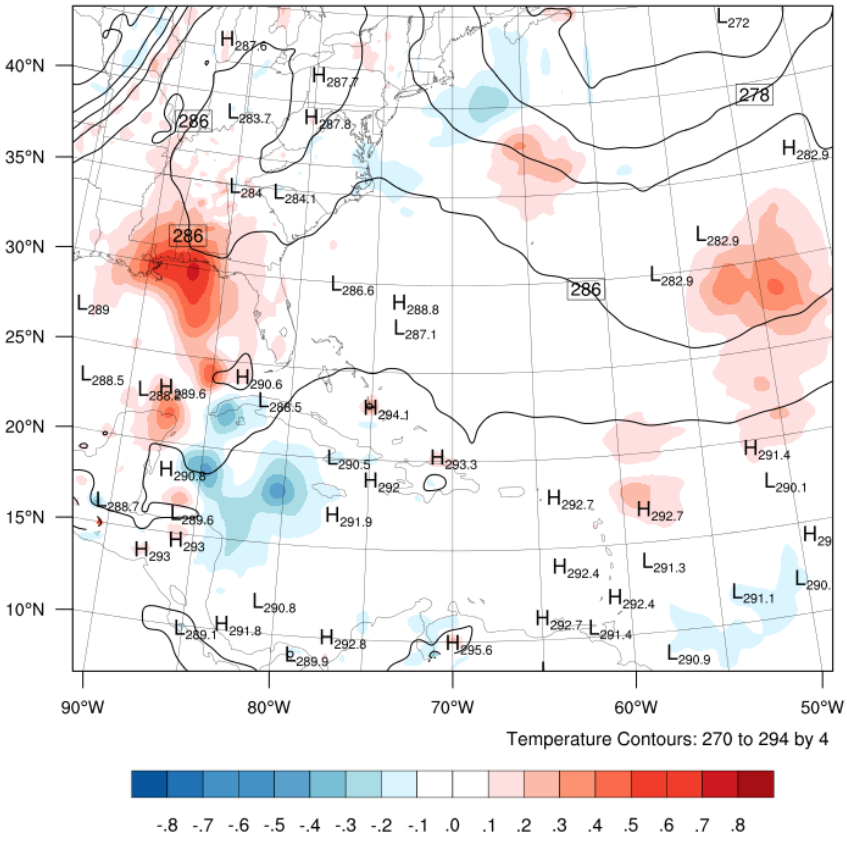

Figure 5.6 The difference in temperature (shaded, unit: K) analysis between AIRS (MOD cld-clr) and AIRS (MOD clr) with temperature (contour, unit: K) of AIRS (MOD cld-clr) at 850 hPa at 1800 UTC 25 October 2012.

The differences shown in Figure 5.5 and Figure 5.6 are due to the differences between analysis with AIRS cloud-cleared radiances and the background. The warmer background in

those regions is decreased from assimilation of AIRS (MOD cld-clr) compared with that from assimilation of AIRS (MOD clr).

5.2.3 Comparing the analysis temperature profiles with radiosondes

The temperature profiles extracted from the analyses are compared with radiosondes at the analysis time. Temperature BIAS (radiosondes minus the analysis profiles) and STD (standard deviation) between the analysis profiles and radiosondes for Hurricane Sandy (2012) are shown in Figure 5.7, and for Hurricane Irene (2011) are shown in Figure 5.8. Approximately 200 radiosondes profiles located within the model domain are used for verification of the analysis filed. The number of radiosondes varied with pressure levels (Table 5.1). One example of the radiosondes map at 0000 UTC 26 October, 2012 is shown in Figure 5.9. The radiosondes are the standard observed stations in the U.S. continent. Usually there are around 30 – 35 radiosondes at one time on each pressure level, and the whole 6 groups of experiments make the sum of radiosondes between 200 and 222.

Table 5.1. The number of radiosondes at different pressure levels from 1000 hPa to 150 hPa for Hurricane Sandy.

Levels (hPa)	**1000**	**850**	**700**	**500**	**400**	**300**	**200**	**150**
Analysis time	137	221	217	218	215	214	214	214
24-hour forecast	149	223	221	220	219	219	215	217
48-hour forecast	135	223	222	223	224	220	217	218
72-hour forecast	105	221	222	222	222	220	217	218

In Figure 5.7, all temperature BIAS ranges from -0.2 K to 0.33 K, indicating the high quality of the temperature analysis field. For temperature BIAS, there are obvious differences among the three: the AIRS (GSI clr) appears to have a slightly smaller bias compared with AIRS (MOD clr) and AIRS (MOD cld-clr) between 300 and 850 hPa; the AIRS (MOD cld-clr) appears to have a slightly smaller bias than AIRS (MOD clr). For temperature STD, there are few differences between AIRS (MOD clr) and AIRS (MOD cld-clr), both of which have slightly smaller STD than AIRS (GSI clr) except around 600 hPa.

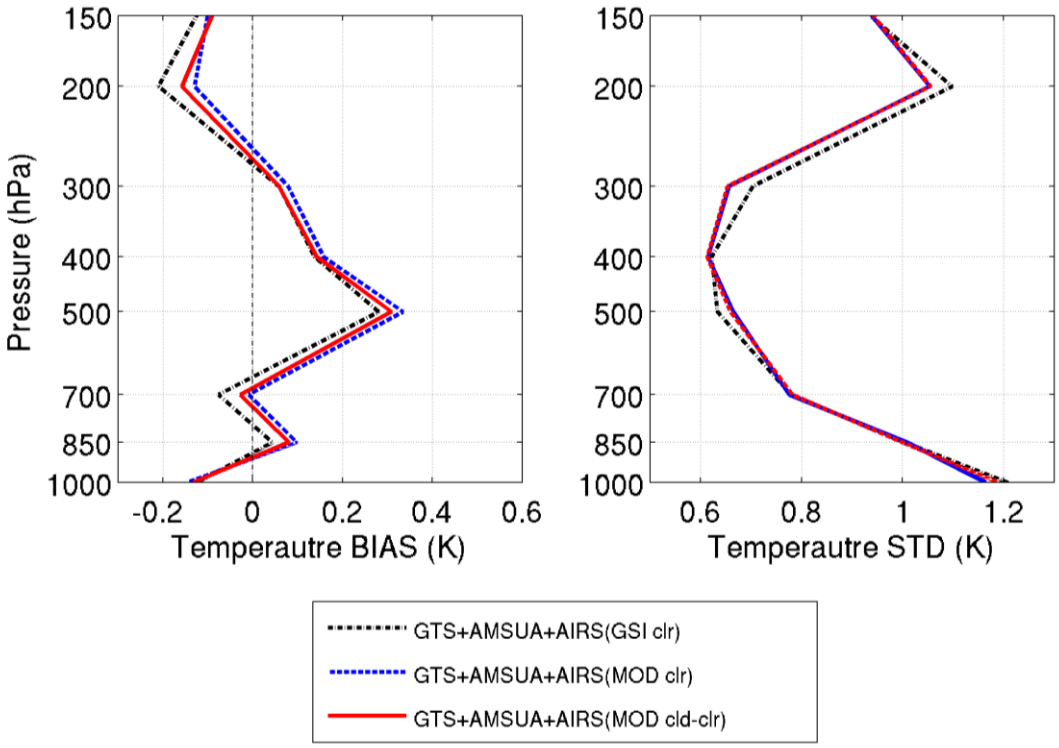

Figure 5.7 Temperature BIAS (left) and STD (right) using radiosonde for AIRS (GSI clr) (dash-dot black, unit: K), AIRS (MOD clr) (solid blue, unit: K) and AIRS (MOD cld-clr) (dashed red, unit: K) at analysis time for Hurricane Sandy.

From Figure 5.8, the temperature BIAS is from -0.4 K to 0.3 K, and the STD ranges from 0.5 K to 1 K from surface to 150 hPa. From temperature BIAS, from surface to 750 hPa and 500 hPa to 300 hPa, AIRS (MOD cld-clr) gives the smallest value; from 750 hPa to 500 hPa, the temperature BIAS of AIRS (MOD clr) is the smalles; and from 300 hPa to 150 hPa, the temperature BIAS of AIRS (GSI clr) is the smallest. For temperature STD, the three experiments are quite similar, especially in the mid and low troposphere.

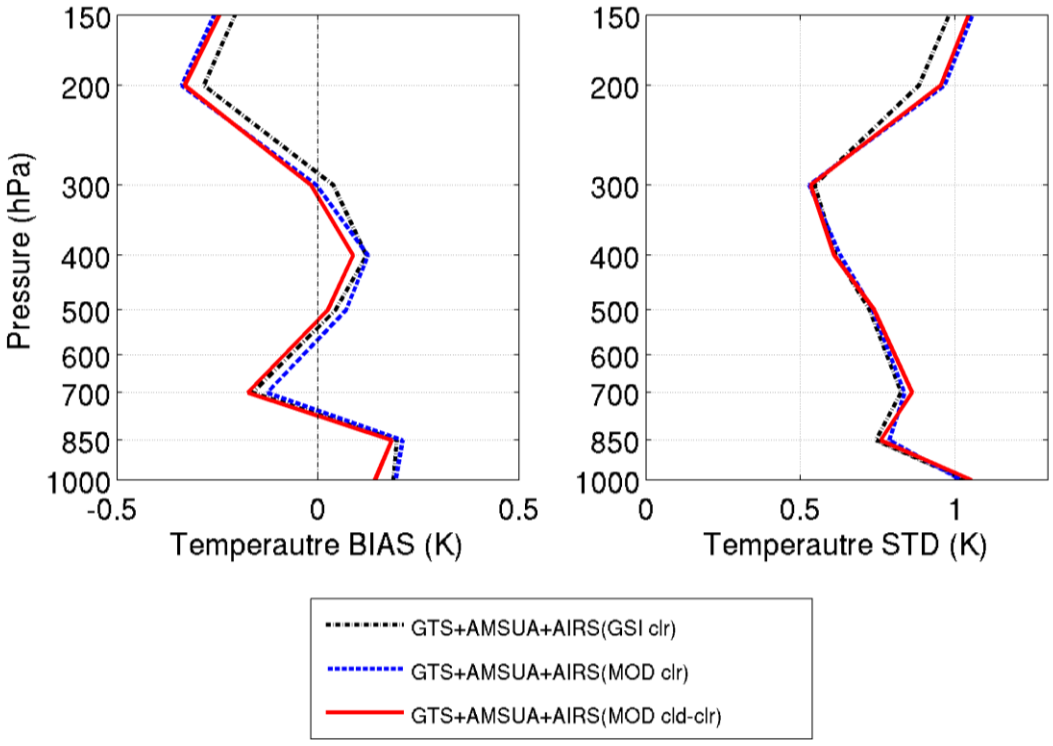

Figure 5.8 Temperature BIAS (left) and STD (right) using radiosonde for AIRS (GSI clr) (dash-dot black, unit: K), AIRS (MOD clr) (solid blue, unit: K) and AIRS (MOD cld-clr) (dashed red, unit: K) at analysis time for Hurricane Irene.

These results indicate that the MODIS cloud detection and the cloud-clearing have impacts on the analysis temperature fields. However, the impacts are so subtle that no single experiment is significantly better than the other two. Although the comparisons with radiosondes in all three types of analysis are very close, it can be seen in next section that impacts on forecasts are quite different.

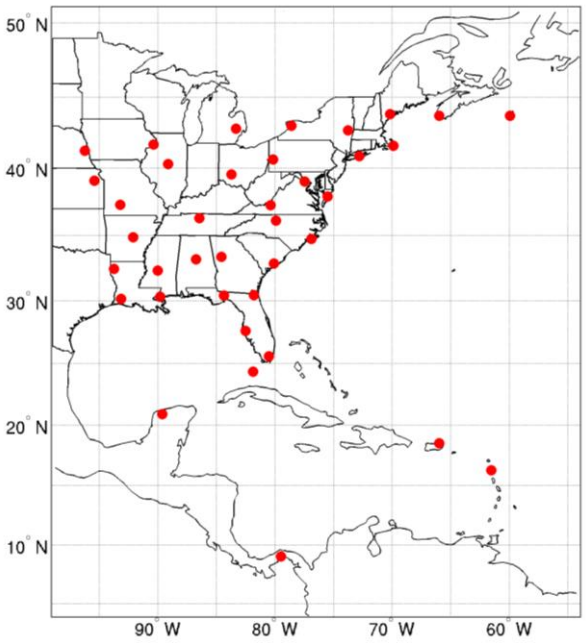

Figure 5.9 The locations of radiosondes are used to compare with analysis fields at 0000 UTC 26 October 2012.

5.2.4 The hurricane locations at the analysis time

The hurricane track error is calculated the distance between the simulated hurricane center and the best track from NHC. The hurricane track error is a quantity way to evaluate the performance of the simulated hurricane. If the simulated hurricane location is close to the

observation at the analysis time, it is believed that the analysis fields are good to have a reliable weather forecast.

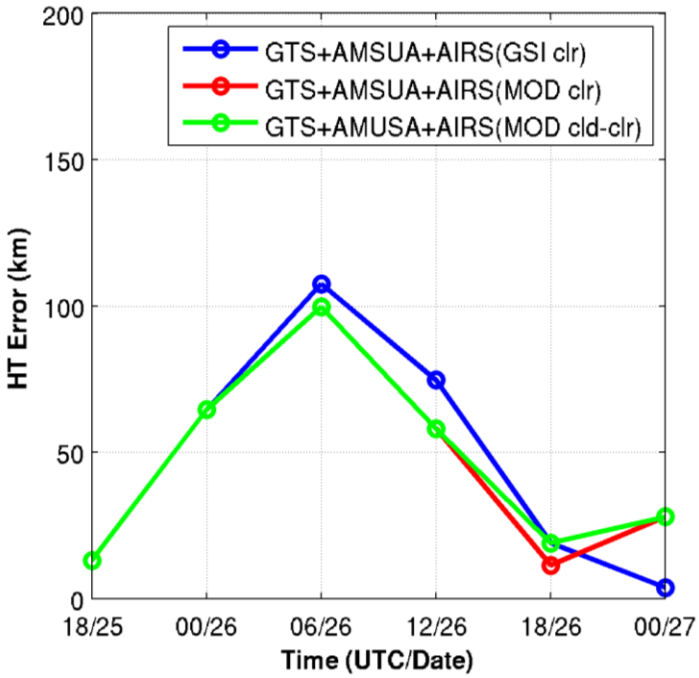

Figure 5.10 The track error of Hurricane Sandy (2012) at analysis time from 1800 UTC 25 October to 0000 UTC 27 October, 2012.

The Figure 5.10 shows the track error of Hurricane Sandy (2012) at the analysis time. At 1800 UTC 25 and 0000 UTC 26 October, the difference of track error among the three experiments are very small, from 0600 UTC 26 October, the track error of AIRS (MOD clr) and AIRS (MOD cld-clr) is becoming smaller than AIRS (GSI clr). And then with the accumulated forecasting time, the difference of track error among the three experiments is becoming obvious. The numbers of the assimilated AIRS radiances data of channel 210 are also plotted in Figure 5.11. In the three experiments, the AIRS (GSI clr) is always assimilated the most radiances data,

the AIRS (MOD clr) assimilated fewest data due to the cloud mask. The AIRS (MOD cld-clr) can assimilate more data than AIRS (MOD clr), because some of the AIRS data can be cloud-cleared and assimilate into the data assimilation system as equivalent clear radiances.

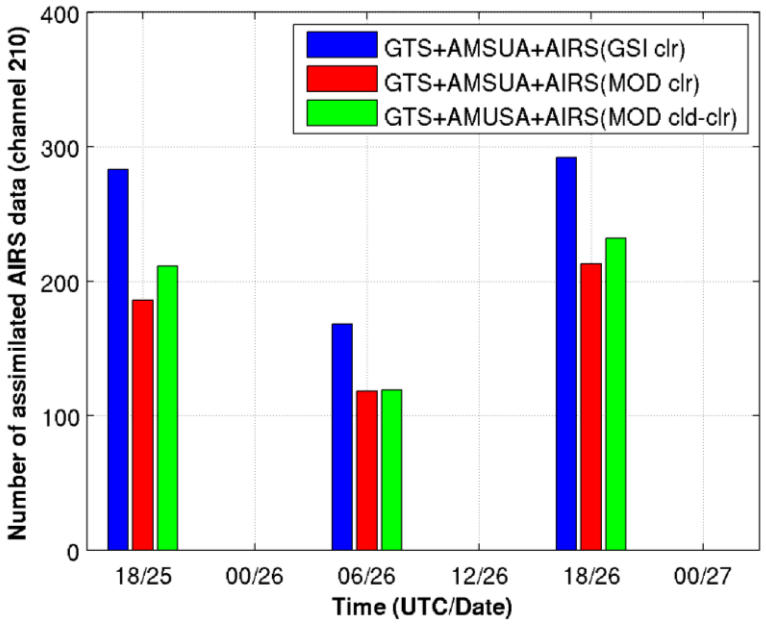

Figure 5.11 The number of assimilated AIRS radiances at channel 210 of Hurricane Sandy (2012) at analysis time from 1800 UTC 25 October to 0000 UTC 27 October, 2012.

In general, the hurricane track error is less than 110 km at the 6 analysis time, and the track error is as small as 10 km at 1800 UTC 25 and 1800 UTC 26. The AIRS data are available at every 0600 UTC and 1800 UTC. And from the hurricane error at the analysis time, the hurricane track error of AIRS (MOD clr) and AIRS (MOD cld-clr) is reduced compared to the track error of AIRS (GSI clr) at 0600 UTC 26 and 1800 UTC 26. For the three experiments, the location of simulated hurricane is very close to the observations, which indicates that the model can simulate the hurricane locations very well.

5.3 Impact on cloud-cleared radiances forecasts

5.3.1 Comparison with GOES-13 Imager brightness temperature observations

The simulated brightness temperature of the 72-hour forecast at 11 μm is compared with the observations from GOES-13 imager channel 4 at 1800 UTC 28 October 2012 (Figure 5.12). The Pressure-Layer Fast Algorithm for Atmospheric Transmittance (PFAAST) model (Hannon et al., 1996, Li et al., 2009) is used as radiative transfer model to calculate the clear-sky GOES 13 radiances. The cloudy radiances are calculated by coupling the clear-sky optical thickness from PFAAST with the cloud optical thickness (COT) at 0.55μm, which is calculated using a fast radiative transfer cloud model developed by University of Wisconsin–Madison (UW) and Texas A&M University [Baum et al., 2000; Wei et al., 2004]. For ice clouds, COT is calculated from the ice water path [Heymsfield et al., 2003]; and for water clouds, the cloud droplet is assumed to be spherical and the classical Lorenz-Mie theory is used to calculate the single-scattering properties.

At 1800 UTC 28 October, Hurricane Sandy passed southeast of North Carolina, with cold clouds (brightness temperature (BT) around 230 K) northwest of the hurricane center, and relatively few clouds and a warm area (BT around 280 K) southeast of the hurricane center. Comparing the simulated GOES-13 Imager brightness temperature from AIRS (MOD clr) and AIRS (MOD cld-clr), substantial differences are seen around the hurricane center (Figure 6, bottom panels). The brightness temperature from AIRS (MOD cld-clr) better reflects the curly structure of the clouds around the hurricane center, and the relatively few clouds and warm area

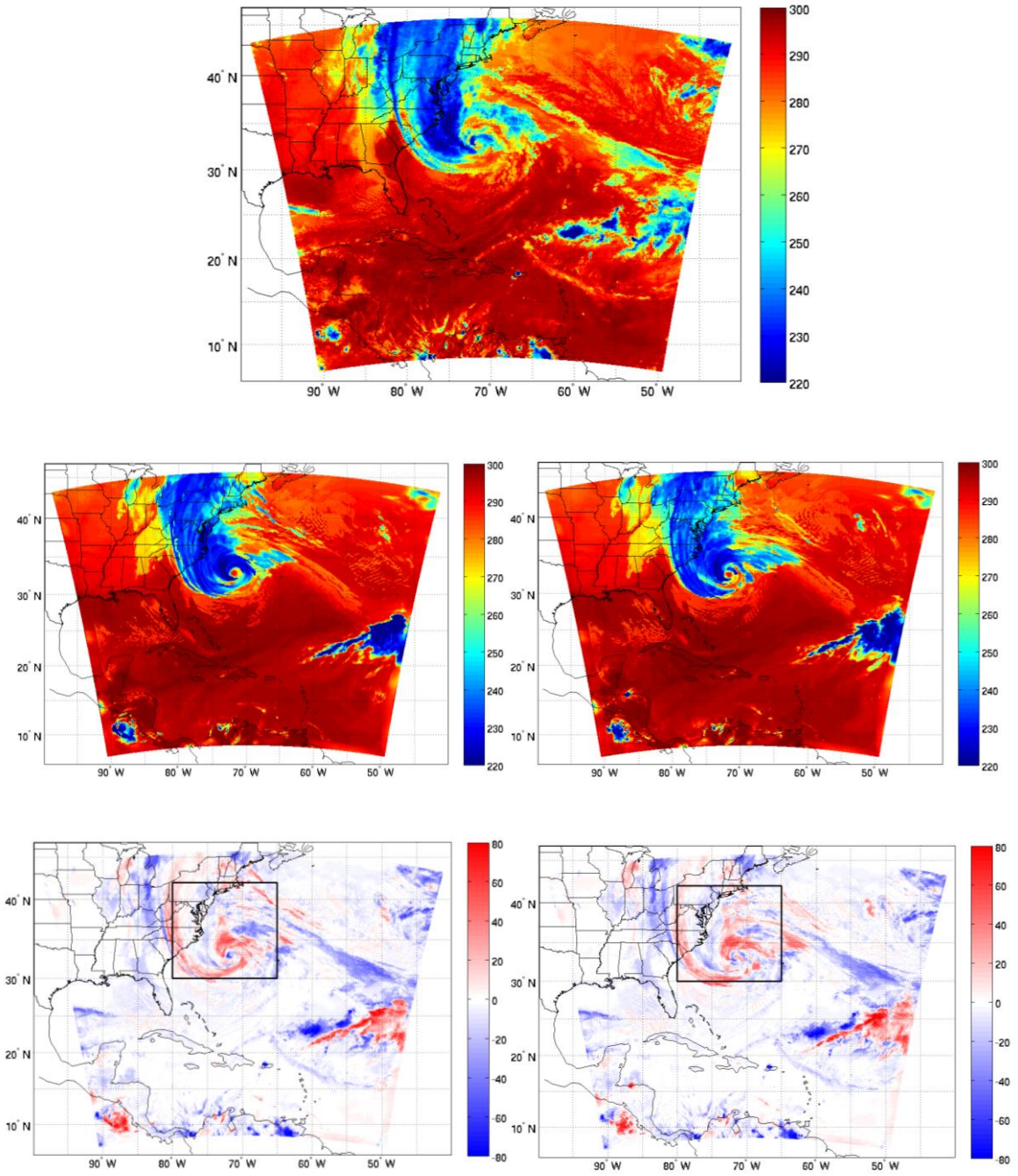

Figure 5.12 The brightness temperature of GOES-13 channel 4 (11 μm) observations (upper, unit: K), simulated 72-hour forecast brightness temperature of AIRS (MOD clr) (mid left) and AIRS (MOD cld-clr) (mid right), the difference of brightness temperature between observations and AIRS (MOD clr) (lower left) and between observations and AIRS (MOD cld-clr) (lower right) at 1800 UTC 28 October 2012.

southeast of the center. Quantitatively, this can be verified using the standard deviation of the difference (STD) of brightness temperature between the observations and the simulations. For the whole domain, the STD is 13.78 K from AIRS (MOD clr) and 13.77 K from the AIRS (MOD cld-clr). If we focus on the region of hurricane center (black box in Figure 6 bottom panel), the STDs are 17.29 K from AIRS (MOD clr) and 17.15 K from AIRS (MOD cld-clr). These results indicate that the assimilation of AIRS (MOD cld-clr) generates forecasted radiances closer to GOES-13 Imager than AIRS (MOD clr).

5.3.2 Forecasts validation with radiosondes

The radiosondes could also be used to validate the performance of the forecasts fields. To validate the temperature of forecast fields against the radiosondes, the temperature profiles are extracted from the 72 hours forecasts. Temperature BIAS (radiosondes minus the temperature of forecast fields) and STD at 24-hour, 48-hour and 72-hour forecast times are shown in Figure 5.13. The number of radiosondes profiles used differs with levels (Table 5.1). An example map of the radiosondes sites at one time period is shown in Figure 5.9. More than half of the stations are near the coast. Both the stations near the coast and over the CONUS could be used to verify the improvements of the forecast fields with assimilation of AIRS (MOD clr) and AIRS (MOD cld-clr), respectively, over that with the assimilation of AIRS (GSI clr). From the 24-hour forecast to 72-hour forecast, AIRS (MOD cld-clr) shows a consistent improvement over AIRS (MOD clr) and AIRS (GSI clr). At the 24-hour forecast time, the difference of temperature BIAS among the three experiments is small (less than 0.1 K). Around 300 hPa, the forecast BIAS is around 1 K in absolute value, which is larger than atmosphere beneath, where BIAS is mostly

less than 0.5 K. This is likely due to the model simulation error near the tropopause. At the 48-hour forecast time, the differences among the three experiments become more substantial. The AIRS (MOD cld-clr) shows substantial improvements over AIRS (GSI clr) and AIRS (MOD clr). The BIAS of AIRS (MOD cld-clr) at 300 hPa is about 0.08 K smaller than AIRS (GSI clr) and 0.1 K smaller than AIRS (MOD clr). The RMSE is also evident between 250 and 750 hPa with an averaged improvement of 0.1 K where AIRS (MOD clr) and AIRS (GSI clr) show similar performance. At the 72-hour forecast time, the improvement from AIRS (MOD cld-clr) becomes more profound. The averaged improvement between 250 and 700 hPa is 0.25 K over AIRS (GSI clr) and 0.2 K over AIRS (MOD clr). Similar improvements are seen in RMSE. It is important to point out that the AIRS (MOD clr) has slight improvements over MOD (GSI clr), which is consistent with Wang et al. [2014]. The RMSE also increased with forecast hours, which is consistent with the model errors growing over time.

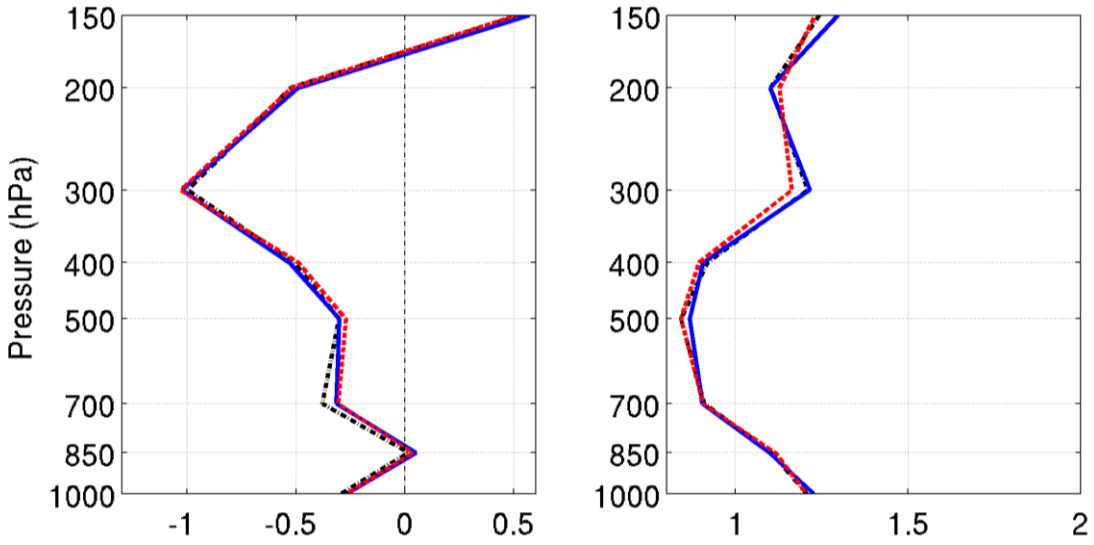

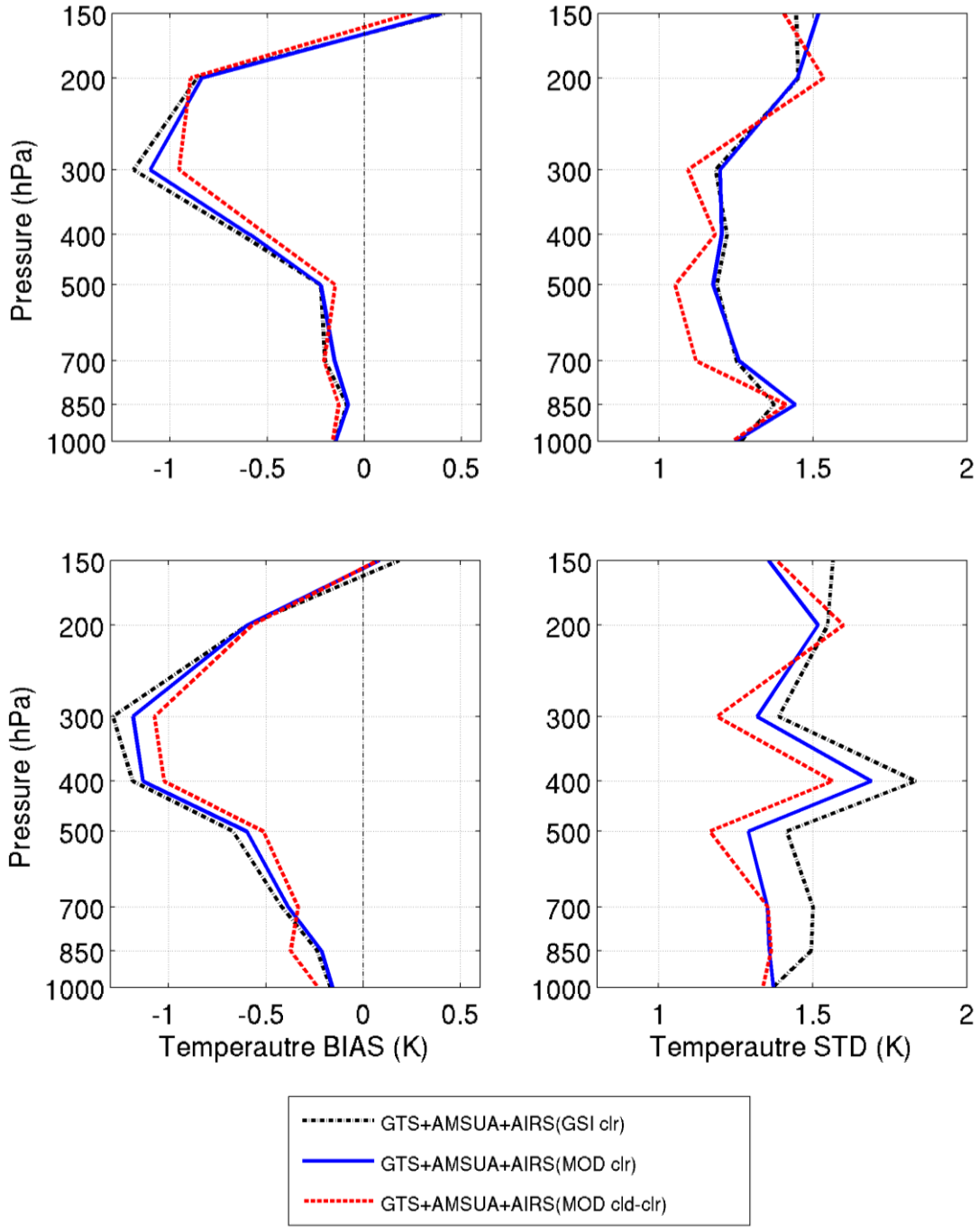

Figure 5.13 BIAS (left column) and STD (right column) for 24-hour (upper panel), 48-hour (middle panel), and 72-hour (lower panel), forecasts of temperature profiles between the AIRS (GSI clr) (dash-dot black, unit: K) and radiosondes, AIRS (MOD clr) (solid blue line, unit: K) and radiosondes, and AIRS (MOD cld-clr) (dashed red line, unit: K) and radiosondes from 1000 hPa to 150 hPa for Hurricane Sandy.

For Hurricane Irene, similar results are seen when comparing forecast temperature with radiosondes. The BIAS of forecast temperature with AIRS (MOD cld-clr) assimilation is about 0.05 K smaller than that of AIRS (MOD clr). These results indicate that the extra cloud-cleared AIRS radiances data provide positive impacts for the temperature forecast.

5.3.3 Hurricane track error and intensity error

Hurricane forecast are validated against the actual storm track and its intensity with time (the best track and observations data were obtained from NOAA's NHC). Intensity is a measure of extreme meteorological conditions, either the maximum sustained (low-level) wind (MSW) or the minimum sea level pressure (MSLP) is used (Merrill, 1988). Figure 5.14 shows the RMSE of the hurricane track (upper) and maximum wind speed (lower) of the 72-hour forecasts for Hurricane Sandy. The RMSE of the hurricane track from AIRS (MOD cld-clr) is the smallest among the three experiments for the whole process, especially after the 18-hour forecasts. The RMSE of the hurricane track from AIRS (MOD clr) is 10 to 25 km smaller than that from AIRS (MOD clr), and is 10 to 50 km smaller than that from AIRS (GSI clr). For the maximum wind speed, the three experiments have comparable results, making it difficult to determine which is better. The RMSE of the hurricane track for Hurricane Irene (Figure 5.15 upper) shows similar results where AIRS (MOD cld-clr) has the smallest track error compared to AIRS (MOD clr) and AIRS (GSI clr), especially after 36-hour forecasts. For the maximum wind speed prediction (Figure 5.15 lower), it is neutral for the three experiments. For Hurricane Ike (Figure 5.16), the RMSE of the hurricane track also shows that the assimilation of the AIRS (MOD cld-clr) improves the track error by 10 km or so compared to that of AIRS (MOD clr) and AIRS (GSI

clr). The maximum wind speed prediction of Hurricane Ike with assimilation of AIRS (MOD cld-clr) gives the slightly smaller error compared to (GSI clr).

It is interesting that assimilation of AIRS (MOD clr and MOD cld-clr) radiances provides positive impacts on hurricane track but neutral impacts on hurricane intensity. Possible reason for that is because of the limited penetration capability of IR radiances. Both AIRS (GSI clr) and AIRS (MOD clr) assimilate clear radiances, which mostly come from environment region and contain little information about cloudy region (i.e. hurricane). Even though cloud-clearing technique extracts clear sky radiances from a cloudy FOV, which contain information within and below clouds, it works better for partly cloudy FOVs, which still account for the environment.

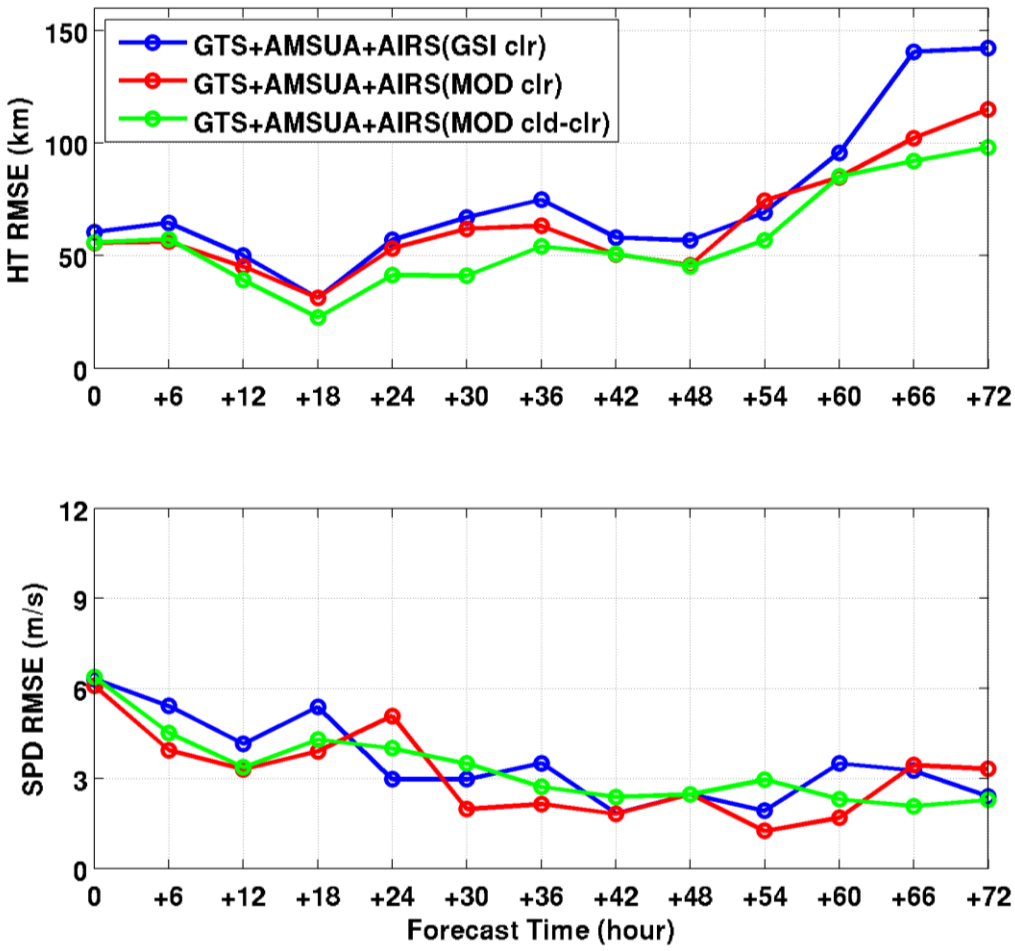

Figure 5.14 The track (top) and maximum wind speed (bottom) forecast RMSE with AIRS (GSI clr) (blue), AIRS (MOD clr) (red) and AIRS (MOD cld-clr) (green). Data are assimilated every 6-hour from 1800 UTC on 25 October to 0000 UTC on 27 October 2012, followed by 72-hour forecasts for Hurricane Sandy (2012).

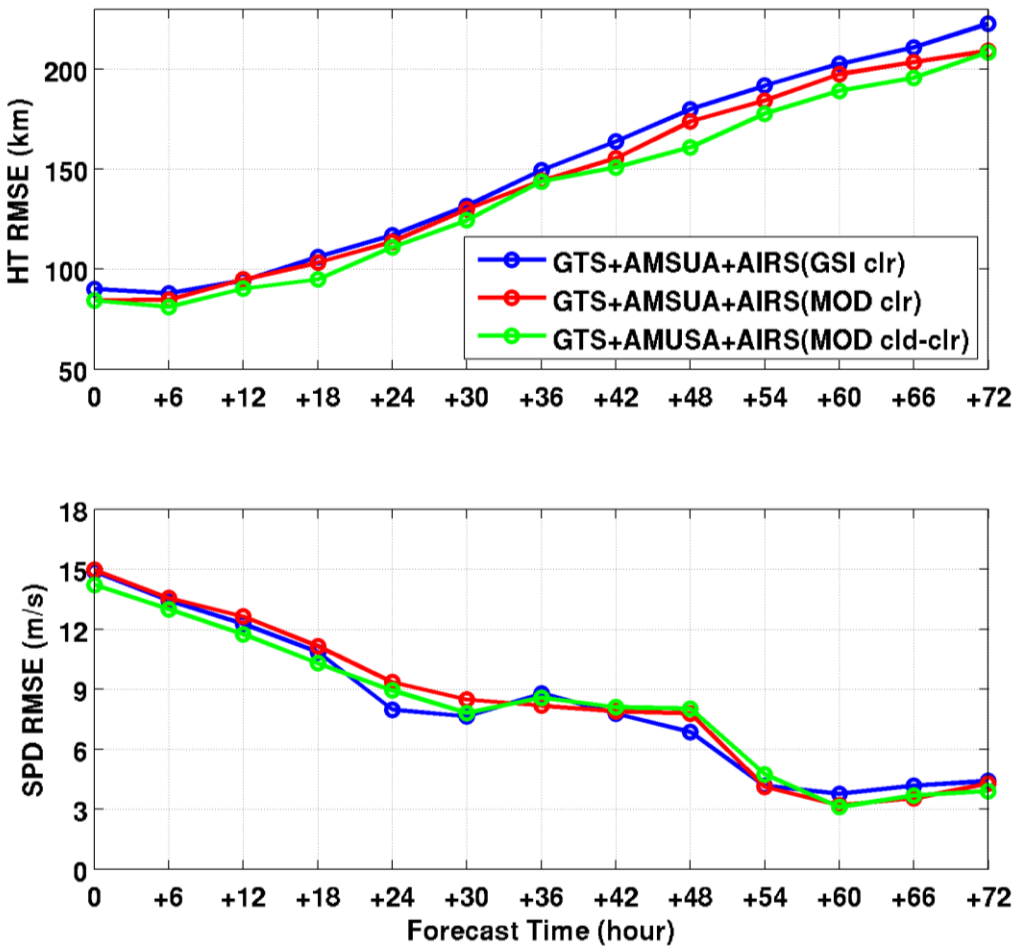

Figure 5.15 The track (top) and maximum wind speed (bottom) forecast RMSE with AIRS (GSI clr) (blue), AIRS (MOD clr) (red) and AIRS (MOD cld-clr) (green). Data are assimilated every 6-hour from 1200 UTC on 22 August to 0000 UTC on 24 August 2011, followed by 72-hour forecasts for Hurricane Irene (2011).

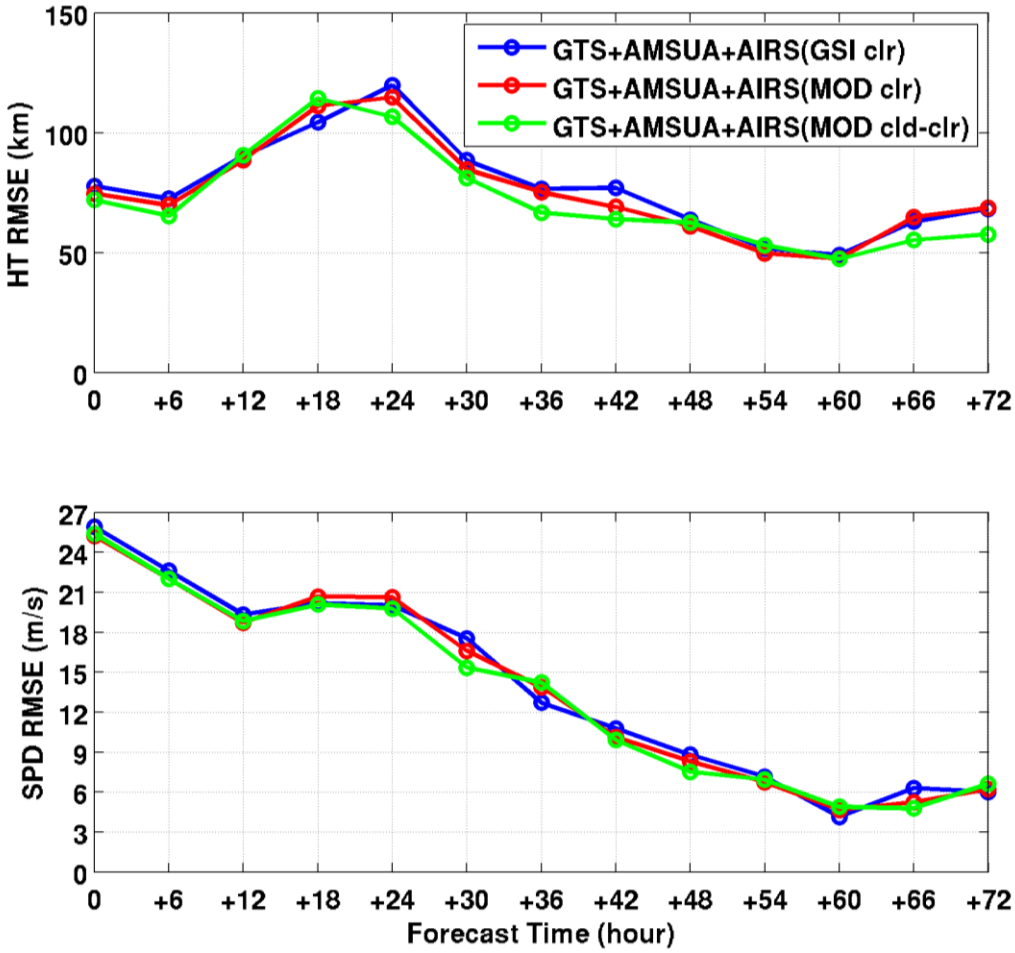

Figure 5.16 The track (top) and maximum wind speed (bottom) forecast RMSE with AIRS (GSI clr) (blue), AIRS (MOD clr) (red) and AIRS (MOD cld-clr) (green). Data are assimilated every 6-hour from 1800 UTC on 5 September to 0000 UTC on 7 September 2008, followed by 72-hour forecasts for Hurricane Ike (2008).

5.4 Summary

Based on the study of Chapter 4, it shows that if the cloudy radiances are assimilated as clear observations, there will be a negative impact on the quality of the NWP analysis and forecast. The reliable cloud detection is essential for data assimilation. With the reliable cloud detection,

the clear observations assimilated in the model are very limited. Cloud-cleared radiance is clear equivalent radiance, but it also includes the information from partially cloudy regions. Therefore, the assimilation of the cloud-cleared radiances data is an alternative way to assimilate thermodynamic information in cloudy regions.

The assimilation of cloud-cleared AIRS radiances is discussed in this chapter. By having collocated high spatial resolution imager measurements, advanced IR sounder sub-pixel cloud characterization, cloud-clearing, and quality control make it possible for effective assimilation of thermodynamic information in cloudy skies. Since the cloud-clearing method retrieves clear equivalent radiances, the same clear radiance assimilation approach can be applied directly to the cloud-cleared radiances. Therefore, the assimilation of thermodynamic information in cloudy skies is not limited by the uncertainty of the cloudy radiative transfer model.

The temperature differences at the analysis fields indicate that the assimilation of the AIRS data can directly affect the atmospheric fields surrounding the hurricane vortex. The comparisons of the analysis temperature profiles with radiosondes for both Hurricane Sandy (2012) and Hurricane Irene (2011) indicate that MODIS cloud detection and the cloud-clearing method have impacts on the analysis temperature fields. But the impacts are different at different vertical levels. The hurricane track error at the analysis time is also studied in this chapter. In general, the track error is less than 150 km, which reflects the model can simulate the hurricane location very well. The different of the track error is subtle at the first 3 experiments, but it is becoming more observations with longer cycling experiments. The assimilation of AIRS (MOD cld-clr) gives the smallest hurricane track error among the three experiments.

The forecast results of Hurricane Sandy, Irene, and Ike showed that assimilating cloud-cleared AIRS radiances in cloudy skies reduces the SD of the temperature difference between the 72-hour forecast and radiosondes by approximately 0.3 K compared to assimilating AIRS (GSI) stand-alone clear radiances. The track forecasts are substantially improved by 10 to 50 km, compared to only clear radiance. The intensity forecast has neutral impact, possibly due to limited penetration capability of the IR radiances. A complementary data set could be microwave radiance observations. In the cloud-clearing method, the accuracy of the cloud-cleared radiances highly depends on the uniformity of the atmosphere, surface, cloud geometric, and optical properties (known as "scene uniformity") across the FOVs. Uniformity occurs more over ocean than over land, thus imager/sounder cloud clearing provides a way for indirect assimilation of thermodynamic information in cloudy regions, especially for TC forecasts over oceans. Since a minimum of two FOVs is required for extrapolation, the cloud-clearing process reduces the spatial resolution of the original observations. Theoretically, it is much more complicated to require more than two FOVs when clouds exist in the cloud-clearing domain. However, under these cases the valid assumption of "scene uniformity" is less frequent and a reliable cloud-cleared solution is rare. Despite all of the shortcomings inherent in the cloud-clearing method, it remains as a possible way to potentially increase the yield of using some of the cloudy hyperspectral infrared data indirectly, as indicated by TC forecasts from Hurricane Sandy, Irene and Ike.

Chapter 6

Analysis of thermodynamic fields of Hurricane Sandy

The assimilation of satellite IR radiances can provide atmospheric information and improve the hurricane forecasts. Based on the discussion in Chapter 4 and Chapter 5, collocated high spatial resolution cloud mask removes the cloud contamination, and improves the IR radiances assimilation. The cloud-clearing method is to calculate the equivalent clear sky radiances under partially cloudy regions. The assimilation of cloud-cleared IR radiances provides more clear equivalent radiances, which brings the thermodynamic and hydrometric information under partially cloudy regions. Based on the hurricane track and intensity forecasts, using high spatial resolution cloud mask for IR clear detection can improve the track forecasts, and assimilating cloud-cleared radiances IR data can further reduce the hurricane track forecast error. The improvement of hurricane track is directly related to the atmospheric environmental fields. In this chapter, one of the hurricane forecasts is selected and the atmospheric environmental structures are analyzed. The thermodynamic fields, sea level pressure, winds and potential vorticity are discussed in the following sections.

6.1 Case study of Hurricane Sandy

Based on the assimilation and forecast results in Chapter 4 and Chapter 5, the track error of Hurricane Sandy (2012) reduces substantially with assimilation of cloud-cleared AIRS radiances. One of the Hurricane Sandy (2012) experiments is selected to analyze the differences of atmospheric environmental fields between GSI stand-alone cloud detection and the cloud-clearing IR assimilation.

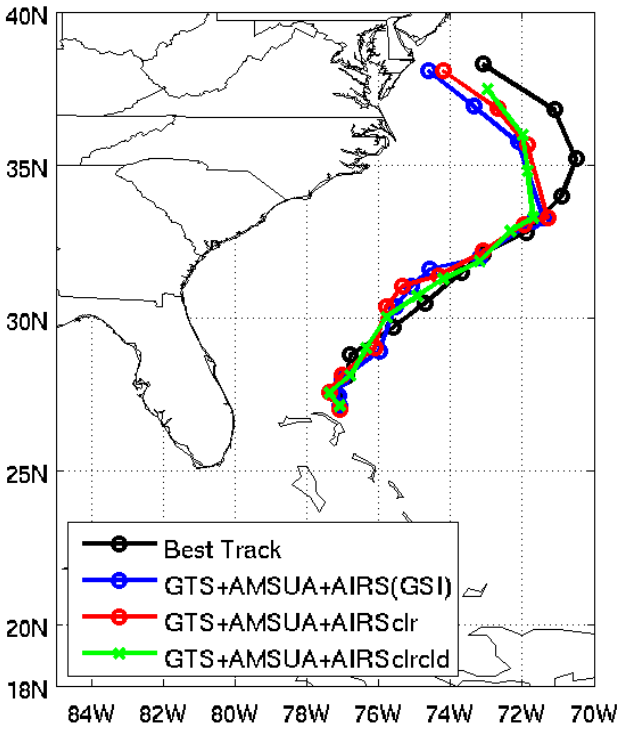

Figure 6.1. The tracks of Hurricane Sandy (2012) for a 72-hour forecast from 1800 UTC 26 October to 1800 UTC 29 October 2012.

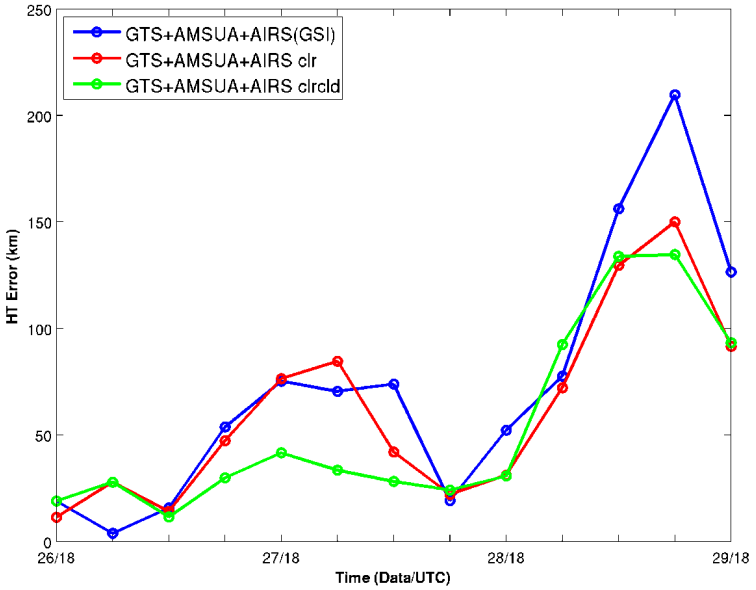

Figure 6.2 The track error of GTS+AMSUA+AIRS (GSI) (blue line), GTS+AMSUA+AIRS clr (red line) and GTS+AMSUA+AIRS clrcld (green line) comparing to the best track for 72-hour forecast of Hurricane Sandy (2012) from 1800 UTC 26 October to 1800 UTC 29 October 2012.

Figure 6.1 is the 72-hour track forecasts of Hurricane Sandy (2012) from 1800 UTC 26 October to 1800 UTC 29 October 2012. The black line is the best track from NHC; the blue is the forecast results of assimilating the AIRS radiances with GSI stand-alone cloud detection (GTS+AMSUA+AIRS (GSI)); the red is the forecast results of assimilating the AIRS radiances with collocated MODIS cloud mask (GTS+AMSUA+AIRS clr); and the green is the forecast results of assimilating the cloud-cleared AIRS radiances (GTS+AMSUA+AIRS clrcld). Compared with the best track, the track error of the three experiments are plotted in Figure 6.2. It's obvious to see that the hurricane track error with assimilation of cloud-cleared radiances reduce dramatically compared to using GSI stand-alone cloud detection method and using collocated MODIS cloud mask cloud-detection method. The assimilation of AIRS with GSI

stand-alone cloud detection gives the largest hurricane track error among the three experiments, especially at the 1200 UTC 29 October.

The following discussions of the atmospheric environmental fields are based on this 72-hour forecast. The comparison of the results focus on the assimilation of AIRS with GSI stand-alone cloud detection method and the assimilation of cloud-cleared AIRS radiances. The 0-hour, 24-hour, 48-hour and 72-hour forecasts are used to analyze the atmospheric fields.

6.2 The temperature fields on 500 hPa

Large-scale circulation affects the tropical cyclone track forecasts. The different large-scale patterns can lead to varying track forecast results [Harr and Elsberry, 1991, 1993; Lander, 1995]. Thus the differences between large-scale patterns of AIRS (GSI clr) and AIRS (MOD cld-clr) on 500 hPa, and the impacts on the track forecast are discussed in this section, and then shown the impacts on the track forecast.

Before the discussion of temperature fields, the data coverage of the assimilated AIRS radiances in the three groups of experiments at 1800 UTC 26 October are shown in Figure 6.3. The weighting function peak of channel 210 is at around 450 hPa (Figure 4.3). The data coverage of AIRS with GSI stand-alone cloud detection is marked in blue dots, the data coverage of AIRS with MODIS cloud detection is shown in red dots, and the coverage of AIRS cloud-cleared radiances is shown in green dots. The differences among the three experiments are at the northeast coast of the U.S. continent, and the northern part of South America. The AIRS with

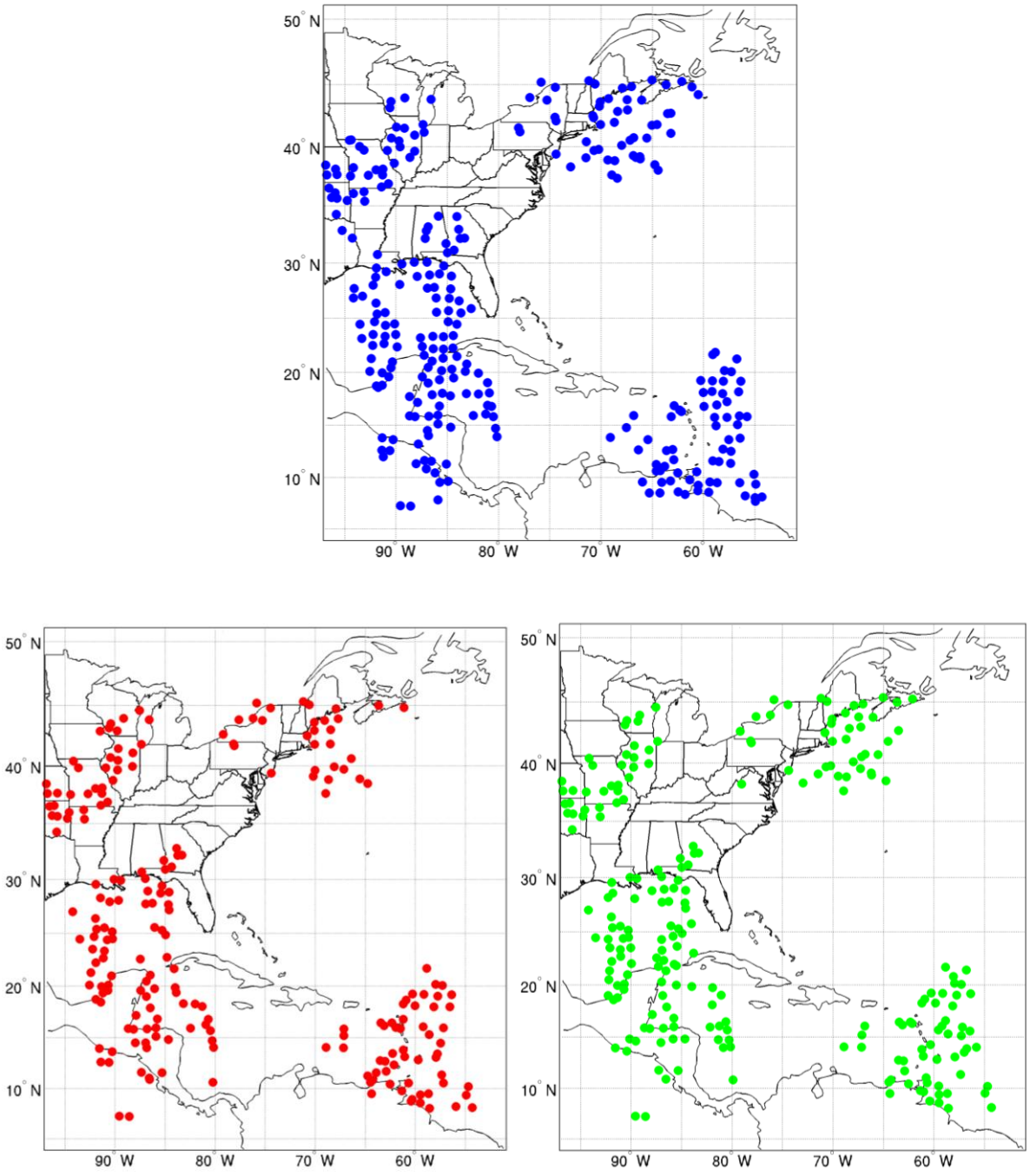

Figure 6.3 The locations at 1800 UTC 26 October 2012 where AIRS channel 210 (709.5659 cm^{-1}) is assimilated in GSI for AIRS (GSI clr) (lower left red), AIRS (MOD clr) (upper blue) and AIRS (MOD cld-clr) (lower right green).

MODIS cloud detection removes the cloud contaminated FOVs that assimilated as clear FOVs in GSI stand-alone cloud detection. These AIRS FOVs can be cloud-cleared as equivalent clear radiances, and then assimilated as clear radiance of AIRS (MOD cld-clr) in the GSI system.

Figure 6.4 shows the temperature difference between AIRS (MOD cld-clr) and AIRS (GSI clr) (AIRS (MOD cld-clr) minus AIRS (GSI clr)) at 0-hour, 24-hour, 48-hour and 72-hour forecast time, with geopotential height of AIRS (MOD cld-clr) at 500 hPa. The temperature difference between AIRS (MOD cld-clr) and AIRS (GSI clr) shows that AIRS (MOD cld-clr) is colder near the northeast of the U.S. continent, and varyingly warmer and colder at the northern part of South America (Figure 6.4(a)). These regions are consistent with the regions that assimilated different AIRS data sets in Figure 6.3. So the assimilation of AIRS with different data sets can directly affect the temperature fields. With the accumulated forecast time, the difference of temperature fields becomes larger. For the 24-hour forecast (Figure 6.4 (b)) and the 48-hour forecast (Figure 6.4 (c)), the temperature difference between AIRS (GSI clr) and AIRS (MOD cld-clr) is larger than that at 0-hour forecast. The regions of the difference are quite close to the hurricane center, which is different from the 0-hour forecast. At the 0-hour forecast, the regions of temperature difference are in the surrounding area of the hurricane vortex, not the hurricane center. With the accumulated forecast time, the temperature difference begins to affect the hurricane center, which could further affect the other dynamic parameters, such as geopotential height and sea level pressure. For the 72-hour forecast (Figure 6.4 (d)), the temperature difference between AIRS (GSI clr) and AIRS (MOD cld-clr) is nearly 5K, which is much larger than the previous forecast time. The temperature of AIRS (MOD cld-clr) is warmer southeast of the hurricane center, and colder northwest of the hurricane center. AIRS (MOD cld-

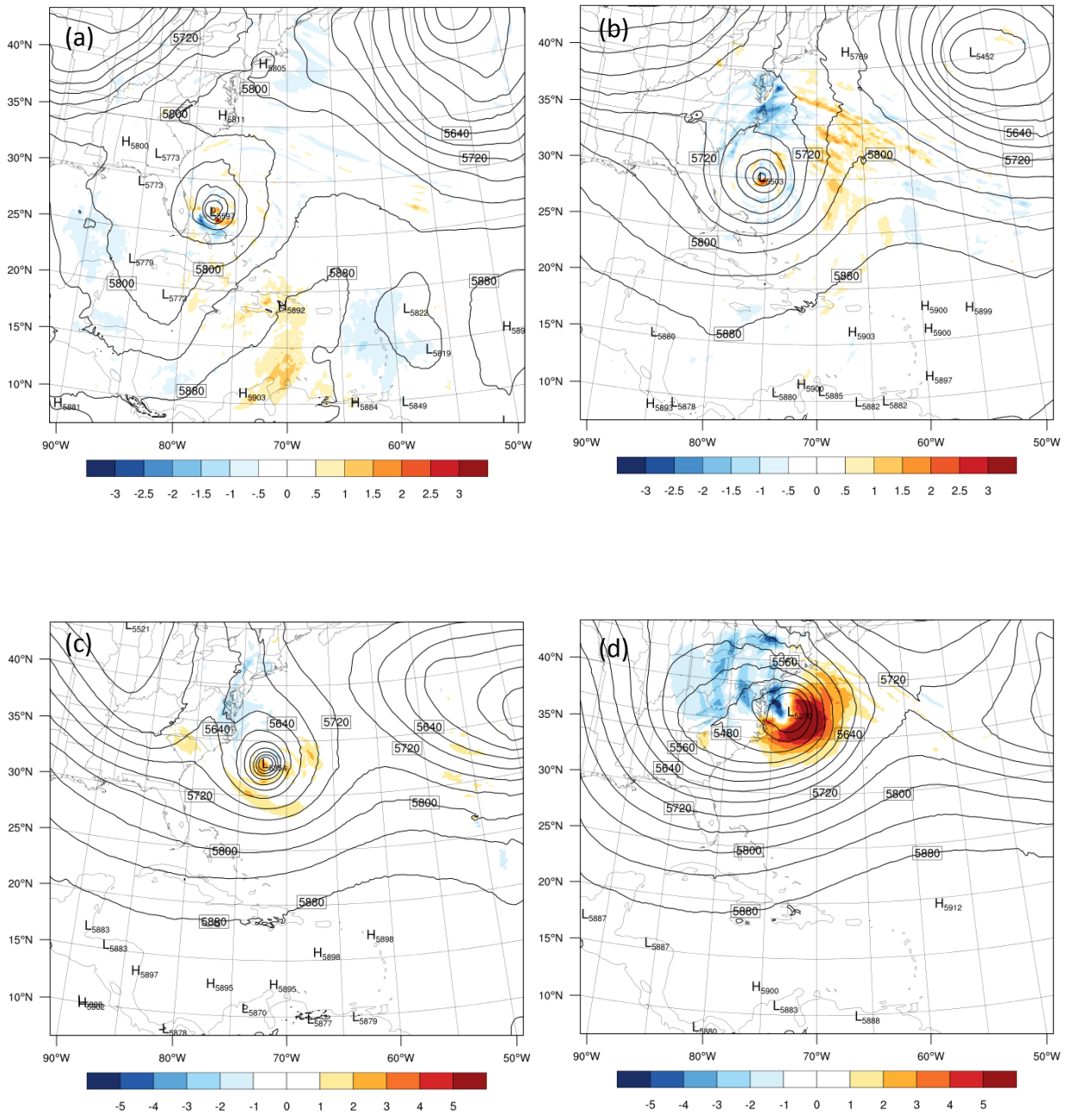

Figure 6.4 The difference in temperature (shaded, unit: K) between AIRS (MOD cld-clr) and AIRS (MOD clr) with geopotential height (contour, unit: m) of AIRS (MOD cld-clr) at 500 hPa for 0-hour forecast (a), 24-hour forecast (b), 48-hour forecast (c) and 72-hour forecast (d) from 1800 UTC 26 October 2012.

clr) minus AIRS (MOD clr) has the similar pattern. It is also indicated that the impacts from different AIRS data set is more significant with longer forecast time.

6.3 Sea level pressure, surface wind and the surface radar reflectivity

The surface pressure and surface wind are important variables for both the hurricane structure and the atmospheric environments study. The surface wind can reflect the hurricane surface vortex structure, and the sea surface pressure can reflect the hurricane intensity. The simulated radar reflectivity is a variable to show the rainband and the rainfall intensity related to the hurricane event.

The sea level pressure, surface wind and the surface radar reflectivity at 0-hour, 24-hour, 48-hour and 72-hour forecast from 1800 UTC 26 October 2012 are shown in Figure 6.5. At 0-hour forecast, the surface variables are quite similar in the experiment of AIRS with GSI stand-alone cloud detection (Figure 6.5 (a)) and the experiment of AIRS with cloud-cleared radiances (Figure 6.5 (b)). The locations and the intensity of the radar reflectivity are also quite similar in the two experiments. At 24-hour forecast, the radar reflectivity is a little bit different in the center of the hurricane. The radar reflectivity in the hurricane center of AIRS (MOD cld-clr) (Figure 6.5 (d)) is stronger than the hurricane center of AIRS (GSI clr) (Figure 6.5 (c)). At 48-hour forecast, the radar reflectivity of the two experiments has large difference. The AIRS (MOD cld-clr) (Figure 6.5 (f)) has much stronger radar reflectivity compared to the AIRS (GSI clr) (Figure 6.5 (e)). There is a large area at the northwest of the hurricane center of AIRS (GSI clr) has no radar reflectivity, which indicates that the intensity of the hurricane is weaker than AIRS (MOD cld-

clr). Till the 72-hour forecast, the asymmetric structure of AIRS (GSI clr) (Figure 6.5 (g)) is more obvious, the no reflectivity region is at the north of the hurricane center. The reflectivity of AIRS (MOD cld-clr) (Figure 6.5 (h)) is much stronger in the center of hurricane than the center of AIRS (GSI clr). The hurricane center of AIRS (MOD cld-clr) is at around west 73.5° longitude, which is on the eastward of the hurricane center of AIRS (GSI clr). This is consistent with the 72-hour hurricane track forecast in Figure 6.1.

From the surface radar reflectivity, it shows that from 24-hour forecast, especially after 48-hour forecast, the reflectivity of AIRS (GSI clr) in the hurricane center is weaker than AIRS (MOD cld-clr), so the hurricane intensity of AIRS (GSI clr) is weaker than AIRS (MOD cld-clr). The dry area with no radar reflectivity regions is much larger in AIRS (GSI clr) than AIRS (MOD cld-clr). At 72-hour forecast, the hurricane center of AIRS (GSI clr) is on the northwest side of the hurricane center of AIRS (MOD cld-clr).

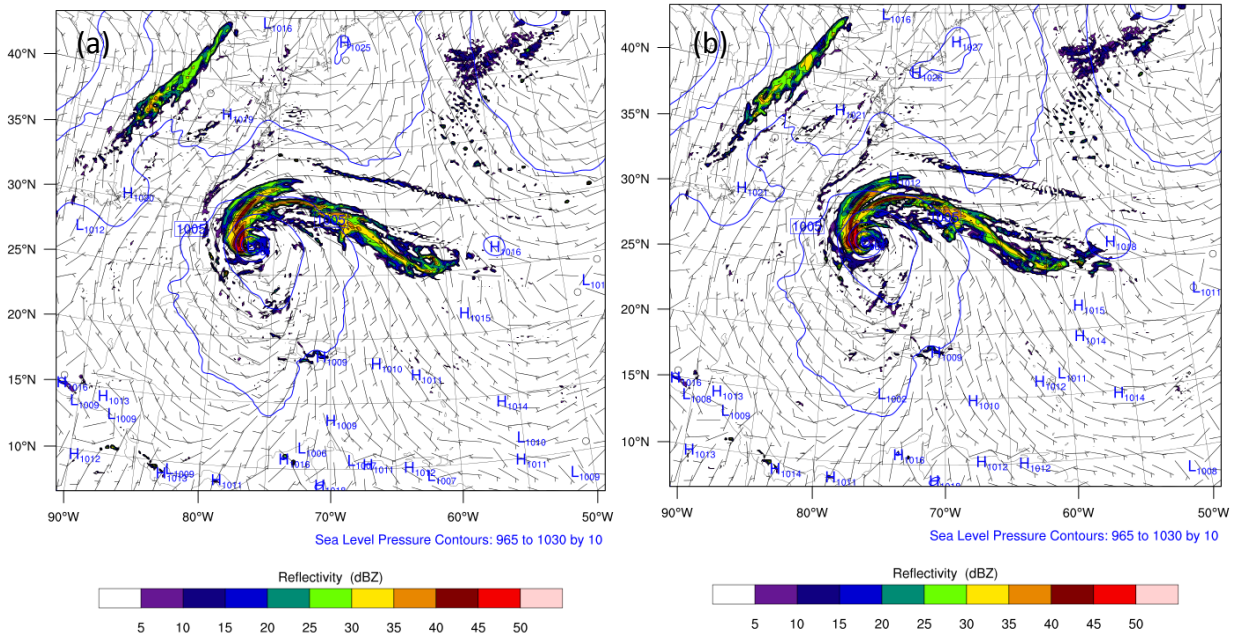

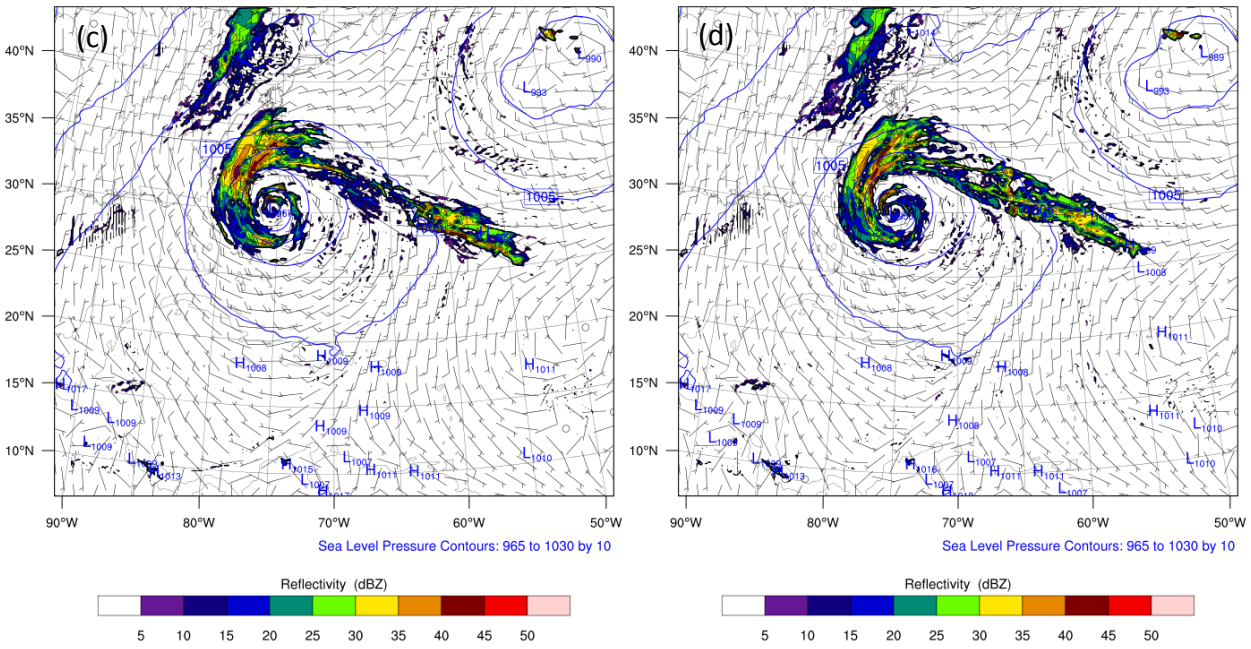
(c)
(d)
40°N
35°N
30°N
25°N
20°N
15°N
10°N
90°W
80°W
70°W
60°W
50°W
Sea Level Pressure Contours: 965 to 1030 by 10
Reflectivity (dBZ)
5 10 15 20 25 30 35 40 45 50

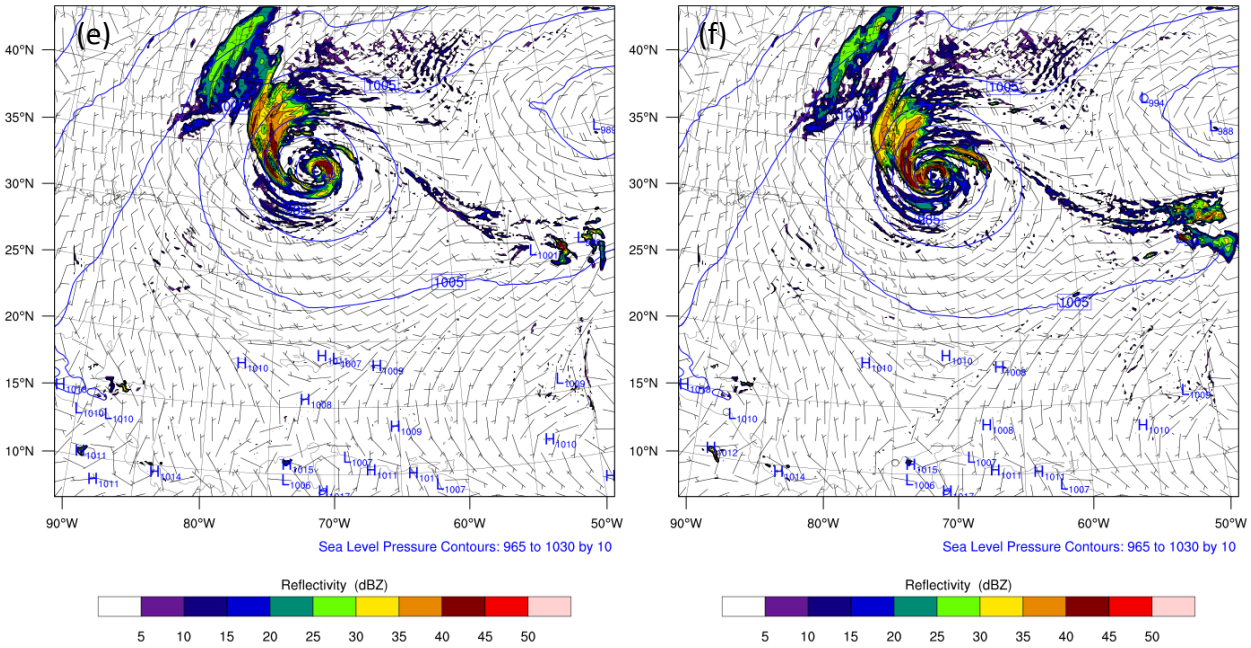
(e)
(f)
40°N
35°N
30°N
25°N
20°N
15°N
10°N
90°W
80°W
70°W
60°W
50°W
Sea Level Pressure Contours: 965 to 1030 by 10
Reflectivity (dBZ)
5 10 15 20 25 30 35 40 45 50

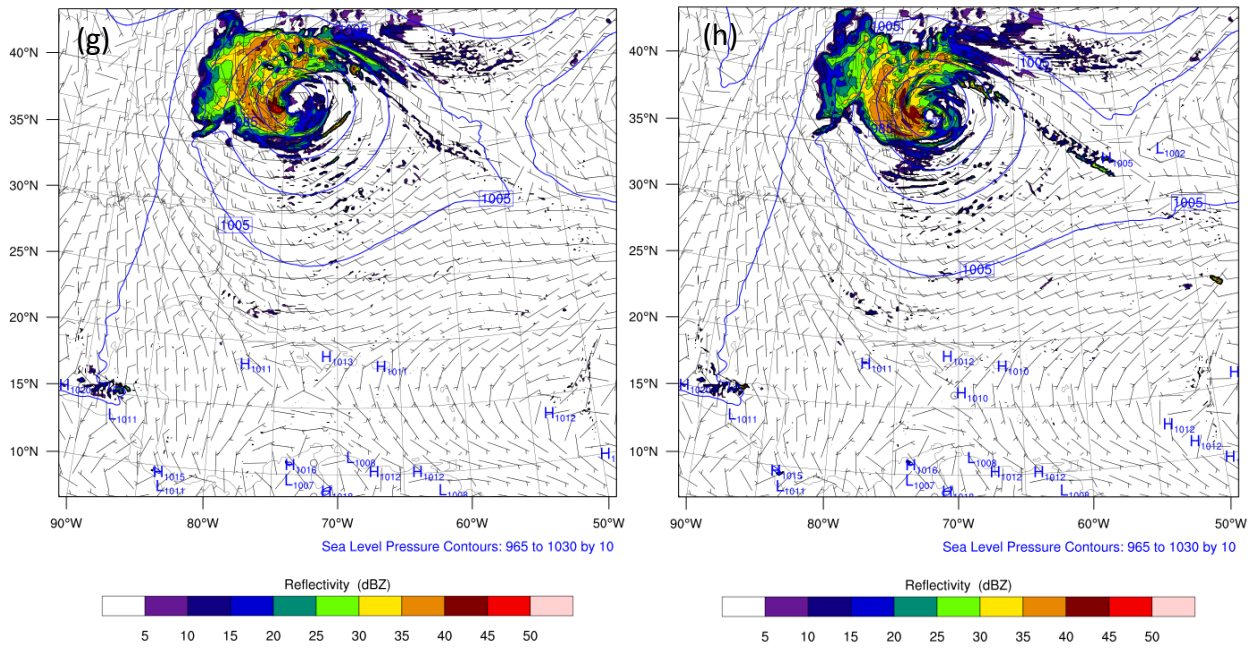

Figure 6.5 The surface radar reflectivity (shaded, unit: dBz), sea level pressure (contour, unit: hPa) and surface wind (vector, unit: m/s) of AIRS (GSI clr) ((a) (c) (e) (g)) and AIRS (MOD cld-clr) ((b) (d) (f) (h)) for 0-hour forecast ((a) (b)), 24-hour forecast ((c) (d)), 48-hour forecast ((e) (f)), and 72-hour forecast ((g) (h)) from 1800 UTC 26 October 2012.

6.4 The temperature fields, winds and geopotential height on 850 hPa

After discussed the variables at the surface level and on 500 hPa, the temperature fields, wind structures and the geopotential heights on 850 hPa are discussed in this section (Figure 6.6). The temperature fields at 0-hour forecast time of AIRS (GSI clr) (Figure 6.6 (a)) and AIRS (MOD cld-clr) (Figure 6.6 (b)) is similar, but there are some differences in the surrounding area away from the hurricane vortex. This difference also can be seen on the 500 hPa temperature fields, and it is believed that the difference of the temperature fields at 0-hour forecast time is from the

impacts of assimilated different AIRS data sets. The data coverage between AIRS (GSI clr) and AIRS (MOD cld-clr) are different (Figure 6.3). The temperature and moisture information from the assimilated AIRS radiances is different, which directly affect the temperature fields at the analysis time. For 24-hour forecast, the temperature fields in the environment area are similar in the two experiments. Compared to AIRS (GSI clr) (Figure 6.6 (e)), the geopotential height of hurricane center of AIRS (MOD cld-clr) (Figure 6.6 (f)) is more symmetric, and the temperature of hurricane center of AIRS (MOD cld-clr) is warmer at the 48-hour forecast. Based on the pattern of temperature and geopotential height on 850 hPa, the hurricane structure of AIRS (GSI clr) is not a typical barotropic structure. At 72-hour forecast, the temperature differences between the two experiments are very obvious. A mature hurricane has a minimum sea level pressure center with a warm-core structure (Ooyama 1969; Kurithrara and Tuleya, 1974; Merrill, 1988). The temperature at the hurricane center of AIRS (GSI clr) (Figure 6.6 (g)) is cooler than AIRS (MOD cld-clr) (Figure 6.6 (h)). For AIRS (MOD cld-clr), the warm center is consistent with the minimum geoportal height. The hurricane center locations of the two experiments are different, which is very similar to the SLP in Figure 6.5. The warmer temperature and lower geopotential height of AIRS (MOD cld-clr) is further southeast compared to AIRS (GSI clr). This difference indicates that the hurricane center of AIRS (MOD cld-clr) is on the southeast of the hurricane center of AIRS (GSI clr). The structure of the AIRS (MOD cld-clr) still keeps the hurricane characters well for the 72-hour forecast, but the hurricane structure of AIRS (GSI clr) is less barotropic and moving faster. Compared the 72-hour simulated hurricane tracks to the best track from NHC (Figure 6.1) at 1800 UTC on 29 October, the hurricane center of AIRS (MOD cld-clr) is on the southeast side of the hurricane center of AIRS (GSI clr). The track error of AIRS (MOD

cld-clr) at 72-hour forecast is around 40 km smaller than the track error of AIRS (GSI clr) (Figure 6.2).

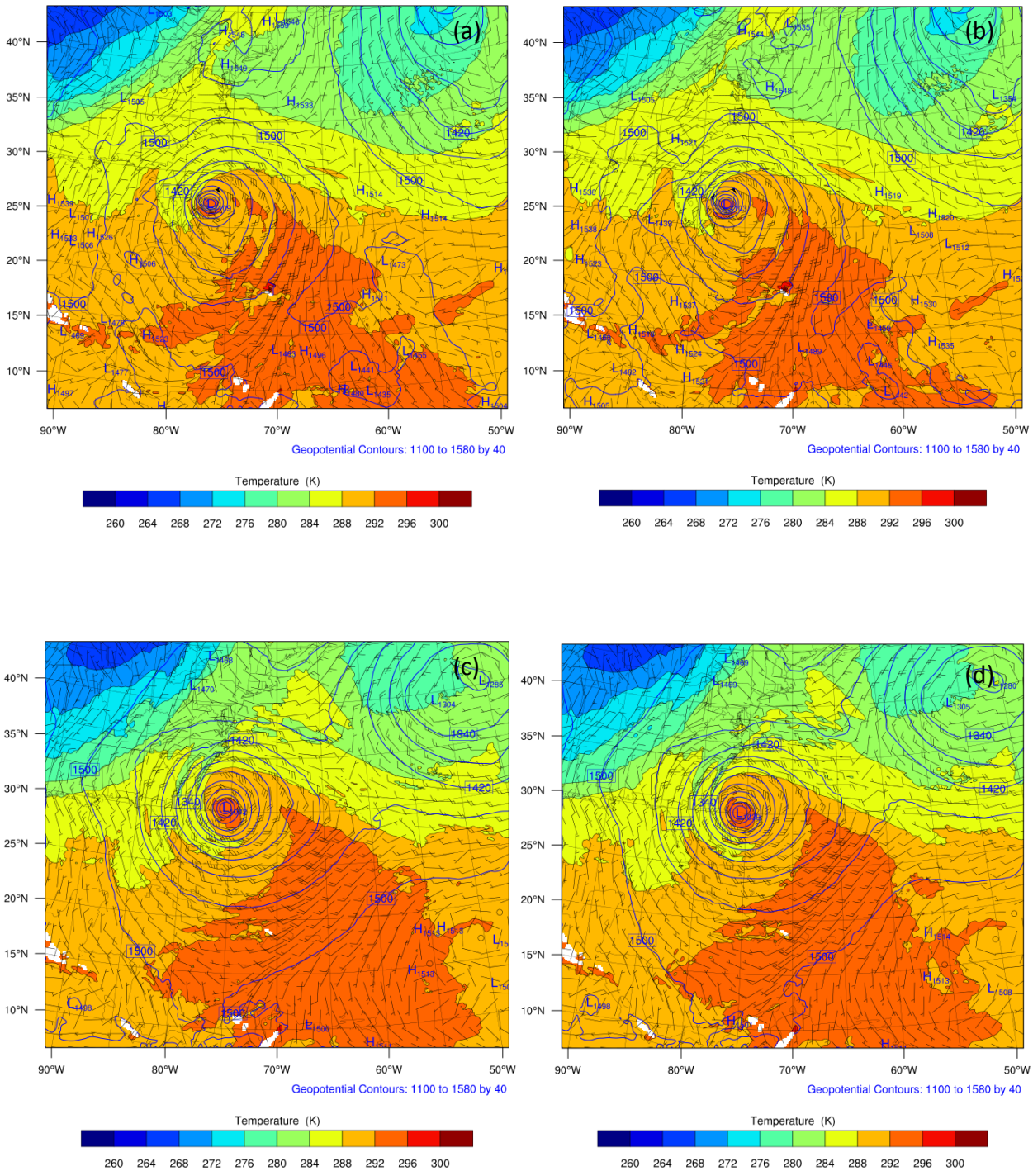

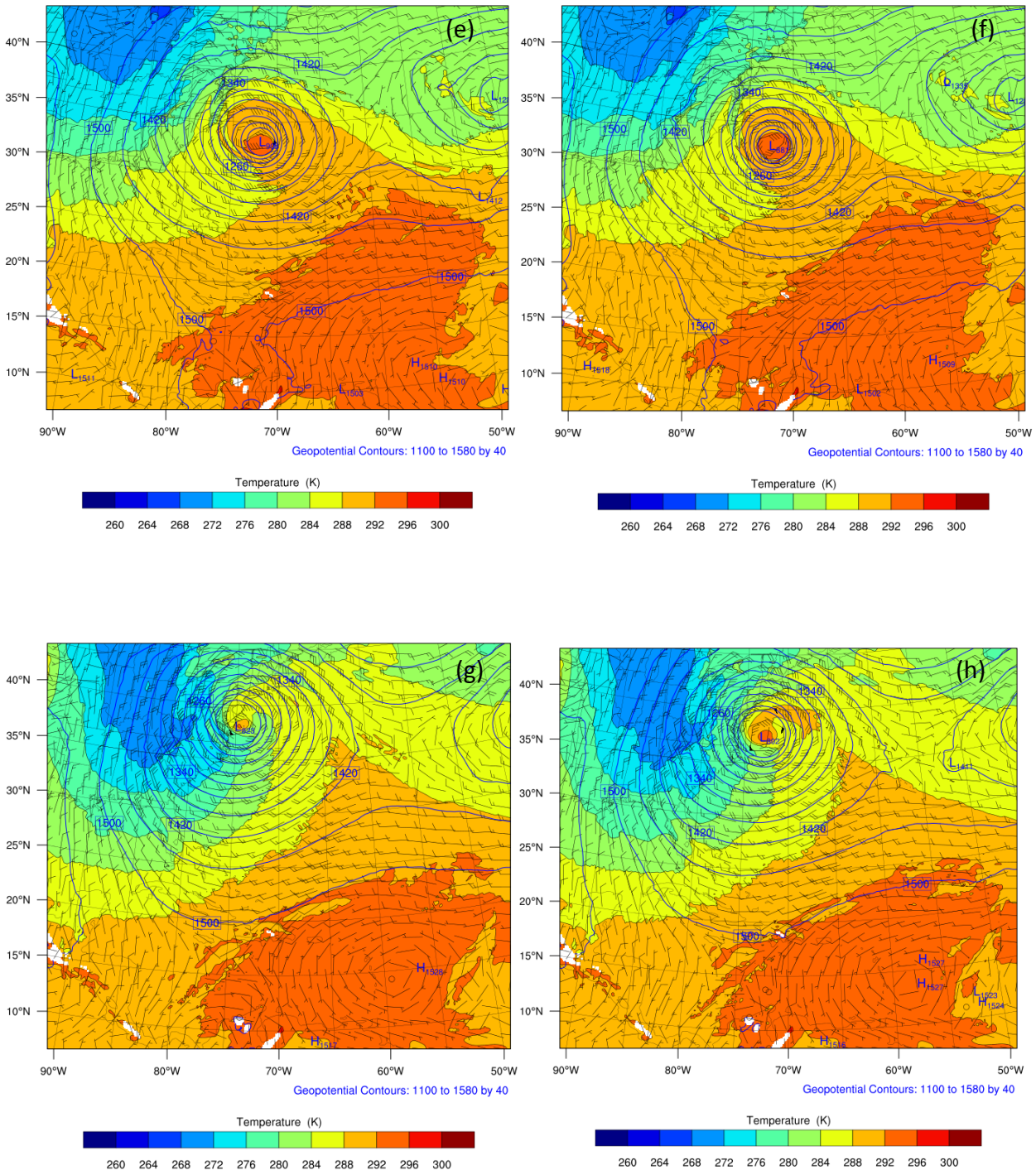

Figure 6.6 The temperature fields (shaded, unit: K), geopotential height (contour, unit: m) and winds (vector, unit: m/s) on 850 hPa of AIRS (GSI clr) ((a) (c) (e) (g)) and AIRS (MOD cld-clr) ((b) (d) (f) (h)) for 0-hour forecast ((a) (b)), 24-hour forecast ((c) (d)), 48-hour forecast ((e) (f)), and 72-hour forecast ((g) (h)) from 1800 UTC 26 October 2012.

6.5 The potential vorticity and the winds on 200 hPa

The potential vorticity (PV) has been used to be a powerful tool for understanding the dynamics of quasi-balanced atmospheric systems (Shapiro and Franklin, 1995). It is a broad used diagnostic variable in the study of mid-latitude weather systems. Based on the definition, PV is conserved following the motion in adiabatic frictionless flow (Holton, 2014). The maxima of PV at a certain level in the atmosphere represent the intrusion of dry air from the upper tropospheric or stratospheric levels into the lower troposphere. The dry air from the upper troposphere is always cold comparing to the lower tropospheric atmosphere. Tracing PV is a good way to track the movement of the cold and dry air.

Figure 6.7 shows the wind vectors and PV on 200 hPa for 0-hour, 24-hour, 48-hour and 72-hour forecasts from 1800 UTC 26 October. The shaded area indicates the PV larger than 2PVU. At 0-hour forecast time, the PV and wind structures of AIRS (GSI clr) (Figure 6.7 (a)) and AIRS (MOD cld-clr) (Figure 6.7 (b)) are very similar. There are two large PV regions (PV is larger than 6 PVU), or two cold dry air sources, at the northwest area and the northeast area of the model domain. At 24-hour, the shaded PV is slightly different between the two experiments (Figure 6.7 (c) and (d)). From the movement of PV, it shows that PV is moving anticlockwise with winds from the north of the hurricane to the southwest of the hurricane. The movement of PV indicates the movement of the cold and dry air, which is also moving from the north to the southwest of the hurricane. At 48-hour forecasting time, the difference between the two experiments is becoming larger. More cold and dry air is brought to the south and southeast of the hurricane. For AIRS (GSI clr) (Figure 6.7 (e)), the PV larger than 4 PVU is found at the eastside of the hurricane vortex, and the PV larger than 2 PVU at the eastside of the hurricane

vortex is between 62° - 70° west longitude. For AIRS (MOD cld-clr) (Figure 6.7 (f)), the PV larger than 2 PVU at the eastside of the hurricane vortex of is between 60.5° - 67° west longitude. So the large PV of AIRS (GSI clr) is more westward compared to the large PV of AIRS (MOD cld-clr). At the 72-hour forecast, the PV continues moving to the south and southeast of the hurricane vortex. For AIRS (GSI clr) (Figure 6.7 (g)), the PV at the eastside of the hurricane vortex has strong connection with the large PV at the northwest of the model domain, and the PV at the eastside is from 65° west longitude. For AIRS (MOD cld-clr) (Figure 6.7 (h)), the PV at the eastside of the hurricane vortex is connected with both the large PV from northwest and northeast of the model domain, and the PV at the eastside is from 70° west longitude.

The movement of PV represents the cold and dry air movement. The whole 72-hour forecast indicates that the large PV moves from the northwest to the south and east of the hurricane vortex. The cold and dry air is moving in the same path from the northwest to the south and east of the hurricane vortex. The cold air moves in and destroys the hurricane structure. Compared to AIRS (MOD cld-clr), the PV at the east of the hurricane vortex of AIRS (GSI clr) is higher and the location is from 65° west longitude, which indicates that the cold air of AIRS (GSI clr) is stronger and the 5° westter. The stronger cold air of AIRS (GSI clr) pushes the hurricane vortex moving to the northwest, which makes the center of the hurricane is on the northwest side of AIRS (MOD cld-clr) (Figure 6,1).

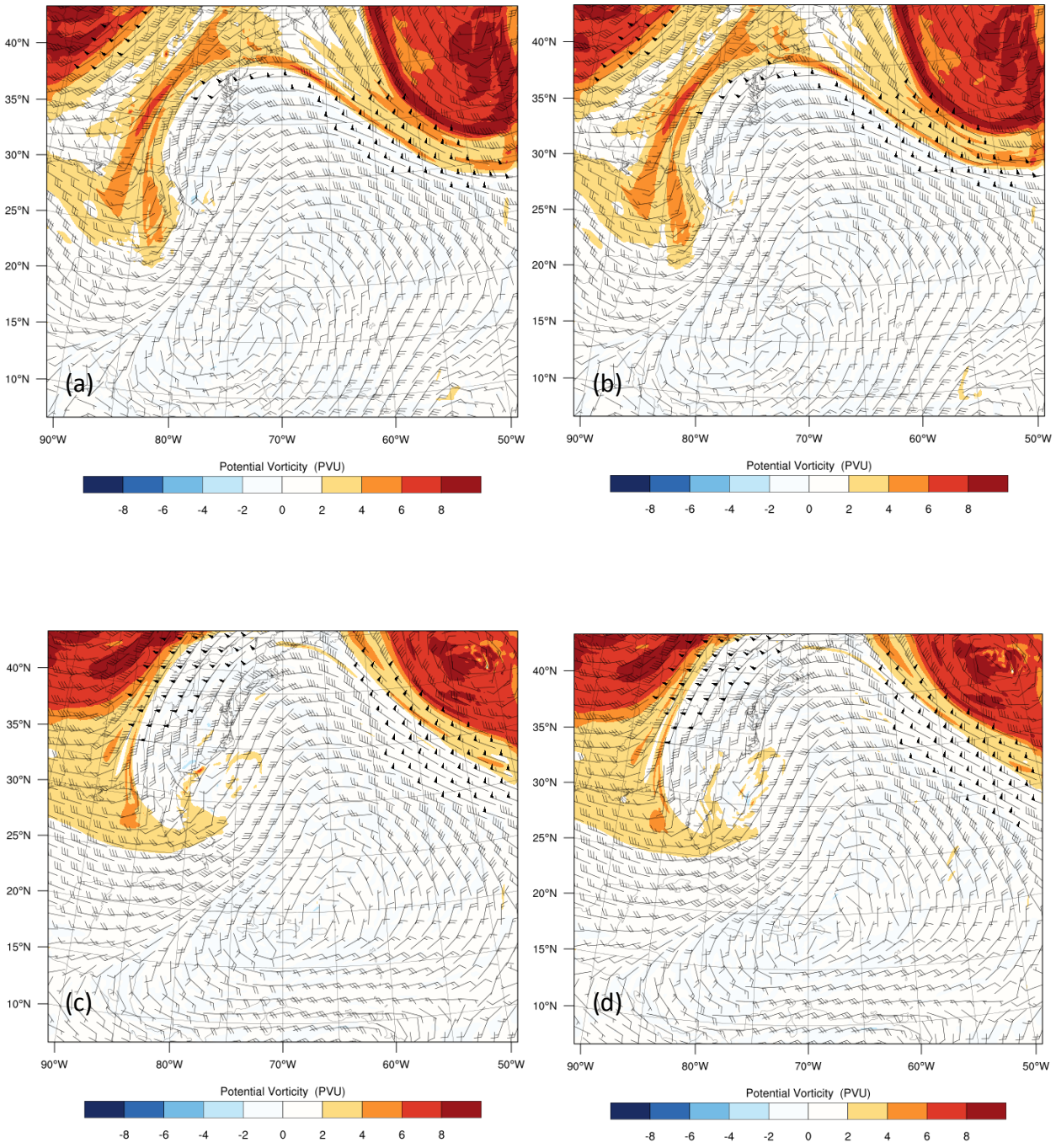
(a)
(b)
(c)
(d)
40°N
35°N
30°N
25°N
20°N
15°N
10°N
90°W
80°W
70°W
60°W
50°W
Potential Vorticity (PVU)
-8
-6
-4
-2
0
2
4
6
8

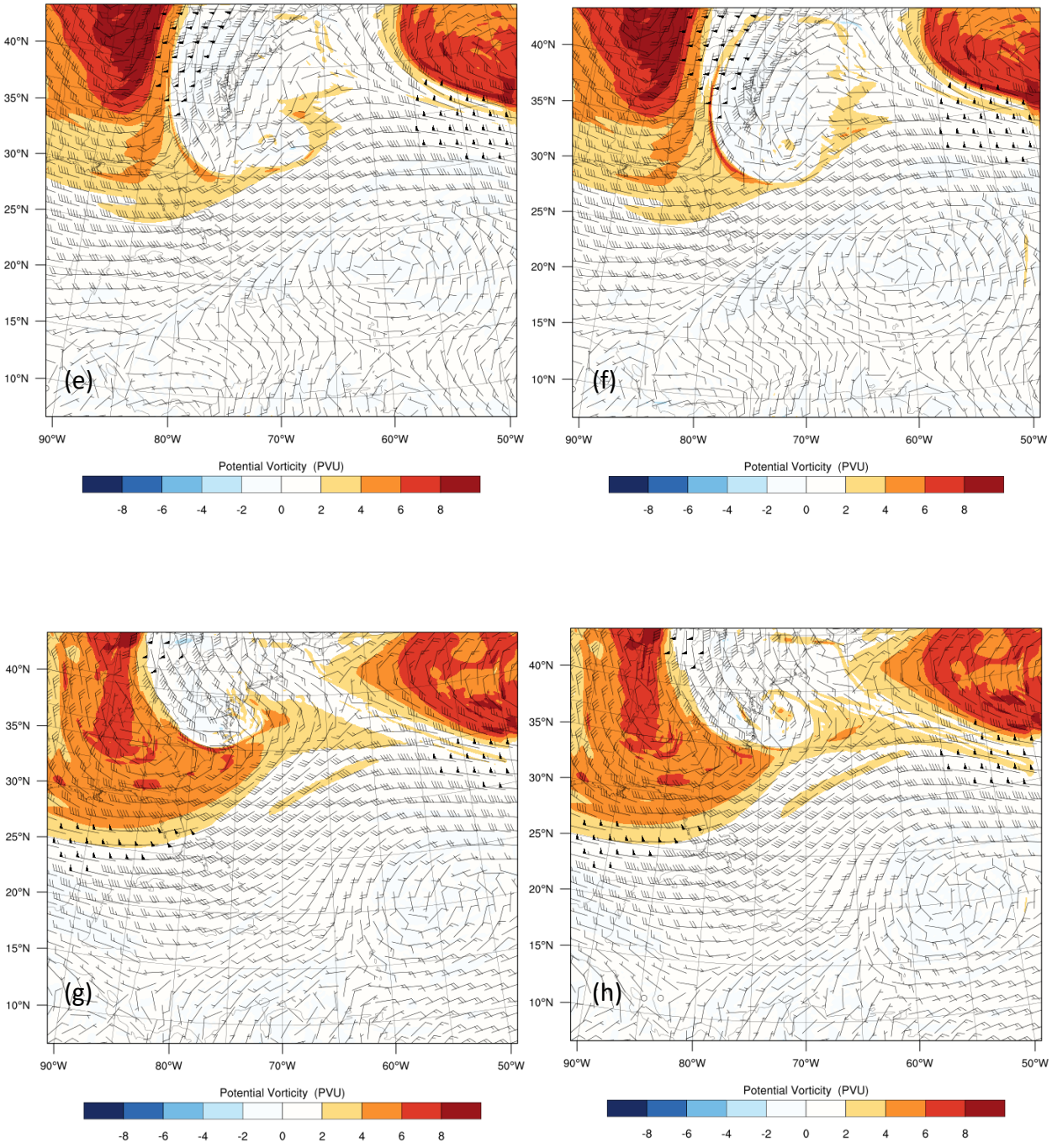

Figure 6.7 The potential vorticity (shaded, unit: PVU) and winds (vector, unit: m/s) on 200 hPa of AIRS (GSI clr) ((a) (c) (e) (g)) and AIRS (MOD cld-clr) ((b) (d) (f) (h)) for 0-hour forecast ((a) (b)), 24-hour forecast ((c) (d)), 48-hour forecast ((e) (f)), and 72-hour forecast ((g) (h)) from 1800 UTC 26 October 2012.

6.6 Summary

To better understand the impacts of different AIRS data set on the hurricane dynamics and the atmospheric environmental structures, the temperature, winds, geopotential heights, PV and etc. on different pressure levels are discussed in this chapter. One of the 72-hour forecasts of Hurricane Sandy (2012), the 72-hour forecast from 1800 UTC 26 October, is used as the case study to analyze the atmospheric structures.

The assimilated AIRS data coverages from AIRS (GSI clr), AIRS (MOD clr) and AIRS (MOD cld-clr) are compared, and the temperature difference on the 500 hPa between AIRS (GSI clr) and AIRS (MOD cld-clr) is further discussed to understand the impacts of the assimilated AIRS data on the temperature fields. It is shown that the assimilated AIRS data could directly affect the temperature fields on 500 hPa. Since the AIRS data are under clear or partially cloudy regions, the assimilated AIRS data affect the temperature fields outside the hurricane regions at 0-hour forecast. With the accumulated forecast time, the differences from the temperature in the hurricane environmental regions are transferring to affect the center of the hurricane. At the 72-hour forecast time, the temperature difference is in the hurricane center as large as 5 K. The temperature of AIRS (MOD cld-clr) is warmer southeast of the hurricane center, and colder northwest of the hurricane center.

The simulated surface radar reflectivity represents the rainband and rainfall intensity around the hurricane center. The comparison of the radar reflectivity indicates that the rainfall of AIRS (GSI clr) is weaker than the rainfall of AIRS (MOD cld-clr). For AIRS (GSI clr), there are more dry air moving into the northeast of the hurricane center, which also degrades the hurricane intensity and the hurricane structure. The comparison of 850 hPa temperature fields shows that

the temperature of hurricane eye is warmer of AIRS (MOD cld-clr) than AIRS (GSI clr). And the hurricane center of AIRS (GSI clr) is on the northwest side of AIRS (MOD cld-clr), which is consistent with the track forecast.

Since PV is an important variable to trace the movement of cold and dry air, PV and wind on 200 hPa is analyzed in this chapter. The PV pattern of the two experiments are quite similar at 0-hour forecast, there are two big PV large centers (PV larger than 6 PVU) at the northwest and the northeast area. The high PV is moving with winds from the northwest to the west, south and east of the hurricane vortex. With the accumulated forecast time, the difference of PV in the two experiments is becoming larger. At 72-hour forecast, the high PV is moving to the east of the hurricane vortex. The PV of AIRS (GSI clr) is 2 PVU larger than AIRS (MOD cld-clr), which indicates the cold air moving to the eastside of the hurricane vortex is stronger than AIRS (GSI clr). The location of PV at the east of hurricane vortex is from 65° west longitude of AIRS (GSI clr), and the location of PV is from 70° west longitude of AIRS (MOD cld-clr). The strong cold and dry air moving into the hurricane vortex of AIRS (GSI clr) degrades the hurricane structure, and pushes the hurricane northwestwards, which makes the hurricane center of AIRS (GSI clr) is on the northwest side of the hurricane center of AIRS (MOD cld-clr).

The assimilation of cloud-cleared radiances can remove the cloud contamination and provide the thermodynamic information under partially cloudy regions. Through the comparison of the atmospheric variables and the hurricane structures between AIRS (GSI clr) and AIRS (MOD cld-clr), it is shown that the assimilation of AIRS cloud-cleared radiances directly affect the atmospheric fields in the environments outside the hurricane center at the analysis time. With the accumulated forecast time, the impacts from the environments are transferring to the center of the hurricane, and then further affect the speed of hurricane moving and the hurricane center

locations. For the assimilation of AIRS cloud-cleared radiances, the cold air from both the surface level and on the 200 hPa is moving slower and weaker than the results using GSI stand-alone cloud detection method. The hurricane warm core and the radar reflectivity of AIRS (MOD cld-clr) are stronger than AIRS (GSI clr). The differences between the two experiments are from the different assimilated AIRS data set. The differences from the environmental fields largely affect the atmospheric fields in the hurricane center with the forecast time accumulation.

Chapter 7

Conclusions and future perspectives

It is generally agreed that the role of satellite observations is becoming important for both operational weather forecasts and the atmospheric research studies. Data assimilation is the key step to connect the satellite observations with the weather forecasts. The assimilation of the satellite observations has great progress since late 20^{th} century. The contributions from satellite data, especially from IR and MV sounders are the largest in operational centers. There are still some spaces to improve the satellite data assimilation, especially under cloudy skies. This dissertation focuses on the cloud detection and cloud-cleared IR radiances assimilation under cloudy skies in the regional NWP model.

The contributions of the satellite observations are from the clear radiances assimilation. The core parts of data assimilation model, such as the control vectors, the radiative transfer model, the background and observation error covariance, and etc., are suitable for the clear radiances assimilation. Therefore, the cloud detection is an important step of satellite data assimilation. The current cloud detection method is based on the first-guess check, but this method has potential risk of assimilating cloudy radiances as clear skies. In this dissertation, a new cloud detection method is applied on the IR radiances assimilation. The new cloud detection method is collocated the high spatial imager resolution cloud mask on the IR FOV and helps the

IR radiances remove cloud FOV. MODIS and AIRS are onboard the same platform, MODIS can provide cloud properties and high spatial resolution cloud mask. Collocated MODIS cloud mask on AIRS FOVs and removes the cloud contained FOVs, and then the clear AIRS FOV is kept to assimilate in the models. Since CrIS and VIIRS are onboard the same platform, this cloud detection method can also be applied on CrIS/VIIRS cloud detection. The data coverage with GSI stand-alone cloud detection method and the sub-pixel cloud detection method are compared for AIRS channel 120 and 1447 and CrIS channel 96. The data coverage shows that the stand-alone cloud detection allows more cloud-contaminated radiances into the GSI system. So with sub-pixel cloud detection, few but high quality of the clear radiances are assimilated. Compared to the GSI stand-alone cloud detection, the cold bias and wet bias are moved out from the analysis fields with sub-pixel cloud detection. With the better analysis fields, the hurricane track forecasts are improved using the sub-pixel cloud detection method.

The reliable cloud detection is essential for data assimilation. Using the strict collocated cloud mask detection algorithm, the high-quality clear radiances are ensures to assimilate in the models. A limitation, however, is a reduction in the number of observations. The cloudy regions are forecast sensitive regions that include useful thermodynamic and hydrometric information for weather forecast. However, direct assimilation of the cloudy IR radiances will continue to be challenging before we can link more adequately model cloud parameters and equivalent radiance observations. The assimilation of cloud-cleared radiances is an alternative way to use the information under partially cloudy regions. The cloud-cleared radiance is to calculate the clear equivalent radiance under partially cloudy regions. Therefore, the cloud-cleared radiance can be directly assimilated in the current data assimilation models as clear radiance.

Three experiments of AIRS radiances with different data set are compared: AIRS using GSI stand-alone cloud detection, AIR (GSI clr); AIRS using MODIS cloud mask detection, AIRS (MOD clr); and AIRS using MODIS cloud mask detection plus the cloud-cleared radiances, AIRS (MOD cld-clr). The temperature difference of analysis fields indicates that the assimilation of AIRS data can directly affect the temperature fields. Since the assimilated data are clear radiances or cloud-cleared radiances, the temperature difference regions are in the surrounding area of hurricane vortex. The comparison of the temperature profiles and radiosondes represent that the temperature impacts on different vertical levels are different. In general the temperature BIAS and STD is smallest for AIRS (MOD cld-clr) in the mid and low troposphere. The hurricane track error at the analysis time is discussed to study the simulated hurricane locations. In general the hurricane track error is between 20 km to 130 km, which indicates that the simulated hurricane locations are close to the observations. The difference of the hurricane locations using the three data sets is subtle in the first analysis time. With more cycling experiments, the difference of the track error is becoming obvious among the three groups data sets.

The difference of the BIAS and STD of simulated temperature in the three groups of experiments is small at 24-hour forecast, but it grows with the accumulated forecast time. At 720hour forecast, the temperature BIAS and STD of AIRS (MOD cld-clr) is around 0.3 K smaller than AIRS (GSI clr). For the hurricane track and intensity forecast, the AIRS (MOD cld-clr) gives the smallest hurricane track RMSE, but the impact on the hurricane intensity is neutral using the three data sets. The track error reduces 10 to 50 km with assimilation of AIRS (MOD cld-clr) compared to the assimilation of AIRS (GSI clr). Due to the assimilated AIRS are under clear and partially cloudy regions, which mostly come from the environmental regions and

contain little information about the cloudy region (i.e. hurricane vortex). Therefore, the improvement of assimilating AIRS radiances is on hurricane track forecast, but natural impacts on the hurricane intensity.

To better understand how the assimilation of the AIRS clear radiances and the AIRS cloud-cleared radiances affects the environment and the hurricane structures, one of the 72-hour forecasts of Hurricane Sandy (2012), the 72-hour forecast from 1800 UTC 26 October, is selected as the case study. The analysis of the atmospheric variables focuses on the results of AIRS (GSI clr) and AIRS (MOD cld-clr). From the comparison of the temperature fields, it is found that the assimilated AIRS data can directly affect the temperature fields at the 0-hour forecast, or the analysis time. Since the assimilated AIRS data are clear radiances or equivalent clear radiances, the data are in the surroundings away from the hurricane vortex. The temperature difference is at the surrounding are away from the hurricane vortex at the 0-hour forecast. With the long time forecasting, the temperature difference is from the surrounding area to the hurricane center. At 72-hour forecast, the temperature difference on 500 hPa of AIRS (GSI clr) and AIRS (MOD cld-clr) is very obvious.

Based on the analysis of the surface radar reflectivity, it is found that more dry air moves into the northeast of the hurricane center of AIRS (GSI clr), which weakens the hurricane intensity. The radar reflectivity in the hurricane center is stronger of AIRS (MOD cld-clr) than AIRS (GSI clr). The pattern of 850 hPa temperature and geopotential height also reflects that the warm core of AIRS (MOD cld-clr) is stronger than AIRS (GSI clr). The minimum geopotential height of AIRS (MOD cld-clr) is on the southeast side of the minimum geopotential height of AIRS (GSI clr) at 72-hour forecast, which is consistent with the simulated track forecast.

The movement of high PV on 200 hPa is following the wind anticlockwise from the west to the south and southeast of the hurricane vortex. At 72-hour forecast time, the strong cold and dry air moving into the hurricane vortex of AIRS (GSI clr) degrades the hurricane intensity, and pushes the hurricane northwestwards, which makes the hurricane center of AIRS (GSI clr) is on the northwest side of the hurricane center of AIRS (MOD cld-clr). So for AIRS (GSI clr), the cold and dry air from both the surface and the upper troposphere move into the hurricane center, and then weakened the hurricane intensity.

From the analysis of the atmospheric fields, it is interesting that the impacts from the assimilation of AIRS radiances slightly adjust the surrounding temperature fields away from the hurricane center at 0-hour forecast. With the longer forecast time, the adjustment from the surrounding area is moving into the hurricane center, and the small difference is becoming more significant. The large difference in the hurricane center makes the hurricane track and intensity different at 72-hour forecast.

Although the cloud-cleared radiances can improve the yield of radiance assimilation, for example, expand radiance assimilation to partly cloudy cover, there are still some limitations that need to be considered in radiance assimilation. First, the cloud-cleared radiances have amplified instrument noise depends on the cloudiness of the FOV to be cloud-cleared, usually this can be taken into account by increasing the observation error in radiance assimilation; Second, atmospheric temperature and moisture might have inhomogeneity in partly FOV, especially for moisture, since the moisture in clear portion and cloudy portion within one sub-pixel might be different; Third, the correlated errors both spectrally and spatially should be represented in assimilation but are difficult to quantify. So these limitations would affect the results of the assimilation of cloud-cleared radiances.

For the future research plan, the cloud detection method can be further improved with the combination of clear channel detection (McNally and Watts, 2003) and clear pixel detection (English et al., 1999; Li et al., 2004; Wang et al., 2014). The clear channel detection is assimilated the channels that not affected by clouds, this method is based on the background fields. For high spectral IR sounders, the clear channel detection can keep more data assimilated into the models, especially for the upper channels. But there is the potential risk of miss assimilating the observed cloudy radiances as clear radiances. The clear pixel detection is collocated the cloud mask on IR sounders, which is based on the observations. So this would avoid the miss assimilating of the cloudy radiances into the models. But if the FOV is contaminated by clouds, the whole FOV is removed even for the channels with weighting function peak in the stratosphere. So the combined clear channel detection and the clear pixel detection would keep the channels with high weighting function peak, and avoid the cloud contamination in the troposphere.

The ultimate goal for some operational centers is to directly assimilate the cloud-affected or all-sky radiances. The direct assimilation of cloud-affected radiances is a big improvement for global satellite data assimilation. But due to the less understood observation and background errors in cloudy and rainy situations, the uncertainties of the nonlinearity of the moisture physics process and some other issues, the direct assimilation of cloud-affected radiances is still hard to carry out. The direct assimilation of cloudy radiances relies on the improvement of RTM in cloudy skies. RTM used in the current operational assimilation is mainly a geometric model which assumes an effective cloud emissivity and an effective cloud-top (Vidot, 2015), which can be still useful with improvement on the predetermination of cloud-top pressure, for example, with help of collocated high resolution imager cloud-top pressure (Eresmaa, 2014). Ideally,

cloud particle absorption and scattering model (Wei et al., 2004) should be considered, but this model needs to be accurate on both radiance and Jacobian calculations for direct radiance assimilation in cloudy skies. Considering the current advancement on RTM with cloudy particle absorption and scattering in cloudy skies, the focus should be on radiance assimilation in single layer cloud situation (e.g., satellite sees single layer clouds), priority should be given to water cloud situations followed by ice cloud situations, therefore, IR sub-pixel cloud characterization from high resolution collocated imager cloud products is very important and has been recommended by the International TOVS Working Group (ITWG) to the NWP community at ITSC20 (27 October – 03 November, 2015 in Lake Geneva, Wisconsin, U.S.A) for radiance assimilation. The IR sounder subpixel cloud characterization can contain cloud fraction, cloud phase, cloud-top pressure, cloud type etc. for improving radiance assimilation in cloudy skies. Other alternative approaches include assimilation of cloud-cleared radiances, and/or assimilation of hydrometers (e.g., liquid water path, ice water path) (Jones and Stensrud, 2015; Chen et al., 2015) retrieved from satellite cloudy radiances. Research continues on cloudy radiances assimilation to improve the analysis fields and the forecast skills.

References

Ackerman, S. A., K. I. Strabala, W. P. Menzel, R. A. Frey, C. C. Moeller, and L. E. Gumley , 1998: Discriminating clear sky from clouds with MODIS, *J. Geophys. Res.*, 103, 32 141-32 157. doi: 10.1029/1998JD200032.

Aumann, H. H., M. T. Chahine, C. Gautier, M. D. Goldberg, E. Kalnay, L. M. McMillin, H. Revercomb, P. W. Rosenkranz, W. L. Smith, D. H. Staelin, L. L. Strow, and J. Suskind, 2003: AIRS/AMSU/HSB on the Aqua mission: design, science objectives, data products, and processing system. *IEEE Trans. Geosci. Remote Sens.*, 41, 253-264.

Avila, L. A., and J. Cangialosi, 2011: Hurricane Irene (AL092011) 21-28 August 2011, *Tropical Cyclone Report*, 1-45.

Baker, N., 2012: Joint Polar Satellite System (JPSS) cloud top algorithm theoretical basis document (ATBD), 474-0041, 73pp., NASA Goddard Space Flight Center, Greenbelt, Md.

Barnes, W. L., T. S. Pagano and V. V. Salomonson, 1998: Prelaunch characteristics of the Moderate Resolution Imaging Spectroradiometer (MODIS) on EOS-AM1, *IEEE Trans. Geosci. Remote Sens.*, 36, 1088-1100.

Bauer, P., P. Lopez, A. Benedetti, D. Salmond, E. Moreau, 2006a: Implementation of 1D+4D-Var assimilation of precipitation-affected microwave radiances at ECMWF. I: 1D-Var. *Q. J. R. Meteorol. Soc.* 132: 2277-2306.

Bauer, P., P. Lopez, D. Salmond, A. Benedetti, S. Saarinen, E. Moreau, 2006b: Implementation of 1D+4D-Var assimilation of precipitation-affected microwave radiances at ECMWF. II: 4D-Var. *Q. J. R. Meteorol. Soc.* 132:2307-2332.

Bauer, P., G. Ohring, C. Kummerow and T. Auligne, 2011: Assimilating satellite observations of clouds and precipitation into NWP Models, *Bull. Amer. Meteor. Soc.*, 92, ES25-ES28.

Baum, B. A., D. P. Kratz, P. Yang, S. C. Ou, Y. Hu, P. F. Soulen, and S. C. Tsay, 2000: Remote Sensing of cloud properties using MODIS airborne simulator imagery during SUCCESS, 1. Data and models, *J. Geophys. Res.*, 105, 11 767- 11 780. doi: 10.1029/1999JD901089.

Benjamin S. G., D. Devenyi, S. S. Weygandt, K. J. Brundage, J. M. Brown, G. A. Grell, D. Kim, B. E. Schwartz, T. G. Smirnova, T. L. Smith, G. S. Manikin, 2004a: An hourly assimilation/forecast cycle: The RUC., Mon. Wea. Rev., 132, 495-518.

Benjamin S. G., J. M. Brown, S. S. Weygandt, T. L. Smith, B. Schwartz., W. R. Moninger, 2004b: Assimilation of surface cloud, visibility, and current weather observations in the RUC, *In Preprints for 16th Conference on Numerical Weather Prediction*, Seattle. Amer. Meteorolog. Soc: Boston, MA.

Berg, R., 2009: Hurricane Ike (AL092008) 1-14 September 2008, *Tropical Cyclone Report*, 1-55.

Blake, E. S., T. B. Kimberlain, R. J. Berg, J. P. Cangialosi and J. L. Beven II, 2013: Hurricane Sandy (AL182012) 22-29 October 2012, *Tropical Cyclone Report*, 1-157.

Bjerknes, V., 1991: Dynamic Meteorology and Hydrography. Part II. Kinematics. *Carnegie Institute*, Gibson Bros, New York, USA.

Cardinali, C., 2009: Monitoring the observation impact on the short-range forecast. *Q.J.R. Meteorol. Soc.*, 135: 239–250. doi: 10.1002/qj.366.

Chen, Y., Y. Han, P. Van Delst, and F. Weng, 2010: On water vapor Jacobian in fast radiative transfer model, *J. Geophys. Res.*, 115, D12303. doi:10.1029/2009JD013379.

Chen, Y., Y. Han, and F. Weng, 2012: Comparison of two transmittance algorithms in the community radiative transfer mode: Application to AVHRR, *J. Geophys. Res.*, 117, D06206. doi: 10.1029/2011JD016656.

Courtier, P., and Coauthors, 1993: Variational assimilation at ECMWF. *ECMWF Tech. Memo.* 194, pp 84.

Cucurull, L., R. A. Anthes, and L.-L. Tsao, 2014: Radio Occultation Observations as Anchor Observations in Numerical Weather Prediction Models and Associated Reduction of Bias Corrections in Microwave and Infrared Satellite Observations. *J. Atmos. Oceanic Technol.*, 31, 20–32. doi: http://dx.doi.org/10.1175/JTECH-D-13-00059.1

Daley, R., 1991: Atmospheric Data Analysis, Cambridge University Press, UK.

Deber, J. C., D. F. Parrish, and S. J. Lord, 1991: The new global operational analysis system at the National Meteorological Center, *Wea. Forecasting*, 6, 538-547

Derber, J. C., and F. Bouttier, 1999: A reformation of the background error covariance in the ECMWF global data assimilation system, *Tellus*, 51A, 195-221.

Derber, J. C., and W. –S. Wu, 1998: The use of TOVS cloud-cleared radiances in the NCEP SSI analysis system. *Mon. Wea. Rev.*, 126, 2287-2299.

Dey, C. H., R. A. Petersen, B. A. Ballish, P. M. Caplan, L. L. Morone, H. J. Thiebaux, G. H. White, H. E. Fleming, A. L. Reale, D. G. Gray, M. D. Goldberg, and J. M. Daniels, 1989: An evaluation of NESDIS TOVS physical retrievals using data impact studies. *NOAA Tech. Memo.* NWS NMC 69, National Meteorological Center, Washington D. C., pp 25.

Diak, G. R., D. Kim, M. S. Whipple, and X. Wu, 1992: Preparing for the AMSU. *Bull. Amer. Meteor. Soc.*, 73, 1971-1984. doi:10.1175/1520-0477(1992)073<1971:PFTA>2.0.CO;2.

DTC, NCAR, and NOAA, 2012: Gridpoint Statistical Interpolation (GSI) Version 3.1 User's Guide, http://www.dtcenter.org/com/GSI/users/docs/users_guide/GSIUserGuide_v3.1.pdf

English, S., J. Eyre, and J. Smith, 1999: A cloud-detection scheme for use with satellite sounding radiances in the context of data assimilation for numerical weather predictions. *Q. J. Roy. Meteor. Soc.*, 125, 2359–2378.

Errico, R. M., P. Bauer, and J. –F. Mahfouf, 2007: Issues Regarding the Assimilation of Cloud and Precipitation Data. *J. Atmos. Sci.*, 64, 3785–3798.

Evensen, G., 1994: Sequential data assimilation with a nonlinear quasi-geostrophic model using Monte Carlo methods to forecast error statistics, *J. Geophys. Res.*, 99(C5), 10143-10162.

Eyre J. R., G. A. Kelly, A. P. McNally, E. Andersson and Persson A., 1993: Assimilation of TOVS radiance information through one-dimensional variational analysis. *Q. J. Roy. Meteor. Soc.*, 119, 1427-1463.

Gambacorta, A., and C. Barnet, 2013: Methodology and information content of the NOAA NESDIS operational channel selection for the Cross-Track Infrared Sounder (CrIS), *IEEE Trans. Geosci. Remote Sens.*, 51, 3207-3216.

Garand, L., M. Buehner, S. Heilliette, S. R. Macpherson, and A. Beaulne, 2013: Satellite radiance assimilation impact in new Canadian ensemble-variational syste, *Proceedings of the 2013 EUMETSAT Meteorological Satellite Conference*, 16-20 September, 2013, Vienna, Austria.

Gauthier, P., Charette, C., Fillion, L., Koclas, P., Laroche, S., 1999: Implementation of a 3D variational data assimilation system at the Canadian Meteorological Centre. Part I: The global analysis. *Atmosphere Ocean* 37 (2), 103–156.

Geer, A. J, P. Bauer, P. Lopez, 2008: Lessons learnt from the operational 1D + 4D-Var assimilation of rain- and cloud-affected SSM/I observations at ECMWF. *Q. J. R. Meteorol. Soc.* **134***:* 1513–1525.

Geer, A. J. and Bauer, P., 2011: Observation errors in all-sky data assimilation. *Q.J.R. Meteorol. Soc.*, 137: 2024–2037.

Godin, R., 2014: Joint Polar Satellite System (JPSS) cloud effective particle size and cloud optical thickness algorithm theoretical basis document (ATBD), 474-0042, 148 pp., NASA Goddard Space Flight Center, Greenbelt, Md.

Goldberg, M. D., Y. Qu, L. M. McMillin, W. Wolf, Z. Lihang, and M. Divakarla, 2003: AIRS near-real-time products and algorithms in support of operational numberical weather prediction, *IEEE Trans. Geosci. Remote Sens.*, 41(2), 379-389.

Goldberg, M. D., T. S. King, W. W. Wolf, C. Barnet, H. Gu and L. Zhou, 2005: Using MODIS with AIRS to develop an operational cloud-cleared radiance product, *Proc. SPIE 5655*, Multispectral and Hyperspectral Remote Sensing Instruments and Applications II, 128. doi:10.1117/12.578824 .

Han, Y., P. van Delst, Q. Liu, F. Weng, B. Yan, R. Treadon and J. Derber, 2006: JCSDA Community Radiative Transfer Model (CRTM) - Version 1, *NOAA Tech Report 122.*

Han, Y., *et al.*, 2013: Suomi NPP CrIS measurements, sensor data record algorithm, calibration and validation activities, and record data quality, J. Geophys. Res. Atmos., 118, 12,734–12,748. *doi:*10.1002/2013JD020344.

Heilliette, S. and L. Garand, 2007: A practical approach for the assimilation of cloudy infrared radiances and its evaluation using airs simulated observations, Atmosphere-Ocean, 45:4, 211-225.

Hong. S. –Y., and J.-O. J. Lim, 2006: The WRF single-moment 6-class microphysics scheme (WSM6), *J. Korean Meteor. Soc.*, 42, 129-151.

Holton, J. R., 2004: An introduction to dynamic meteorology, Academic Press, Fourth Edition, London, p535.

Hu, M., and M. Xue, 2006: Implementation and evaluation of cloud analysis with WSR-88D reflectivity data for GSI and WRF-ARW, *Geophy. Res. Letters.*, 34, L07808. doi: 10.1029/2006GL028847.

Huang, H.-L. and W. L. Smith, 2004: "Apperception of clouds in AIRS data", *Proc. ECMWF Workshop on Assimilation of High Spectral Resolution Sounder in NWP*, Jun. 28-Jul. 1, 2004, p155-169.

Hutchison, K. D., J. K. Roskovensky, J. M. Jackson, A. K. Heidinger, T. J. Kopp, <. J. Pavolonis, and R. Frey, 2005: Automated cloud detection and typing of data collected by the Visible Infrared Imager Radiometer Suite (VIIRS), *Int. J. Remote Sens.*, 20, 4681-4706.

Iacono, M. J., J. S. Delamere, E. J. Mlawer, M. W. Shephard, S. A. Clough, and W. D. Collins, 2008: Radiative forcing by long-lived greenhouse gases: Calculations with the AER radiative transfer models, *J. Geophys. Res.*, 113, D13103. doi:10.1029/2008JD009944.

Joo, S., J. Eyre, and R. Marriott, 2013: The Impact of MetOp and Other Satellite Data within the Met Office Global NWP System Using an Adjoint-Based Sensitivity Method. *Mon. Wea. Rev.*, 141, 3331–3342. doi: http://dx.doi.org/10.1175/MWR-D-12-00232.1.

Jung, J. A., 2008: The assimilation of hyperspectral satellite radiances in global numerical weather prediction. *UMD These and Dissertations.* http://hdl.handle.net/1903/8166

Kain, J. S., 2004: The Kain-Fritsch convective parameterization: An update. *J. Appl. Meteor.*, 43, 170-181. doi: 10.1175/1520-0450(2004)043<0170:TKCPAU>2.0.CO;2.

Kalnay, E., 2003: Atmospheric Modeling, Data Assimilation and Predictability, *Cambridge University Press*, Cambridge, UK.

Kelly, G., E. Anderson, A. Hollingsworth, P. Lonnberg, J. Pailleux and Z. Zhang, 1991: Quality control of operational physical retrievals of satellite sounding data. *Mon. Wea. Rev.*, 119, 1866-1880.

Kelly, G., and J.-N. Thepaut, 2007: Evaluation of the impact of the space component of the Global Observation System through observing system experiments. *ECMWF Newsletter*, *No. 113*, ECMWF, Reading, United Kingdom, 16–28. [Available online at http://www.ecmwf.int/publications/newsletters/pdf/113.pdf.]

Kim, D., and S.G. Benjamin, 2001: An initial RUC cloud analysis assimilating GOES cloud-topdata. *Preprints, 14th Conf. Num. Wea.* Pred., Ft. Lauderdale, FL, Amer. Meteor. Soc., P113-115.

King, M. D., W. P. Menzel, Y. J. Kaufman, D. Tanre, B. Gao, S. Platnick, S. A. Ackerman, L. A. Remer, R. Pincus, and P. A. Hubanks, 2003: Cloud and aerosol properties, precipitable water, and profiles of temperature and water vapor from MODIS, *IEEE Trans. Geosci. Remote Sens.*, 41, 442-458.

Kleist, D. T., D. F. Parrish, J. C. Derber, R. Treadon, W. –S. Wu and S. Lord, 2009: Introduction of the GSI into the NCEP global data assimilation system, *Wea. Forecasting*, 24, 1691-1705. doi: 10.1175/2009WAF2222201.1.

Le Marshall, J. F., 1988: An intercomparison of temperature and moisture fields derived from TIROS operational vertical sounder data by different retrieval techniques. Part I: Basic statistics, *J. Appl. Met.,* 27, 1282-1293.

Le Marshall, J., J. Jung, J. Derber, R. Treadon, S. Lord, M. Goldberg, W. Wolf, H.C. Liu, J. Joiner, J. Woollen, and R. Todling, 2005: AIRS hyperspectral data improves southern hemisphere forecasts. *Aust. Meteor. Mag.,* 54, 57-60.

Lee, T., S. Miller, C. Schueler, and S. Miller, 2006: NASA MODIS previews NPOESS VIIRS capabilities, *Weather Forecasts.*, 21 (4), 649-655.

Li, J., and H.-L. Huang, 1999: Retrieval of atmospheric profiles from satellite sounder measurements by use of the discrepancy principle, Appl. Optics, Vol. 38, No. 6, 916-923.

Li, J., Jinlong Li, Elisabeth Weize, and D. K. Zhou, 2007: Physical retrieval of surface emissivity spectrum from hyperspectral infrared radiances, Geophysical Research Letters, 34, L16812.

Li, J., C. Y. Liu, H.-L. Huang, T. J. Schmit, W. P. Menzel, and J. Gurka, 2005: Optimal cloud-clearing for AIRS radiances using MODIS. *IEEE Trans. Geosci. Remote Sens.*, 43, 1266-1278.

Li. J., and H. Liu, 2009: Improved hurricane track and intensity forecast using single field-of-view advanced IR sounding measurements, *Geophys. Res. Lett.*, 36, L11813.

Li, J., W. P. Menzel, and A. J. Schreiner, 2001: Variational retrieval of cloud parameters from GOES sounder longwave cloudy radiance measurements. J. Appl. Meteorol. 40, 312-330.

Li, J., W. P. Menzel, Z. Yang, R. A. Frey, and S. A. Ackerman, 2003: High-spatial-resolution surface and cloud-type classification from MODIS multi-spectral band measurements, *J. Appl. Meteorol.*, 42, 204-226.

Li. J., W. P. Menzel, F. Sun, T. J. Schmit, and J. Gurka, 2004: AIRS subpixel cloud characterization using MODIS cloud products, *J. Appl. Meteorol.*, 43, 1083-1094.

Li, Z., J. Li, T. J. Schmit, W. P. Menzel, and S. A. Ackerman, 2007: Comparison between current and future environmental satellite imagers on cloud classification using. *Remote Sensing of Environment*, 108, 311 - 326.

Li, J., W. Wolf, W. P. Menzel, W. Zhang, H.-L. Huang, and T. H. Achtor, 2000: Global soundings of the atmosphere from ATOVS measurements: The algorithm and validation, J. Appl. Meteorol., 39: 1248 - 1268.

Lim, A. H. N., J. A. Jung, H.-L. A. Huang, S. A. Ackerman and J. A. Otkin, 2014: Assimilation of clear sky atmospheric infrared sounder radiances in short-term regional forecasts using

community models, *J. Appl. Remote Sens.*, 8, 083655-1 – 083655-27. doi: 10.1117/1.JRS.8.083655.

Liu, H., and J. Li, 2010: An improvement in forecasting rapid intensification of typhoon Sinlaku (2008) using clear-sky full spatial resolution advanced IR soundings, *J. Appl. Meteor. Climatol.*, 49, 821-287.

Lopez, P., Moreau, E., 2005: A convection scheme for data assimilation: Description andinitial tests. *Q. J. R. Meteorol. Soc.*, 131 (606), 409–436.

Lorenc, A. C., 1986: Analysis methods for numerical weather prediction. *Quart. J. Roy. Meteor. Soc.*, 112, 1177-1194.

Lorenc, A., 2003: Modelling of error covariances by 4D-Var data assimilation. *Q. J. R.Meteorol. Soc.*, 129 (595), 3167–3182.

Macpherson B., B. W. Wright, W. H. Hand, A. J. Maycock, 1996: The impact of MOPS moisture data in the UK Meteorological Office data assimilation scheme, *Mon. Wea., Rev.*, 124, 1746-1766.

McCarty, W., G. Jediovec, T. L. Miller, 2009: Impact of the assimilation of Atmospheric Infrared Sounder radiance measurements on short-term weather forecast, *J. Geophys. Res.*, 01/2099, 114.

McPherson, R. M., 1999: The future of the North American radiosonde network. *Third Symposium on Integrated Observing Systems*, 10-15 January, 1999, Dallas, Texas, pp 14-17.

McNally, A. P., 2002: A note on the occurrence of cloud in meteorologically sensitive areas and the implications for advanced infrared sounders. *Q.J.R. Meteorol. Soc.*, 128: 2551–2556.

McNally, A. P. and Watts, P. D., 2003: A cloud detection algorithm for high-spectral-resolution infrared sounders. Q.J.R. Meteorol. Soc., 129: 3411–3423. doi: 10.1256/qj.02.208.

Merrill, R. T., 1988: Environmental Influences on Hurricane Intensification. *J. Atmos. Sci.*, 45, 1678–1687. doi: http://dx.doi.org/10.1175/15200469(1988) 045<1678:EIOHI>2.0.CO;2.

Moreau, E., Lopez, P., Bauer, P., Tompkins, A. M., Janisková, M. and Chevallier, F., 2004: Variational retrieval of temperature and humidity profiles using rain rates versus microwave brightness temperatures. *Q.J.R. Meteorol. Soc.*, 130: 827–852.

Muth, C., W. A. Webb, W. Atwood and P. Lee, 2005: Advanced technology microwave sounder on the National Polar-Orbiting Operational environmental satellite system, *Int'l Geoscience and Remoste Sensing Symposium, IGARSS Proceedings*, 1.

Nagle, F. W., 1998: The association of disparate satellite observations, *Proc. Second Symp. On Integrated Observing Systems*, Phoenix, AZ. Amer. Meteor. Soc., 49-52.

Okamoto, K. and J. C. Derber, 2006: Assimilation of SSM/I Radiances in the NCEP Global Data Assimilation System. *Mon. Wea. Rev.*, 134, 2612–2631.

Otkin, J. A., 2010: Clear and cloudy sky infrared brightness temperature assimilation using an ensemble Kalman filter, *J. Geophys. Res.*, 115, D19207.

Pangaud, T., N. Fourrie, V. Guidard, M. Dahoui, and F. Rabier,, 2009: Assimilation of AIRS Radiances Affected by Mid- to Low-Level Clouds. *Mon. Wea. Rev.*, 137, 4276–4292. doi: http://dx.doi.org/10.1175/2009MWR3020.1.

Parrish, D. F., and J. C. Derber, 1992: The National Meteorologcial Center's spectral statistical interpolation analysis system. *Mon. Wea. Rev.*, 120, 1747-1763.

Pavelin EG, English SJ, Eyre JR. (2008), The assimilation of cloud-affected infrared satellite radiances for numerical weather prediction. *Q. J. R. Meteorol. Soc.*, 134: 737–749.

Pavolonis, M. J. and A. K. Heidinger, 2004: Daytime cloud overlap detection from AVHRR and VIIRS. *J. Appl. Meteor.*, 43, 762-778.

Platnick, S., M. D. King, S. A. Ackerman, W. P. Menzel, B. A. Baum, J. C. Riedi, and R. A. Frey, 2003: The MODIS cloud products: algorithms and examples from Terra, *IEEE Trans. Geosci. Remote. Sens.*, 41, 459-473.

Reale, O., J. Susskind, R. Rosenberg, E. Brin, E. Liu, L. P. Riishojgaard, J. Terry, and J. C. Jusem, 2008: Improving forecast skill by assimilation of quality0controlled AIRS temperature retrievals under partially cloudy conditions, *Geophys. Res. Lett.*, 35, L08809.

Renshaw, R. and P. N. Francis, 2011: Variational assimilation of cloud fraction in the operational Met Office Unified Model. *Q.J.R. Meteorol. Soc.*, 137: 1963–1974.

Schwartz, C. S., Z. Liu, H.-C. Lin, and S. A. McKeen, 2012: Simultaneous three-dimensional variational assimilation of surface fine particulate matter and MODIS aerosol optical depth, *J. Geophys. Res.*, 117, D13202.

Skamarock, W. C., J. B. Klemp, J. Dudhia, D. O. Gill, D. M. Barker, M. G. Duda, X.-Y., Huang, W. Wang and J. G. Powers, 2008: A description of the advanced research WRF version 3, *NCAR Technical Note*, 1-113.

Smith, W. L., et al., 2004: Extraction of profile information from cloud contaminated radiances, *Proc. ECMWF Workshop on Assimilation of High Spectral Resolution Sounder in NW*P, Jun. 28-Jul. 1, 2004, p145-154.

Stengel, M., Lindskog, M., Undén, P. and Gustafsson, N. (2013), The impact of cloud-affected IR radiances on forecast accuracy of a limited-area NWP model. *Q.J.R. Meteorol. Soc.*, 139: 2081–2096.

Strabala, K. I., S. A. Ackerman, and W. P. Menzel, 1994: Cloud properties inferred from 8-12-μ m data. *J. Appl. Meteor.*, 33, 212-229. doi: 10.1175/1520-0450(1994)033<0212:CPIFD>2.0.CO;2.

Wang, P., J. Li, J. Li, Z. Li, T. J. Schmit, and W. Bai *(*2014*),* Advanced infrared sounder subpixel cloud detection with imagers and its impact on radiance assimilation in NWP, *Geophys. Res. Lett.,* 41, 1773–1780. doi:10.1002/2013GL059067.

Wang, P., J. Li, M. D. Goldberg, T. J. Schmit, A. H. N. Lim, Z. Li, H. Han, J. Li, and S. A. Ackerman, 2015: Assimilation of thermodynamic information from advanced infrared sounders under partially cloudy skies for regional NWP. *J. Geophys. Res. Atmos.*, 120, doi:10.1002/2014JD022976.

Warner, T. T., R. A. Peterson, and R. E. Treadon, 1997: A tutorial on lateral boundary conditions as a basic and potentially serious limitation to regional numerical weather prediction. *Bull. Amer. Meteor. Soc.*, 78 (11): 2599-2617.

Weng, F., L. Zhao, R. R. Ferraro, G. Poe, X. Li, and N. C. Grody, 2003: Advanced microwave sounding unit cloud and precipitation algorithms, *Radio Sci.*, 38(4), 8068. doi:10.1029/2002RS002679.

Weng. F., 2007: Advances in radiative transfer modeling in support of satellite data assimilation, *J. Atmos. Sci.*, 64, 3799-3807.

Wu, W. –S.,R. J. Purser, and D. F. Parrish, 2002: Three- dimensional variational analysis with spatially inhomogeneous covariances, *Mon. Wea. Rev.*, 115, 209-232. doi: 10.1175/1520-0493(2002)130<2905:TDVAWS>2.0.CO;2.

Wylie, D. P., W. P. Menzel, H. M. Woolf, and K. I. Strabala, 1994: Four years of global cirrus cloud statistics using HIRS, *J. Clim.*, 7(12), 1972– 1986. doi:10.1175/1520-0442(1994)007<1972:FYOGCC>2.0.CO;2.

Zavodsky, B. T., S. H. Chou, G. Jedlovec, and W. Lapenta, 2007: The impact of atmospheric infrared sounder (AIRS) profiles on short-term weather forecasts. Proc. SPIE 6565, Algorithms and Technologies for Multispectral, Hyperspectral, and Ultraspectral Imagery XIII, 656561J (May 07, 2007).

Zhang, M., M. Zupanski, M.-J. Kim, J. A. Knaff, 2013: Assimilating AMSU-A radiances in the TC Core Area with NOAA Operational HWRF (2011) and a Hybrid Data Assimilation System: Danielle (2010). *Mon. Wea. Rev.*, 141:11.

Zheng, J., J. Li, T. J. Schmit, and J. Li, 2015: The impact of AIRS atmospheric temperature and moisture profiles on hurricane forecasts: Ike (2008) and Irene (2011), Adv. In Atmos. Sci., 32 (3), 319-33.